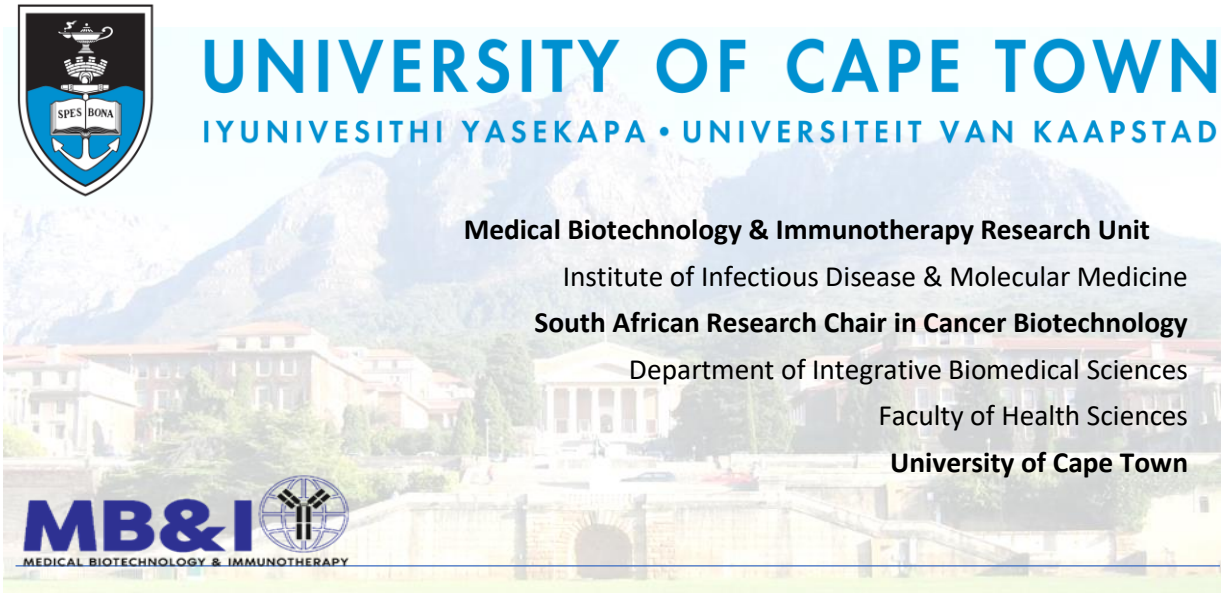

Masters Thesis

Developing novel SNAP tag-based antibody fusion proteins directionally conjugated to fluorophores for immunophenotyping of acute myeloid leukemia.

Tatenda Lovemore Bvudzijena

Supervisor:

Prof. Dr. Dr. Stefan Barth

Co-Supervisors:

Dr Munyaradzi Musvosvi

Bernard Murithi Mirianga

Submitted to the Faculty of Health Sciences, University of Cape Town, in fulfilment of the requirements for the degree of Master of Science (Med) in Chemical Biology.

November 2023

Plagiarism Declaration

1. This thesis/dissertation has been submitted to the Turnitin module (or equivalent similarity and originality checking software), and I confirm that my supervisor has seen my report and any concerns revealed by such have been resolved with my supervisor.
2. I know that plagiarism is wrong. Plagiarism is using another's work and pretending that it is one's own.
3. I have used the Vancouver Referencing Style as the convention for citation and referencing. Each significant contribution to, and quotation in, this thesis/dissertation from the work or works of other people has been attributed and has cited and referenced.
4. This thesis/dissertation is my work.
5. I have not allowed and will not allow anyone to copy my work to pass it off as his or her own work.
6. I acknowledge that copying someone else's assignment or essay, or part of it, is wrong, and declare that this is my own work.

SIGNATURE: Signed by candidate

DATE: 06/11/2023

Acknowledgements

I express my profound gratitude to Prof. Dr. Dr. Stefan Barth for his exceptional guidance and insightful supervision throughout my research. My sincere appreciation also extends to my co-supervisors, Dr. Munyaradzi Musvosvi and Bernard Murithi Mirianga, whose invaluable input and patience significantly contributed to the success of this study. Your exemplary mentorship has been truly invaluable, and I am deeply grateful for your support.

I am also thankful to the dedicated members of the Medical Biotechnology and Cancer Immunotherapy Research Unit, as well as our collaborators from the South African Tuberculosis Vaccine Initiative, for their unwavering support and collaboration.

I want to thank Prof. Davison Sangweme, Prof. Frank Matose, Tamsang Matose, Dr. Alex Akrinimade, Dr. Akhona Vava, Dr. Ramamurthy, Nyasha Sigwadi, Atli Molope, Elis T Mutyanda and Denis Dogbey in particular for their invaluable help with my experimental work and writing.

Furthermore, I would like to express my heartfelt gratitude to my parents, especially Mazani S. and the late Bvudzijena G, for their unwavering emotional and material support throughout this journey. My gratitude also extends to my brother Mugweni Allen, my friends, and numerous others whose contributions, though unmentioned, have played a significant role in the completion of this work. Thank you all for your support and encouragement.

Lastly, I extend my sincere appreciation to the National Research Fund (NRF) and the University of Cape Town (UCT) for their generous financial support, which made my pursuit of postgraduate education a reality. Your assistance has been instrumental in enabling me to achieve my academic goals, and I am profoundly grateful for your investment in my education.

List of publications

Dogbey, D.M., Andong-Koung-Edzidzi, U.C., **Bvudzijena, T.L.**, Molope G.A Singh, J., Krupa, N., Barth, S. (2023). EpCAM-specific anti-cancer immunotherapy: evidence from clinical studies and the way forward. Journal: Clinical Oncology, *Submitted for review*.

Table of Contents

Index of Figures and Tables

Figures

Tables

List of Abbreviations

ADC	Antibody-Drug Conjugate
AGT	O6-Alkylguanine-DNA Alkyl transferase
AKT	AKT Protein kinase B
ALL	Acute Lymphoblastic Leukemia
AML	Acute Myeloid Leukemia
AMP	Ampicillin
AMPR	AMPR Ampicillin resistance
BG	Benzyl guanine
BG-Alexa Flour 488	BG-modified SNAP-Surface® Alexa Fluor® 488
BG-Alexa Flour 647	BG-modified SNAP-Surface® Alexa Fluor® 647
BSA	Bovine Serum Albumin
CD14	Cluster Differentiation Antigen 14
CDR	Complementary determining region
Comm	Commercial
dH_20	Deionized water
DMSO	Dimethyl Sulphoxide
DNA	Deoxyribonucleic acid
eGFP	eGFP Enhanced Green Fluorescent Protein
FBS	Fetal Bovine Serum
FDA	Food and Drug Administration (United States)
FR	Framework Regions
HEK293T	Human Embryonic Kidney cells
HLA-DR	Human Leukocyte Antigen-DR
HSPCs	Hematopoietic Stem and Progenitor Cells

IMAC	Immobilised Metal Affinity Chromatography
mAb	Monoclonal antibody
MB&I	Medical Biotechnology and Immunotherapy Research Group
MPO	Myeloperoxidase
ORF	open reading frame
PS	Penicillin Streptomycin
PVDF	Polyvinylidene Fluoride
RCF	Relative centrifugal force
RE	Restriction Enzyme
RPM	Revolutions per minute of rotor
RPMI	Roswell Park Memorial Institute
FBS	Fetal Bovine Serum
FDA	Food and Drug Administration (United States)
RT	Room temperature
scFv	Single chain variable fragment
SDS-PAGE	Sodium Dodecyl sulphate Polyacrylamide Gel Electrophoresis
SOC	Super Optimal Broth with Catabolite repression
TAA	Tumour Associated Antigen
TAE	Tris-acetate EDTA buffer
TKI	Tyrosine Kinase Inhibitor
UV	UV Ultraviolet

Abstract

Acute Leukemia comprising of acute myeloid leukemia (AML) and acute lymphoblastic leukemia (ALL), represents a clonal malignant transformation of hematopoietic cells originating in the bone marrow or lymphoid organs. This is often associated with fundamental genetic abnormalities, and these malignancies are also characterised by persistent proliferation of hematopoietic progenitor cells or maturation arrest at a particular developmental stage, which is specific to each subtype of leukemia. The treatment strategies for acute myeloid leukemia include chemotherapy, bone marrow transplantation, radiotherapy, and immunotherapy, with current research focusing on antibody-based immunotherapy because of its advantages including higher tumour selectivity and increase of drug tolerability.

Acute leukemia is diagnosed by combining information from the patient's past medical records, clinical presentations and laboratory results from the studies performed by a pathologist. Pathologist-led studies include haematological investigations like the total blood count, meticulous peripheral blood film review and bone marrow aspiration smear examination. Specific genetic abnormalities linked to AML can be identified through molecular genetic tests, including chromosomal analysis, next-generation sequencing, real-time polymerase chain reaction and cytogenetic analysis. Immunophenotyping by flow cytometry and immunohistochemistry can be used to identify specific proteins or antigens upregulated in AML.

In low and middle-income countries, particularly Africa, AML diagnosis is primarily based on leukemic cells or blast morphology, which has significant drawbacks in terms of providing accurate and timely diagnosis. This method utilizes the identification of myeloid blasts primarily through their visual characteristics under the microscope and counting them in bone marrow aspirate samples stained with a suitable Romanowsky stain, such as the Wright-Giemsa stain. Additionally, molecular genetic testing, mostly (RT) polymerase chain reaction (PCR), is also being utilized for AML diagnosis.

Using advanced technologies like flow-cytometric immunophenotyping and immunohistochemistry is limited due to the current costs of antibody-based diagnostics in these already strained developing countries' economies Utilizing immunophenotyping by flow cytometry and immunohistochemistry would allow clinicians to clearly define each subtype of acute leukemia, timely diagnose the disease, and initiate therapy on time. These methods utilise monoclonal antibodies targeting uniquely overexpressed markers on leukemic blasts. To address the challenges posed by the costs and limited availability of antibody-based immunodiagnostics in Africa, an alternative approach would be the use an easy-to-tailor fashion of smaller antibody fragments (single chain variable fragments) coupled with a SNAP-tag, which can be readily produced recombinantly under cost-controlling conditions.

SNAP-tag is a modified version of the human DNA repair enzyme alkylguanine-DNA alkyltransferase (AGT), which reacts specifically with *O*6-benzylguanine (BG)-modified molecules via irreversible transfer of an alkyl group to a cysteine residue within its active site. Benzylguanine can be chemically attached to a variety of synthetic labels, such as fluorophores. SNAP-tag can be coupled to scFvs (single chain variable fragments), forming unique SNAP-tag antibody fusion proteins which undergo self-labelling covalent conjugation reactions with benzylguanine derivatives, and this provides an innovative alternative approach to develop next-generation recombinant immunodiagnostics targeting different biomarkers upregulated in AML.

Therefore, this study aimed to explore SNAP tag-based antibody fusion proteins as supplementary or companion diagnostic tools for acute myeloid leukemia targeting cluster of differentiation 14 (CD14), myeloperoxidase (MPO), and the human leukocyte antigen DR (HLA-DR) which are antigens overexpressed on leukemic cells. The variable gene sequences encoding for scFv antibody fragments were obtained from publicly available resources (patents, journals, and antibody databases) and were fused to SNAP by *in-silico* expression plasmid design. The SNAP fusion protein encoding open reading frames (ORFs) were then cloned into the pCB plasmid vector backbone, containing all the unique features for protein expression in mammalian systems. Following that, scFv-SNAP fusion

proteins were generated by transfecting mammalian HEK 293T cells with the recombinant plasmids containing an Ig-Kappa leader, which allowed secretion of the proteins into the cell culture supernatant. After extraction, proteins were purified using immobilised metal affinity chromatography (IMAC) and characterised by SDS-PAGE and western blot before being conjugated to BG Alexa fluorophores. Proof of binding of the generated fluorescently labelled SNAP fusion proteins was demonstrated *in vitro* using leukemic cell lines for CD14 and MPO, while peripheral blood mononuclear cells were used for HLA-DR through confocal microscopy and flow cytometry.

The results of the study demonstrated specific binding of the newly generated SNAP fusion proteins, confirming their suitability for diagnostic applications. The future direction of the study will involve testing the generated fusion proteins on South African leukemia patient samples to determine the disease subtypes and comparing them with already existing tools. Additionally, developing new bivalent formats to increase affinity is a potential avenue for future research. In summary, the use of SNAP fusion proteins promotes local development and invention of next generation immunodiagnostics and therapeutics in Africa, and this could be considered as a cost-containment strategy for cancer remedies which are being priced for the first-world markets.

Chapter 1: Literature review

1.1 Leukemia

Leukemia, which includes acute and chronic leukemias, refers to a group of malignant blood disorders that arise due to genetic abnormalities in the bone marrow or lymphoid organs (1) (2). This is often associated with fundamental genetic abnormalities such as chromosomal translocations, gene mutations and gene amplifications. These genetic abnormalities disrupt normal cell proliferation, differentiation and apoptosis regulation resulting in the development and progression of leukemia (3). Despite their wide genetic heterogeneity, leukemia's have limited set of typical cancer hallmarks including poor differentiation, enhanced cell survival, uncontrolled proliferation and immune system evasion (4). These distinct features lead to the accumulation of immature and dysfunctional cells, which compromise the physiological functions of normal haematological cells (5). Acute lymphoblastic leukemia, acute myeloid leukemia, chronic lymphoblastic leukemia, and chronic myeloid leukemia are the four most frequently diagnosed types of leukemia (2).

1.2 Epidemiology

Currently, leukemia accounts for approximately 5% of all human cancers globally (6), with acute myeloid leukemia accounting for around 20-25% of acute leukemia cases and ranks as the 15th most prevalent cancer worldwide, causing the 11th highest number of cancer-related deaths (7). Acute leukemia is often thought to be predominant in children than in adults, but it is diagnosed 10 times more in adults than in children. (8) (9). The incidence rates of acute leukemia varies geographically, with sub-Saharan African countries, particularly those with a high prevalence of HIV, having the highest number of new cases in Africa, and is currently estimated to be 30–40 thousand per year (10,11). South Africa is one of the countries with the highest incidence and mortality rates of leukemia, as illustrated in **Figure 1**. In many parts of Africa, timely diagnosis, and treatment of acute leukemia is a challenge due to limited healthcare infrastructure and resources. As a result, the mortality rate is

higher in the African continent compared to many parts of the world (12). However, despite these challenges, ongoing efforts are being made to improve early detection and access to treatment for acute leukemia to alleviate the disease burden on the continent.

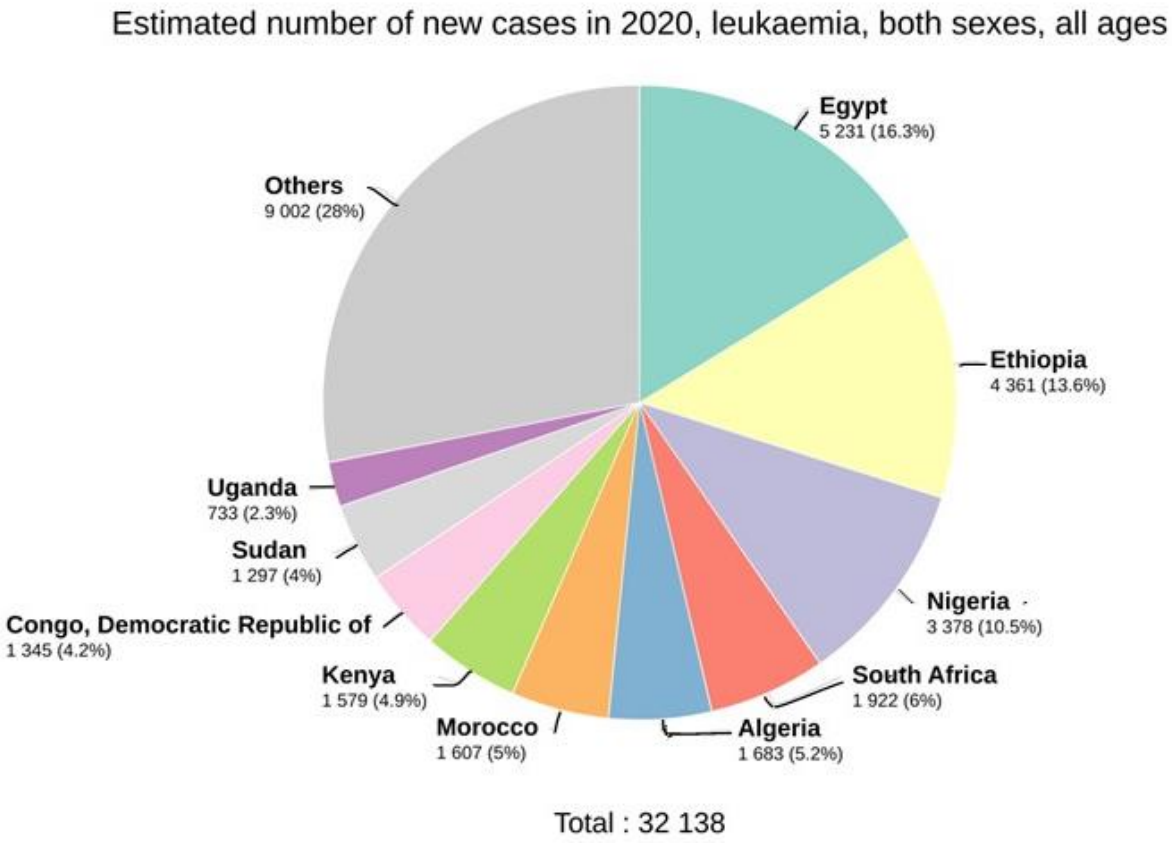

Figure 1. Estimated number of leukemia cases in selected African countries by gender and age group. GLOBOCAN, a global observatory for cancer trends, reported an incidence of 32,138 cases and 23,891 deaths in Africa, with Egypt, Ethiopia, Nigeria, and South Africa having the highest incidence and mortality rates (7).

1.3 Leukemia Classification

Leukemia is a type of cancer that can be categorized into two distinct types, acute and chronic, depending on the rate of progression of dysfunctional cells (blasts) and how quickly they leave the bone marrow and replace healthy cells, leading to the rapid onset of symptoms in patients (2) (13). Furthermore, it is classified as lymphoid or myeloid depending on the haematopoietic cells of origin (14). Acute leukemia's are fast growing cancers that progress quickly without treatments. This category includes acute myeloid leukemia (AML) and acute lymphoblastic leukemia (ALL). AML

develop from myeloid stem cells and myeloblasts, these cells represent immature white blood cells, which ultimately develop into red blood cells, platelets, monocytes, and granulocytes as illustrated in **Figure 2** (5) (15). On the other hand, ALL targets lymphoid stem cells and lymphoblasts that differentiate into either B cells or T cells (16). Under chronic leukemia's, which are slow-growing cancers that can be governed by treatments, we have chronic myeloid leukemia (CML), which primarily affects myeloid stem cells and granulocytes responsible for compacting infections (15). On the other hand, chronic lymphocytic leukaemia (CLL) affects B lymphocytes which are responsible for generating antibodies (17).

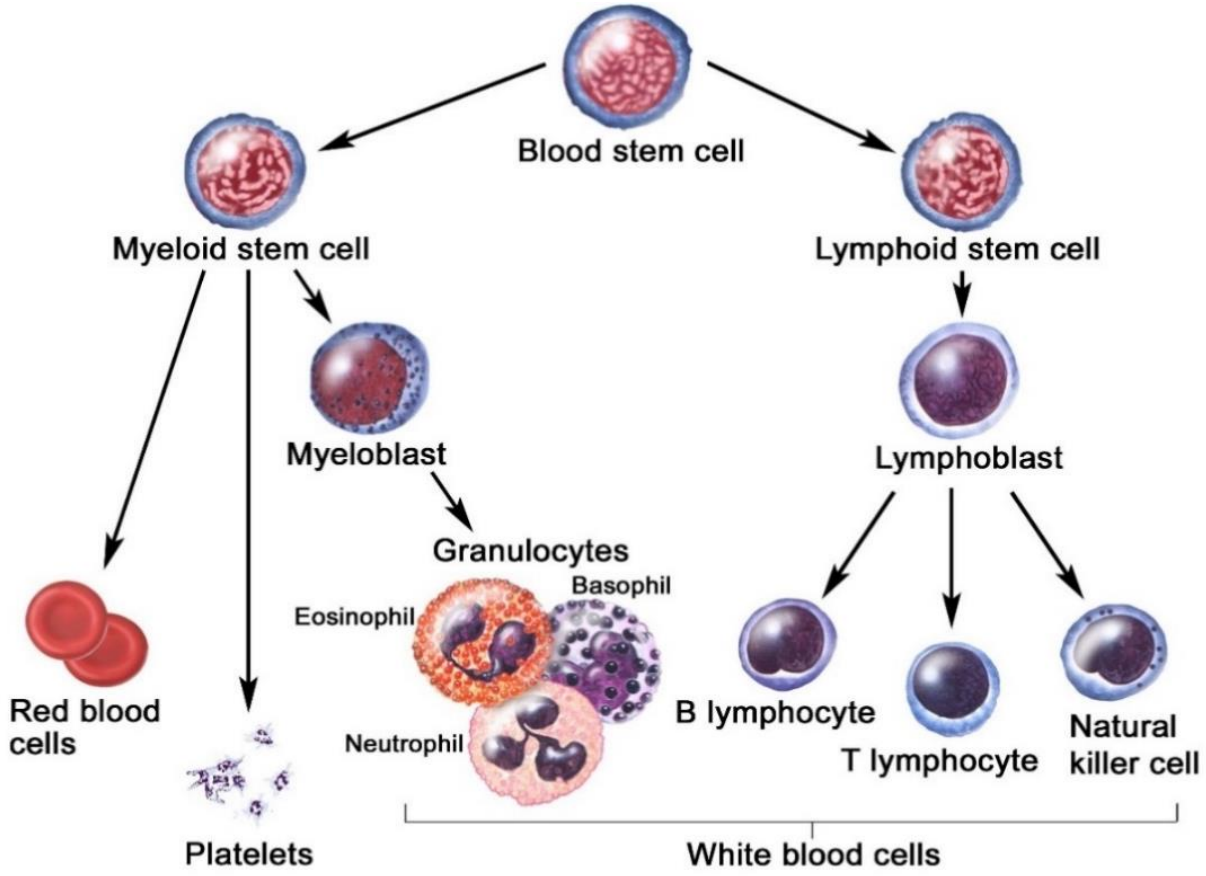

Figure 2. Blood cells development. The bone marrow produces blood stem cells (immature cells) that becomes mature over time. These stem cells may assume a form of myeloid stem cell or a lymphoid stem cell. Myeloid stem cells are transformed to red blood cells (RBC), platelets and myeloblasts (AML can develop from these cells). These cells later differentiate into white blood cells granulocytes (eosinophils, basophils, and neutrophils) and monocytes. Lymphoid stem cells turn into lymphoblasts (ALL can develop from these cells) and these later differentiate into white blood cells including B lymphocytes, T lymphocytes and Natural killer cells (NK cells). Siddhika, 2020 (5)(14) (24).

1.3.1 Aetiology of acute myeloid leukemia

Genetic mutations in hematopoietic stem cells are the first stage in the development of AML (18). These mutations are usually due to congenital anomalies and environmental risk factors, which have been the subject for various studies (19) (20) (21).

1.3.1.1 Congenital anomalies

A few congenital abnormalities have been associated with an elevated risk of acquiring AML (22) (23). According to the National Cancer Institute, children with Down syndrome have a cumulative risk of developing acute leukemia of around 2.1% by the age of 5 years and 2.7% by the age of 30 years (24). These rates reflect a 20- to 30-fold greater risk of ALL and a 100-fold increased risk of AML (25,26). The specific explanation for this is unknown, however it is thought that the presence of trisomy or on extra copy of chromosome 21 leads to increased proliferation of megakaryocyte progenitors (MKPs) and children with Down syndrome are more likely to develop acute megakaryoblastic leukaemia (AMKL) (27). AMKL exhibit immunophenotypic markers including CD33, CD117 and CD34 as illustrated in **Table 1** (28). Similarly, other genetic disorders such as Klinefelter syndrome (29), Li-Fraumeni syndrome (30) , Fanconi anaemia (31), and neurofibromatosis have all been linked to an increased chance of developing AML (32).

1.3.1.2 Environmental factors

Environmental factors including prolonged exposure to ionising radiation has been recognised as a risk factor for AML. According to studies on survivors of the Japanese atomic bomb blasts, the highest prevalence of AML was developed 5-7 years after exposure (33) (34). AML risk has also been related to repeated exposure to chemicals such as benzene, pesticides, ethylene oxide, embalming fluids, and other potentially toxic agents (35) (36). The relationship between smoking and the development of AML, particularly the M2 subtype **(Table 1)** in those over the age of 60, is widely debated (37).

1.3.2 Acute myeloid leukemia pathophysiology

Acute myeloid leukemia is characterised by mutated cells, due to their genetic self-renewal advantage, have the ability to multiply more quickly and survive longer compared to normal stem cells (18). Consequently, an imbalance arises in the production of mature cells, as the unchecked self-renewal of mutated cells leads to an accumulation of aberrant cells. This buildup of immature or undifferentiated cells in the bone marrow disrupts the normal maturation of blood cells at various stages (38). Additionally, the mutated stem cells undergo clonal expansion, overpowering the population of healthy cells and interfering with their normal development (39). In advanced stages of AML, the aberrant cells can invade tissues and spread to other organs through the bloodstream or lymphatic system. This process, known as metastasis, does not only affect multiple organs but also worsens the prognosis. During metastasis, the aberrant cells may establish secondary growths in distant locations including the central nervous system and the liver (40).

Some of the most common mutations observed in AML include Nucleophosmin 1 (NPM 1) mutations, which are present in approximately 25% to 35% of AML patients (41). The NPM 1 gene encodes for a protein involved in the transportation of proteins within the nucleus. Mutations in NPM 1 can disrupt this nuclear transport mechanism, leading to impaired function and increased cell survival (42). In patients with NPM 1 mutations, it has been observed that they are highly responsive to aggressive chemotherapy, regardless of age (43). This sensitivity to chemotherapy is seen in both young and older patients, indicating a favourable treatment response (44).

Another frequently occurring mutation in AML is observed in the FLT3 gene, which is abundantly expressed in hematopoietic stem cells. The FLT3 gene plays a crucial role in cell survival and proliferation. In approximately 30% of AML cases and 30% to 45% of cases with normal cytogenetics (CN-AML), internal tandem duplications (ITD) and tyrosine kinase domain (TKD) mutations in the FLT3 gene are detected (45). These mutations lead to increased activation of the FLT3 receptor, thereby enhancing the proliferation and survival of leukemic cells. FLT3 mutations can result in a

condition called severe leucocytosis, characterized by an abnormally high number of white blood cells (46). Furthermore, AML patients with FLT3-ITD mutations have an increased risk of disease recurrence, highlighting the prognostic significance of these mutations (47).

Similarly, the Runt-related transcription factor (RUNX1) translocation is observed in approximately 12% of all AML cases and is generally associated with a poor prognosis (48). RUNX1 is located on chromosome 21 and frequently translocate with the ETO (eight two one)/RUNX1T1 gene on chromosome 8q22, resulting in AML-ETO or t(8;21) (q22;q22) AML (49).RUNX1 is an essential component of haematopoiesis, the process of blood cell formation (50).

Other mutations occurring in AML include Isocitrate dehydrogenase 1 or 2 (IDH) genetic alterations found in about 20% of AML patients. These mutations occur in the IDH1 or IDH2 genes, which encode enzymes involved in glucose metabolism (51). Mutations in IDH1/2 can lead to the production of abnormal metabolites that promote the growth of AML cells (52). Moreover, approximately 10% of AML patients exhibit mutations in the CEBPA gene (53). This gene encodes for a transcription factor crucial for the differentiation of blood cells. Mutations in CEBPA disrupt this process, leading to uncontrolled proliferation of AML cells (54). Lastly, about 8% of AML patients also reveal TP53 mutations. Which is a tumour suppressor gene responsible for detecting and repairing DNA damage. Mutations in TP53 impair its function, resulting in uncontrolled growth of AML cells (55). Understanding the various mutations in AML is very important in the diagnosis and development of new targeted therapies.

1.3.3 FAB classification of acute myeloid leukemia

In the 1970s, leukemia specialists from France, the United States, and Britain classified AML into eight subtypes from M0 to M7 based on the maturity level of the cells and the type of cells in which leukemia originates (1) (56). This classification was primarily governed by the appearance of leukemia cells under the microscope after routine staining, as shown in **Table 1** (57) (58) (59). Several important factors need to be considered for the classification and accurate diagnosis of AML.

Table 1. FAB classification of acute myeloblastic leukemia

FAB Subtype	**% of adults with AML and Cytogenetics** (60)**.**	**Morphology**(61)	**Immunophenotype** (61)**.**
AML-M0	**5%**	**Acute myeloblastic leukemia with minimal differentiation:** Characterised by medium sized blasts, round nucleus with fine chromatin, cytoplasm is basophilic and non-granular, and they have prominent nucleoli**.**	CD11b+, CD15+, CD33+, CD11c+
AML-M1	**15%**	**Acute myeloblastic leukemia with minimal differentiation:** The blasts are medium sized and have a high ratio of nucleus to cytoplasm. They possess rounded nuclei with immature, dispersed chromatin and one or more prominent nucleoli. The cytoplasm may contain fine azurophilic granulation or isolated Auer rods.	CD117+, MPO+, CD33+, CD34+/-, CD13+
AML-M2	**t(8;21) (q22;q22), t(6;9)** **25%**	**Acute myeloblastic leukemia with maturation**: Cells are small to medium-sized with a high nucleo: cytoplasm ratio, rounded nuclei that contain immature and dispersed chromatin with one or more prominent nucleoli. The cytoplasm is basophilic and may contain traces of azurophilic granulation or isolated Auer rods.	CD34+/-, CD15+, CD13+, MPO+, Sudan Black +, HLA-DR+/-, CD117+/-
AML-M3	**t(15;17)** **10%**	**Promyelocytic leukemia:** Cells with abundant azurophilic granulation, the nucleus is usually monocytic in appearance and either irregular or bilobed with a cleft on it, scarcely basophilic cytoplasm due to abundant azurophilic granules.	CD13+, CD33+, CD34-, HLA-DR-
AML-M4	**inv(16)(p13q22), del(16q)** **20%**	**Acute myelomonocytic leukemia:** Cells are larger in size and have a moderate nucleo: cytoplasm ratio. The nucleus can be round, kidney-shaped or irregular and the nucleoli are typically prominent.	CD13+, CD64+, CD11c+ CD11b+, CD15+, CD33+

AML-M5	**del (11q), t(9;11), t(11;19)** **10%**	**M5a Acute monoblastic leukemia:** large blasts with round nuclei, immature chromatin that is dispersed and Auer rods in the cytoplasm. **M5b Acute Monocytic leukemia:** nuclei of promonocytes are rounded and their cytoplasm is less basophilic and highly granulated.	CD14+, CD11c+, HLA-DR+, CD64+
AML-M6:	**5%**	**M6a Acute erythroid leukemia with mixed blast multiplication:** red blood cells appearance in the blood is significantly changed with the presence of schistocytes. The blood contains more than 50% erythroid progenitor cells and 30% myeloblasts. **M6b Erythroid Leukemia Pure:** Cells contains 80% erythroid cells and 3% myeloid cells.	Glycophorin A+, CD33+, CD13+, CD15+
AML-M7	**t(1;22)** **5%**	**Acute megakaryocytic leukemia:** The blasts are polymorphic and highly immature, with scattered and reticular nuclei and dispersed chromatin. The cytoplasm is non-granular.	CD13+, CD33+, CD34+, CD42+, CD41+, CD61+, CD117+

Adapted from W. Ladines-Castro *et al*. 2016 (61).

1.3.4 WHO classification of AML

The World Health Organization (WHO) expanded the classification of AML in 2001 from the FAB Classification to include genetic and molecular abnormalities present in the leukemic blast cells (62). The latest classification published in 2016 includes six major classes, with the aim of integrating the latest advancements in the diagnosis and treatment of AML (63). **Table 2** provides an overview of the different WHO classifications of AML.

Table 2. WHO classification of AML

Subtype	**Description** (64) (65)
AML with recurrent genetic abnormalities:	AML in this category is distinguished by chromosomal abnormalities, such as translocations or inversions examples include: • AML with t(8;21) (q22;q22) RUNX1-RUNX1T1 • AML with inv(16) (p13q22) or t(16;16) (p13;q22); CBFB-MYH11 • APL with t(15;17) (q22;q12) PML-RARA • AML with t(9;11) (p21.3;q23.3); MLLT3-KMT2A • AML with t(6;9) (p23;q34.1) DEK-NUP214 • AML with inv(3)(q21.3q26.2) or t(3;3) (q21.3;q26.2); GATA2, MECOM • AML (megakaryoblastic) with t(1;22) (p13.3;q13.3); RBM15-MKL1 • AML with BCR-ABL1 (provisional entity) • AML with mutated NPM1 • AML with biallelic mutations of CEBPA • AML with mutated RUNX1 (provisional entity).
Myelodysplasia related AML:	This category includes AML that consists of myelodysplastic syndrome (MDS) features including abnormal blood cell counts or abnormal chromosomes before progressing to AML. This is due to deletions or loss of chromosomes examples include: del(5q)/t(5q), i(17q)/t(17p), del(11q), del(12p)/t(12p), and translocations between chromosomes: t(11;16)(q23.3;q13.3), t(3;21)(q26.2;q22.1), t(1;3)(p36.3;q21.2).
Therapy Related AML:	AML cases that develop due to prior treatment with chemotherapy or radiation therapy.
AML, not otherwise specified:	AML cases that do not fit into any of the other classes Including AML with minimal differentiation, AML without maturation, AML with maturation, Acute myelomonocytic leukemia, Acute monoblastic/monocytic leukemia, Acute erythroid leukemia, Pure erythroid leukemia, Acute megakaryoblastic leukemia, Acute basophilic leukemia and Acute panmyelosis with myelofibrosis
Myeloid sarcoma:	These are AML cases in which the cancerous cells develop a solid tumour outside of the bone marrow
Myeloid proliferations related to Down syndrome:	This category includes cases of AML that develop in people with Down syndrome and have recognisable genetic abnormalities.
Blastic plasmacytoid dendritic cell neoplasm:	This unusual form of AML involves the abnormal proliferation of specific white blood cells known as plasmacytoid dendritic cells.

The classification of AML according to FAB and WHO is crucial for clinicians to comprehend the morphological disparities in blast cells, helping them determine appropriate treatment and monitoring prognosis (66). Various subtypes respond differently to treatment, and some have better or worse prognoses compared to others (62).

1.4 A succinct description of the different AML treatment options

1.4.1 Chemotherapy

Chemotherapy, a medical approach involving the use of chemical substances, particularly cytotoxic drugs to destroy fast-growing cancer cells (67), is used in the treatment of AML. Currently, the standard of care for AML is seven days of cytarabine-based chemotherapy followed by three days of either daunorubicin or anthracyclines (68), and this is done to achieve complete remission (CR). This "7 + 3" regimen has remained unchanged since its first introduction in 1973 and it has yielded unsatisfactory results in many patients, and does not benefit older patients (69). As a result, the current research in this field is focused on developing new chemotherapeutics for AML and improving the usage of current regimens. Other drugs are being tested to improve the efficacy of standard chemotherapy drugs when used in combination therapy. Preclinical data now demonstrate that venetoclax has anti-leukemic effects in AML, as well as synergistic effects when combined with hypomethylating or chemotherapeutic agents (cytarabine) in the elderly with newly diagnosed AML (70). Fortunately, the US Food and Drug Administration (FDA) recently granted approval for the combined use of Venetoclax, in combination with azacitidine, decitabine, or low-dose cytarabine (LDAC), as a treatment option for newly-diagnosed AML in adults aged 75 years or older, or those who have underlying health conditions that make them ineligible for intensive induction chemotherapy (71). The efficacy of this treatment was confirmed through two randomized, double-blind, placebo-controlled trials. These trials clearly showcased a notable 30% rate of improvement in achieving complete remission (72). In contrast to these recent advancements, conventional chemotherapy is

generally cytotoxic to most cells, including healthy cells and this can lead to dose-limiting off-target effects and inherent drug resistance, which can result in inefficient eradication of leukemic blasts and their survival after remission (73). In other words, minimal residual disease is the term used to describe the small number of cancer cells that remain in the body after treatment and is the leading cause of recurrence. Therefore, more specific and efficient approaches are needed to eradicate malignant cells while sparing healthy cells as well as clearing the minimal residual disease which causes disease recurrence.

1.4.2 Bone Marrow transplantation

Bone marrow transplants are medical procedures where healthy blood-forming stem cells are introduced into the body to replace bone marrow stem cells that are no longer capable of producing enough healthy blood cells. Relapse after conventional chemotherapy remains a major problem in patients with myeloid malignancies such as AML, and the major cause of death after diagnosis of AML is from relapsed disease (74). The only potentially curative treatment option currently available is allogeneic hematopoietic stem cell transplantation (allo-HSCT), which through its graft-vs.-leukemia effects has the ability to eliminate residual leukemia cells. The use of bone marrow transplants in AML treatment dates back to 1956, when a medical breakthrough occurred in Cooperstown, New York, that changed the landscape of cancer treatment. It was there that, Dr. E. Donnall Thomas achieved the first successful bone marrow transplant, a procedure that has since become a critical tool in the fight against AML and other blood cancers (75). This remarkable breakthrough was achieved through bone marrow transplantation of healthy stem cells from an identical twin to another twin suffering from leukemia. Nowadays, bone marrow transplants are used in combination with chemotherapy (76). Healthcare professionals can now administer increased doses of chemotherapy medications to eradicate a higher number of cancerous cells. In conjunction, healthy stem cells are collected from the donor and transplanted into the patient's bone, allowing the healthy stem cells to repopulate the recipient's bone marrow. This process aids patients in recuperating from chemotherapy treatment (77). However,

despite the success of bone marrow transplants, relapse following allo-HSCT is still a major challenge and is associated with poor prognosis. Furthermore, there are several other limitations associated with this treatment including the availability of suitable donors, risks of complications associated comprising of graft-versus-host disease, stem cell (graft) failure, organ damage, infections, and development of new cancers (78).

1.4.3 Targeted therapy

1.4.3.1 Genetic targeted therapies

Genetic targeted therapies work by specifically inhibiting or modifying the activity of proteins or pathways changed in cancer cells due to genetic mutations. Recent advancements in next-generation sequencing have enabled a deeper understanding of the pathogenesis of acute myeloid leukemia (AML) (46), particularly the development of small molecules that target the disease at the molecular level (45).

FLT3 inhibitors

The FLT3 gene encodes a receptor tyrosine kinase (RTK) expressed on normal hematopoietic stem cells. RTK, upon binding to receptor-specific ligands, it activates the intracellular tyrosine kinase domain (TKD) and these processes require adenosine triphosphate (ATP) (79). Activation of TDK causes phosphorylation of downstream molecules, thereby activating signalling cascades that promote transcription of genes regulating survival, proliferation and differentiation of cells (79). When a mutation occurs in the FLT3 gene, it causes immature blood cells to multiply uncontrollably resulting in a more aggressive form of AML that is more likely to relapse after treatment and has a lower survival rate (47). As mentioned in section **1.3.2** above, these mutations are detected in approximately 30% of patients with AML and this has led to the development of new targeted therapies for this subgroup of patients (46). FLT3 inhibitors work by inhibiting or interacting with the ATP-binding site of the intracellular tyrosine kinase domain (TKD) and competitively block ATP binding. This mechanism

prevents receptor autophosphorylation and the activation of downstream signalling pathways thereby regulating proliferation of AML cells. In 2017, Midostaurin (Rydapt) became the first FDA drug approved for the treatment of adult patients with newly diagnosed FLT3-mutated AML (80), in combination with chemotherapy drugs such as cytarabine and daunorubicin (47). A year later in 2018, Gilteritinib became the second drug to receive approval from the FDA and is used to treat relapsed or refractory AML with FLT3 mutations (46) (81) . Recently, in July 2023 the FDA granted approval to quizartinib for the treatment of adult patients who have newly been diagnosed with acute myeloid leukemia (AML) characterized by the FLT3 internal tandem duplication (ITD) genetic mutation (82).

IDH inhibitors

Isocitrate dehydrogenase (IDH) enzymes IDH1 and IDH2 play a pivotal role in converting isocitrate into alpha-ketoglutarate as part of the tricarboxylic acid cycle as mentioned above **(1.3.2).** Alterations of specific amino acids at conserved sites result in abnormal enzymatic activity and the production of an oncometabolite known as 2-hydroxyglutarate (R-2-HG) (83). This metabolic shift triggers DNA hypermethylation, disrupts gene expression, promotes cell proliferation, and interferes with normal cell differentiation. Within the context of AML, approximately 20% of AML patients exhibit mutations in either IDH1 or IDH2 enzymes which contribute to the development and progression of AML (51) (84). In recent years, innovative therapies targeting mutant IDH have emerged as a promising avenue for treating AML patients with these mutations. IDH inhibitors function by obstructing the activity of mutant IDH proteins, causing leukemia cells to differentiate normally (84). In 2017, the FDA granted approval for enasidenib, a small molecule IDH2 inhibitor effective against IDH2 R140 and IDH2 R172 variants, for the treatment of relapsed or refractory AML(85) (86). A year later in 2018, ivosidenib was also approved to treat relapsed or refractory AML cases associated with IDH1 mutations (87) (88). Recently in December 2022, olutasidenib gained FDA approval for adult patients with relapsed or refractory AML harbouring susceptible IDH1 mutations, as confirmed by an FDA-approved diagnostic

test (89). This drug has been approved for the treatment of both treatment-naïve and relapsed or refractory AML cases.

BCL-2 inhibitors

B cell lymphoma 2 (BCL-2) family proteins play a crucial role in regulating apoptosis, a process involving both inhibitors and inducers of cell death (90). These proteins regulate and facilitate the intrinsic apoptosis pathway, in which mitochondria contribute to cell death (91). When BCL-2 mutations occur, it causes a significant increase in BCL-2 expression, these proteins block the cells from triggering apoptosis (92). When this happens, cancer cells do not self-destruct and as a result, they build up in the body. To address this challenge, specific inhibitors like venetoclax have emerged as promising therapeutic options, these drugs target BCL-2 proteins and attach to them resulting in restoration of apoptosis allowing cancerous cells to self-destruct (93). Initially, this drug was approved in April 2016 for the treatment of patients with chronic lymphocytic leukemia (CLL) who have a chromosomal abnormality called 17p deletion and who have been treated with at least one prior therapy (94). Subsequently, it received accelerated approval in 2018 for its use in acute myeloid leukemia (AML), with full approval granted in 2021 (71).

Hedgehog (Hh) pathway inhibitors

The Hedgehog (Hh) pathway is a crucial signalling pathway involved in normal embryonic development that also plays an important role in adult tissue maintenance, renewal, and regeneration (95). In this pathway, binding specific ligands to the transmembrane receptor patched (PTCH1) promotes activation of the transcriptional regulators GL11, GL12 and regulation of gene expression via SMO-mediated signalling (96). The Smoothened (SMO) receptor has been implicated in several aspects of AML stem cell development, maintenance, and growth. As a result, various Hh pathway inhibitors have been developed targeting the SMO receptor, a transmembrane protein crucial for Hh signal transduction, influencing both cellular differentiation and cancer growth (97). Glasdegib was approved by the FDA in November 2018 for the treatment of newly diagnosed AML patients 75 years

of age or older and those with comorbidities that exclude them from undertaking aggressive induction chemotherapy (98).

1.4.3.2 Immunotherapy

Immunotherapy, which is defined as the manipulation of human immune system components to selectively target diseased cells, represents a highly promising approach within the realm of precision medicine (99). Over the past decade, it has transitioned from a hopeful concept to a robust clinical reality. Notably, many immunotherapeutic methods have gained approval from the FDA for the treatment of cancer patients, while others are currently in the pipeline for approval either as standalone therapies or in combination with standard treatments (100). Cancer immunotherapy can be broadly categorized into two main types of interventions: passive and active, based on their underlying mechanisms. Passive immunotherapy involves the administration of ex vivo-generated immune elements including monoclonal antibodies. While active immunotherapy aims to stimulate the host's immune system or a specific immune response to a disease (101). This includes the administration of cancer vaccines, chimeric antigen receptor T-cell (CAR-T) therapy, checkpoint inhibitors, peptide-based therapies, and natural killer cell therapies (102).

Passive Immunotherapy

The first FDA approved therapeutic antibody was muromonab-CD3 (Orthoclone OKT3) in 1986 (103) (104). This comprises of a naked murine mAb against T cell expressed CD3 that functions as an immunosuppressant for the treatment of acute transplant rejection (105). Naked antibodies operate without directly delivering potent cytotoxic drugs, instead they function through binding to specific antigens on the cell, blocking a particular signalling pathway, triggering the immune system or recruiting immune cells to combat diseased cells (104). Whereas, antibody drug conjugates (ADCs) are bifunctional molecules combing the monoclonal antibody targeting specific antigens on diseased cells with a cytotoxic drug with a cell killing ability (105). To date, more than 100 mAbs have been

approved since 1985, and new additions are regularly approved for the treatment of cancer and immunological diseases (106). These new drugs have been approved because of the development of promising new treatments resulting from a better understanding of disease pathophysiology and heterogeneity. In comparison to conventional chemotherapeutic bioactive compounds, the use of antibody drug conjugates has benefits including increased cell-killing potential, higher tumour selectivity, improved drug tolerability, and limited systemic exposure (107) (108).

The FDA approved gemtuzumab ozogamicin (Mylotarg) in May 2000 for CD33-positive patients with relapsed AML and older patients 60 years of age or older who were not candidates for conventional chemotherapy (109). Mylotarg is a humanised anti-CD33 monoclonal antibody covalently conjugated to a semisynthetic component of calicheamicin, a potent cytotoxic antibiotic agent that blocks the growth of cancerous cells and causes cell death (110). In 2010, it was voluntarily withdrawn from the market following the Southwest Oncology Group (SWOG) S0106 phase III trial which yielded disappointing results, indicating that there was no additional benefit to combining gemtuzumab ozogamicin with chemotherapy compared to chemotherapy alone. Moreover, the trial revealed an increase in treatment-related mortality associated with the combined therapy (111). Based on this data and other unfavorable results from phase III studies, Pfizer decided to voluntarily withdraw gemtuzumab ozogamicin from the market in 2010, a decade after it was originally approved (112). Gemtuzumab ozogamicin was granted reapproval by the FDA in September 2017 for treating adults with newly diagnosed CD33-positive AML, as well as for relapsed or refractory CD33-positive AML in patients aged 2 years and above (113). The FDA specifically mentioned changes to the dosing regimen that improved the safety and efficacy of gemtuzumab ozogamicin and led to its reapproval.

Current research is focusing on different markers upregulated on AML cells including the pan-leukocyte antigen CD45 and the glycoprotein CD66, as potential unique targets against for AML treatment (114) (115). Despite its potential, the current ADC technology has several limitations. One such limitation is the stoichiometrically undefined chemical linkage of the cytotoxic payload, which

can affect the efficacy and specificity of the ADC. Another limitation is the potential immunogenicity of toxins derived from bacteria and plants, which can limit their clinical utility (116). SNAP-tag antibody fusion proteins offer a promising alternative approach by enabling the production of homogeneous, recombinant ADC products and next-generation recombinant fusion proteins that have reduced immunogenicity. This innovative technology offers a potential solution to some of the limitations associated with current ADC technology (117).

Active Immunotherapy

Checkpoint inhibitors using monoclonal antibodies to block immune checkpoints have proven to be highly effective in AML immunotherapy targeting the bone marrow microenvironment (118). These antibodies act to block inhibitory receptors on the surface of T cells and other cells of the immune system (119). Notably, immune checkpoint inhibitors like Programmed Death-ligand 1 (PD-1/PD-L1) and Cytotoxic T-Lymphocyte Antigen 4 (CTLA-4) inhibitors have demonstrated safety and efficacy across various cancer types, earning approvals from regulatory authorities for use in solid tumours and certain lymphoid malignancies (120). It's worth emphasizing that PD-1 inhibitors, including drugs like pidilizumab, nivolumab, pembrolizumab, durvalumab, and atezolizumab, have seen extensive development and application in AML patients (121). Additionally, CTLA-4 inhibitors such as ipilimumab have shown promise, particularly in high-risk AML and patients with myelodysplastic syndromes (MDS), including those that have relapsed after allogenic-hematopoietic stem cell transplants (122). Furthermore, ongoing research is exploring new T-cell checkpoints like TIM-3, LAG-3, and the CD47 macrophage checkpoint in AML patients. These investigations aim to uncover additional avenues for enhancing the immune response against AML (123).

In the field of adoptive therapy, chimeric antigen receptor (CAR) T cells that target CD19 have shown remarkable success in treating certain B-cell malignancies. Extensive efforts are underway to extend this success to myeloid malignancies. The first clinical trial demonstrating CAR T cell activity in AML used second-generation CD28-CAR T cells targeting the Lewis Y antigen (124). While the trial

showed limited efficacy, it was significant because it established CAR T cell biological activity in AML patients without causing significant harm to healthy blood-forming tissues. Substantially, CAR T cell therapy has emerged as a powerful tool in the arsenal of immunotherapy and is currently undergoing clinical testing for AML. Currently, there are over twenty CAR T cell clinical trials actively enrolling AML patients and these trials are primarily focusing on targeting CLL-1, CD33, or CD123 (74). The CD33 and CD123 antigens are attractive targets due to their high upregulation on AML blast cells, although they are also present at lower quantities on normal hematopoietic stem and progenitor cells (HSPCs) (125). Nevertheless, this method faces certain limitations primarily based on the absence of leukemia-specific antigens that would allow CAR T cells to unleash their full therapeutic potential. Many AML antigens are commonly expressed on both leukemia cells and normal HSPCs.

1.5 Diagnosis

The diagnosis of acute leukemia cases is made through clinical features, hematological investigations like the full blood count, meticulous peripheral blood film review and bone marrow aspiration smears examination (125). Although the clinical appearance of AML differs from person to person, there are some shared signs and symptoms including anemia which is caused by a decrease in normal blood cell synthesis. This renders AML patients to be more prone to fatigue, weakness, and shortness of breath (126). Infections and recurrent fevers are particularly common in individuals with AML because their immune systems are weakened. AML also disrupts the normal synthesis of platelets which aid in blood clotting, increasing the likelihood of bruising and bleeding. This might result in easy bruising, prolonged bleeding from injuries, and nosebleeds on a regular basis (127). These symptoms collectively help clinicians in diagnosis of AML and determining the specific characteristics of the disease.

AML requires timely diagnosis for effective treatment and in high-income countries, acute leukemia survival rates have improved dramatically over the last few decades (128). Unfortunately, most African countries (low-income countries) lack up-to-date statistics on the prevalence of various leukemia subtypes. As a result, treatment outcomes remains poor due to poor registry, misdiagnosis and interpretation, therapy related mortalities and therapy neglection (129) (130) (61). Namazzi and colleagues demonstrated in their work on enhancing the diagnosis and treatment of acute leukemia that in order to achieve the best results, it is essential to have access to biological data and be able to diagnose patients quickly and accurately (128). Many AML patients in Africa face significant difficulties in getting good healthcare facilities and diagnosis is delayed which leads to unfavorable treatment outcomes compared to developed countries (131) (132). At this point, there is a need for improvement in AML diagnosis and the most commonly used diagnosis methods for AML include leukemic cell or blast morphology, molecular genetic testing, and immunophenotyping by confocal microscopy and flow cytometry.

1.5.1 Leukemic cell or blast morphology

This method employs morphological classification of leukemia cells by identification of specific cellular features, such as cell size, shape, and the presence or absence of granules to make a diagnosis (133). As well as, determining the type of leukemia by looking at the traits of the cell line and figuring out its stage of differentiation (61), adhering to the 1976 agreement that produced the FAB classification **(Table 1)**. This method has significant drawbacks in providing accurate and timely diagnosis and is mostly used in low and middle-income countries, particularly Africa. Although, morphology may be useful in identifying leukemia subtypes and describing how these affect the prognosis of the patient. Small numbers of leukemia cells in the disease's early stages or blast cells that remain in the bone marrow after treatment cannot be identified using this diagnostic technique. In other words, minimal residual disease (MRD) refers to the small number of cancerous or leukemic cells that remain in the bone marrow but are not detectable by standard morphological (134) (135).

Hence, there is still a need for more sensitive approaches to accurate and timely diagnose AML in low and middle income countries for improved treatment outcomes.

1.5.2 Molecular genetic testing

The identification of specific genetic abnormalities associated with AML is a crucial part of the diagnostic process of the disease (136). There are several types of molecular genetic tests used in AML diagnosis including chromosomal analysis, which involves examining the chromosomes in AML cells to identify any mutations in the form of translocations, inversions, and deletions (137). Adding to that, fluorescence in situ hybridization (FISH) can also be utilized in AML diagnosis and by using fluorescent probes, detection of specific genetic abnormalities in AML cells becomes feasible (138). Furthermore, next-generation sequencing (NGS) has also been a powerful tool in sequencing the entire genome or specific genes in AML cells and identifying mutations in genes that are associated with AML, such as DNMT3A and IDH1 (139). Lastly, real-time polymerase chain reaction (PCR) techniques have shown to be more sensitive compared to cytogenetic techniques like karyotyping or FISH, which are insufficiently sensitive for monitoring minimal residual disease (MRD) (140). This method can be used to detect mutations in genes that are associated with the disease, such as NPM1 and FLT3 (141). For AML patients, molecular genetic testing is very important and can guide clinicians on treatment choices and predict a patient's prognosis since they know that certain genetic abnormalities are usually associated with poor prognosis (142).

1.5.3 Immunophenotyping

In recent years, technological advancements in immunophenotyping have allowed successful development of monoclonal antibodies for selective identification of diseased cell populations including tumour cells in cancer patients (143). This novel idea entails the discovery of a surface membrane antigen or protein that is highly specific or overexpressed on diseased cells. It also includes the use of antibody derivatives that recognize and bind to the identified surface membrane antigen or

protein for targeting diseased cells. Selective identification of diseased cell populations is feasible when immunoconjugates are attached to the specific moiety (73) (144) (145) (146) (147) (148). Immunophenotyping is useful for categorising various leukaemia subtypes based on the distinct proteins that are upregulated on the surface of the diseased cells, and this can be done by using confocal imaging or flow cytometry.

1.5.3.1 AML Immunophenotyping by confocal microscopy

Immunophenotyping by confocal microscopy is a specialised method that enables examination of cells at a high resolution and allows identification of different markers upregulated in AML cells and over the years it has shown to be an effective diagnostic approach (149). Confocal imaging utilises a laser light source which excites fluorescent molecules conjugated to monoclonal antibodies, causing them to emit light, by directing a laser beam at a particular area on the specimen. It also contains a pinhole located in front of the detector which excludes out-of-focus light and detects only light emitted from the focal point. As a result, the high-contrast images produced for this imaging lacks background noise or optical aberrations which is a most common issue associated with the conventional microscopy (150). Immunophenotyping of AML cells by confocal microscopy has remained a reliable technique providing adequate information in diagnosis of haematological malignancies.

1.5.3.2 AML immunophenotyping by flow cytometry

The use of advanced technologies like flow-cytometric immunophenotyping allows clinicians to clearly define each subtype of acute leukemia and reveal the rare biphenotypic and bilineage of acute leukemia (151). Flow cytometry is a helpful tool for analyzing cell maturation phases, differentiation pathways and unusual features which are relevant for the diagnosis of hematological cancers. Using fluorescently labelled antibodies, flow cytometry can identify and quantify specific intracellular and or surface markers, revealing clinically relevant information about the composition of cell populations in a sample (152) (153). The detection of hematological cancers can be aided by the identification of

abnormal cell populations and the monitoring of modifications in cell differentiation and maturation, using flow cytometry we can recognize a single leukemic cell amongst 10000 normal cells (0.01%) (154). At this time, detection of minimal residual disease (MRD) through immunophenotypic analysis is performed by defining abnormal expressions of certain markers denoted as Leukemia-Associated Phenotypes (LAPs) (134). This type of diagnosis would also help in identification of patients that are likely to benefit from emerging targeted immunotherapeutics.

Table 3. Summary of the current AML diagnostic methods, benefits, and limitations

Method	Advantages	Limitations
Bone marrow aspiration and biopsy:	The most definitive diagnostic test for AML. Provides samples of bone marrow cells, that can be analysed under a microscope to look for abnormal cells. It Can also be used to measure the number of blasts in the bone marrow and to collect cells for further testing, such as flow cytometry.	Invasive surgery might cause pain and discomfort. Complications such as bleeding or infection may occur. This method has limitations in making accurate and timely diagnosis (155) (156).
Cytogenetic analysis:	Can identify changes in the chromosomes of AML cells. These changes can help to determine the prognosis of the leukemia and to select the best treatment.	Can be difficult to interpret. Not all labs have the expertise to perform cytogenetic analysis (137) (157).
Fluorescence in situ hybridization:	A molecular test that can detect specific genetic changes in AML cells. This can be used to confirm the diagnosis of AML and to identify specific subtypes of the leukemia.	Can be expensive and time-consuming. Not all labs have the necessary equipment to perform FISH (138)[128] .
Molecular testing:	Can identify genetic changes that are associated with AML. This can be used to predict the risk of relapse and to select targeted therapies.	Can be expensive and time-consuming. (158).
Immunophenotyping by confocal microscopy:	It allows for high-resolution imaging of leukemia cells, providing detailed information about their surface markers and spatial distribution. This aids in precise subtyping and identifying minimal residual disease.	Confocal microscopy is time-consuming and the antibodies used for staining are expensive (149).
Immunophenotyping by Flow cytometry:	Can identify and quantify different types of cells in the blood and bone marrow. This can be used to distinguish between AML and other types of leukemia, as well as to identify specific subtypes of AML.	Can be expensive and not all labs have the necessary equipment to perform flow cytometry (128) (151).

Methods used to diagnose AML can vary depending on the patient and the resources available. Some methods are less sensitive than others, and some are more expensive. Immunophenotyping using fluorescently tagged antibodies is a sensitive method, but it is also expensive (159). Therefore, there is a need to develop new immunodiagnostic methods that are both cost-effective and sensitive for the diagnosis of AML.

1.6 Biomarkers for immuno-diagnosis of AML

In cancer cells, a number of biomarkers may be upregulated or overexpressed, and the identification of these biomarkers may have diagnostic, prognostic, or therapeutic effect (160) (161). Based on where they are found, these biomarkers may be divided into two groups which are: cell surface antigens and intracellular antigens. Cell surface antigens are often used for both therapeutic and diagnostic applications (160). Antibodies conjugated to fluorophores attach to these surface antigens, making it possible to identify and detect cancer cells. AML cell surface biomarkers include CD34, CD33, CD13, CD117, CD14, CD89, CD32, CD45 CD123 and HLA-DR as shown on **Table 1** (162) (163) (161). Alternatively, intracellular antigens can also be employed for the diagnosis of AML. These biomarkers can be found within cancer cells and the enzyme myeloperoxidase (MPO), which is produced by AML cells, is an example of an intracellular antigen utilized in AML detection (164) (165). Above all, it is important to note that various subtypes of AML and individual patients might exhibit variable levels of these biomarkers' expression. CD14, MPO and HLA-DR are used in AML diagnosis due to their relevance and effectiveness in detecting and characterizing acute myeloid leukemia cells (166) (167) (168). These biomarkers are included in the diagnostic panel because they provide valuable information about the phenotypic and differentiation state of AML cells. These combinations as well as other relevant biomarkers, assist hematologists in effectively diagnosing AML patients.

1.6.1 Human leukocyte antigen-Dr (HLA-DR)

In cases where the diagnosis is unclear based on additional clinical and laboratory findings, HLA-DR expression can be used as a diagnostic marker for acute leukemia. HLA-DR is a member of the major histocompatibility complex (MHC) Class II molecules and is composed of an alpha and beta chain heterodimer, which binds to peptides inside the cell and transports them to the cell surface for presentation (169) (170). This is a cell surface receptor that is expressed on B cells and dendritic cells. The differential expression of HLA-DR in AML has diagnostic and prognostic implications. High HLA-DR expression is associated with better prognosis, while low HLA-DR expression is linked to poor prognosis (171). This is supported by the 2017 and 2022 ELN (European LeukemiaNet) recommendations from an international expert panel, which both state that HLA-DR is a precursor marker for AML diagnosis (172) (173). This supports the use of HLA-DR as a biomarker for the diagnosis and prognosis of AML. This marker has also been pursued for antibody-based immunotherapy in a number of hematologic and solid tumours due to the fact that, it is expressed on a variety of these tumour types. However, there are safety concerns with this approach because the antigen is expressed on normal cells (174) (175). Several methods, including flow cytometry and immunohistochemistry can be used to detect the presence of HLA-DR on cells and flow-cytometry is widely used since it allows for the rapid and sensitive analysis of large numbers of cells (176) (177) . The clinical implications of HLA-DR overexpression in leukemia remain unclear. Several AML subtypes have been reported to express HLA-DR at varying levels, with the M3 subtype having the lowest levels of HLA-DR expression in comparison to other AML subtypes (168) (171). The reduced expression of HLA-DR in these cases may further contribute to the poor prognosis by impairing the immune system's ability to recognize and eliminate the cancer cells (178). The M5 subtype of AML, on the other hand, is known to have HLA-DR overexpression, which increases immune response against leukemia cells and may lead to better outcomes for patients because the immune system may

be better able to recognize and eliminate leukemia cells. More research is needed to fully comprehend the role of HLA-DR overexpression in leukemia and its clinical implications (162).

1.6.2 Cluster of differentiation antigen 14 (CD14)

CD14 is a glycoprotein found on the surface of myeloid cells such as monocytes, macrophages, and granulocytes that plays a role in innate immune responses. It exists as both membrane-bound CD14 (mCD14), which is glycosylphosphatidylinositol (GPI)-anchored and shredded soluble CD14 (sCD14), which lacks the glycosylphosphatidylinositol anchor but has the same amino acid sequence as mCD14 (179). In response to bacterial LPS, membrane-bound CD14 (mCD14) acts as a co-receptor for Toll-like receptor 4 (TLR4). When LPS binds to mCD14, it triggers an immune response by activating a signaling cascade that results in the generation of inflammatory cytokines (180). Soluble CD14 (sCD14) is found in blood as well as other bodily fluids such as cerebrospinal fluid and breast milk (181). Proteolytic cleavage by enzyme Phospholipase C on mCD14 releases sCD14 into the extracellular space where it circulates in the blood performing its immunoregulatory functions. sCD14 binds to LPS and other bacterial components, rendering them inactive and preventing them from interacting with mCD14, this aids in the regulation of the immune response and the reduction of excessive inflammation (182). CD14 is highly expressed in acute myelomonocytic leukemia (AML-M4) subtype and acute monocytic leukemia (AML-M5) subtype and therefore it is used to distinguish between monocytic AML and non-monocytic AML (AML-M0 to AML-M3) (183). The identification of CD14 differential expression on AML cells can be done by flow cytometry and confocal imaging using fluorescently tagged antibodies.

1.6.3 Myeloperoxidase (MPO)

During the myeloblast stage of myeloid cell differentiation, the glycoprotein known as myeloperoxidase (MPO) manifests itself in the azurophil (primary) granules of myeloid cells (184). This enzyme belongs to the peroxidase family and is abundant in immune cells including macrophages,

neutrophils and on the other hand, it is not expressed in lymphoid cells (185). Myeloperoxidase (MPO) is the hallmark enzyme of the myeloid lineage. The presence of MPO in the blood or bone marrow can be used to diagnose AML and distinguish it from other forms of leukemia. According to the French-American-British (FAB) classification of AML, the presence of > 3% MPO-containing blasts is considered a positivity for AML, although most blast cells are MPO negative in M0, M5, and M7 (62) (165). The highest levels of MPO are seen in the M3 subtype and the M1 subtype, whereas the M2 subtype shows low MPO expression. This disparity arises from the different lineages of cells that give rise to M1 and M2 subtypes of AML (186). The M1 subtype is thought to originate from early myeloid progenitors, while M2 AML arises from more mature myeloid progenitors (167). The differential expression of MPO in AML has diagnostic and prognostic implications. A few studies have previously shown the prognostic significance of MPO in AML and low expression levels of MPO are associated with poor prognosis (187) (188). Likewise, intracellular MPO can be detected through flow cytometry and confocal imaging, employing fluorescently labelled antibodies after cell permeabilization, which eliminates additional cellular membrane lipids, enabling larger molecules such as antibodies to penetrate the cell (189).

1.7 Structure and diversity of antibodies

Antibodies are proteins produced by the immune system in response to the presence of foreign antigens. These proteins are produced by B lymphocytes and consist of two identical light chains and two identical heavy chains (190). Antibodies have a very diversified structure, with specific antigen-binding sites or paratopes that recognise and bind to unique molecular structures on the surface of pathogens (epitopes) (191). These molecules are divided into three functional domains: The first two are antigen-binding domains (Fab) that are linked by a very flexible hinge domain as shown in **Figure 3**. The variable region of the antibody contains the complementarity determining regions (CDRs) and the framework regions (FRs) (192). The FRs plays a pivotal role in scaffolding and maintaining the overall structure of the variable domains whereas, the CDRs contribute to antigen recognition (193).

Both the heavy and light chains of antibodies variable domains consisting of three complementarity-determining regions (CDRs), denoted as CDR1 CDR2 and CDR3 and among these CDRs, CDR3 exhibits the highest degree of variability contributing to antibody specificity (194) (195). The key mechanism that produces antibody diversity is through the recombination of V(D)J genes, a process in which T cells and B cells randomly assemble different gene segments known as variable (V), diversity (D), and joining (J) segments (196) (197). This process generates unique receptors that recognize and bind to different antigens which results in the creation of a functional coding sequence for either the variable light (by joining their V and J gene segments) or the variable heavy region (by joining the V, D, and J gene segments) of the antibody (197). (198) (196). The third domain is the antibody's fragment crystallizable (Fc) domain, which can interact with various cell receptors as well as components of the complement system (193) (199). This allows the antibody to perform its effector functions for example exerting antitumour effects through a variety of mechanisms, including apoptosis and antibody-dependent cellular death (200).

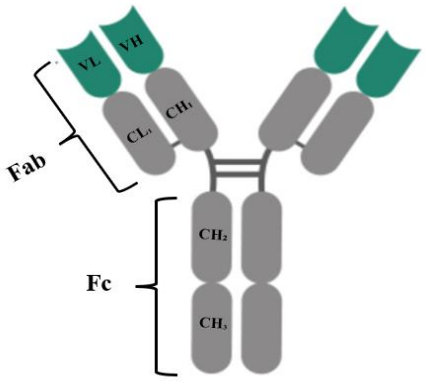

Figure 3. Antibody molecular structure. The heavy and light chains in antibodies are both identical and are joined by disulfide bonds. These two heavy and light chains, respectively, contain the fragment binding region (Fab) and the constant region (Fc). The Fab region contains the variable heavy and light domains, which make up an antibody's binding parts. Additionally, the variable domains VH and VL contain complementary determining regions (CDRs) that contain the antigen-binding residues as well as the framework regions that surround the CDRs to enable proper protein folding and expose the antigen-binding residues to the epitope. They also contain a constant domain that controls the biological functions of the antibody. Adapted from Biteghe *et al*. 2020 and created using BioRender (200).

Building upon the binding abilities and specificity of antibodies in our immune system, scientists have developed diagnostic and therapeutic monoclonal antibodies, which are synthetic molecules that bind and target disease specific intracellular markers or cell surface antigens on diseased cells (192). Most FDA approved mAbs belong to the immunoglobulin G (IgG) isotype or class (193). This classification is differentiated by the heavy chain constant region of the antibody, which in turn determines its effector functions. There are five different antibody isotypes including IgM, IgA, IgE, IgD and IgG. The IgG isotypes have a molecular weight of 150 kDa with two identical heavy and light chains joined by disulfide bonds (194) (195).

1.7.1 Development of monoclonal antibodies

The birth of monoclonal antibodies (mAbs) developments dates back to the 1970s, with Georges Köhler and César Milstein receiving much credit on their invention of the traditional mouse hybridoma technique (201). This innovation involved selecting B-cells that produce antibodies. These B-cells were isolated from mice that were immunized with a specific antigen. Since these B-cells are short lived, they were fused with immortal myeloma cell lines to create hybrid cells known as hybridoma cell lines, which continuously produce specific monoclonal antibodies (202). By using this as a stepping stone, new techniques emerged including the single B cell technique, phage display and use of transgenic mice as illustrated in **Figure 6** (104) (202).

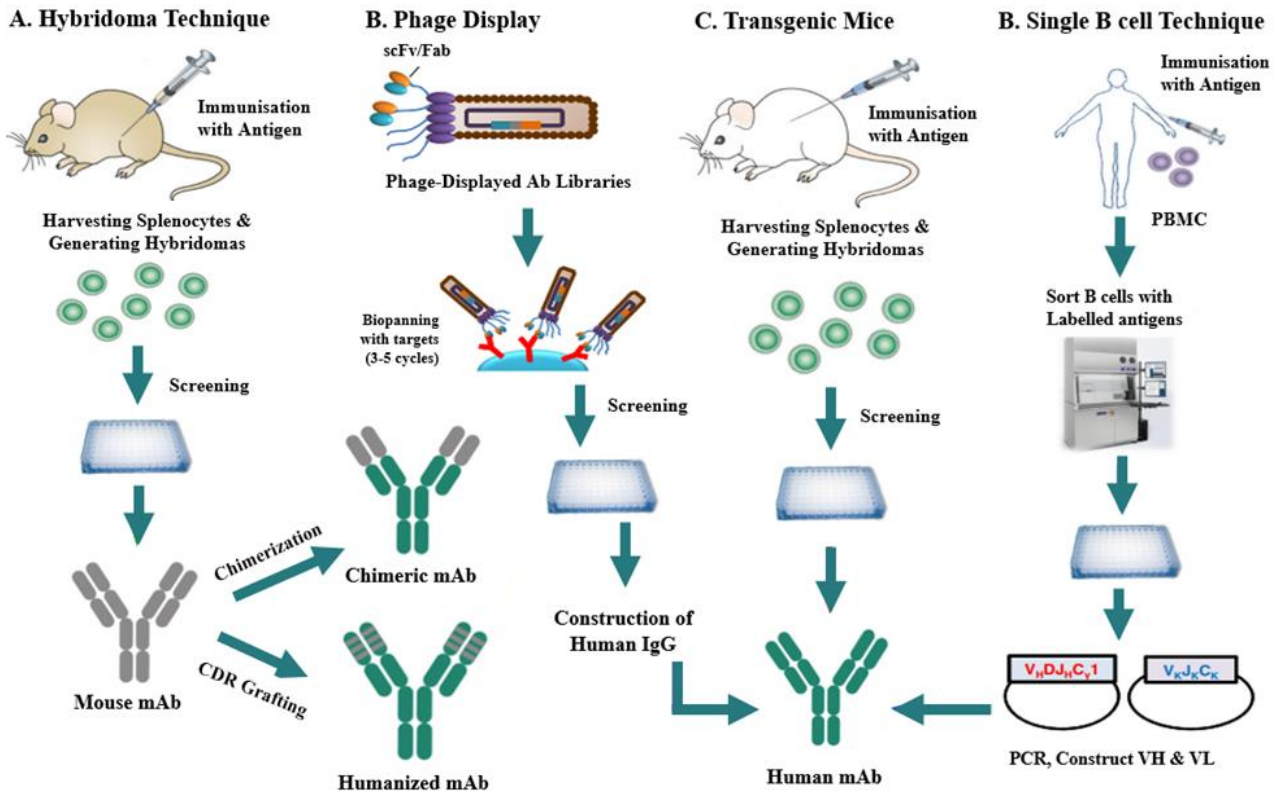

Figure 4. Techniques for developing monoclonal antibodies. **(A)** The mouse hybridoma technique, which starts with injecting mice with the antigen of interest to initiate an immune response. Following that, splenocytes are harvested and fused with myeloma cells to develop hybridoma cells that secrete antibodies of interest. After screening, selected mouse antibodies are used to create chimeric or humanised antibodies. **(B)** The phage display technique which is used to isolate human-derived monoclonal antibodies from a large repertoire of immunoglobulin (Ig) genes. It entails screening libraries for peptides or proteins that bind to a target of interest, as well as genetic fusion of a library of peptides to a bacteriophage coat protein, allowing for the selection of binders through successive rounds of selection and amplification. **(C)** The use of transgenic mouse, which involves inserting human immunoglobulin loci into the germline of mice to generate transgenic mice that produce fully human antibodies. **(D)** The single B cell technique is a powerful method that relies on the direct amplification of VH and VL region encoding genes from single human B cells. It begins by isolating B-cells from an animal immunised with a specific antigen, then fusing the B-cells with myeloma cells to create hybridoma cells, which can produce identical monoclonal antibodies specific to the antigen. The image was adapted from Ruei-Min *et al.* 2020 (104).

1.7.2 Engineered antibody formats

Antibody technologies encompass a wide range of techniques and methods for creating and manipulating antibodies. When combined with protein engineering, it has resulted in derivatives that allow for optimization of affinity, tumour penetration, and internalisation of the antibody-based

moiety while retaining mAbs specificity (203). Reduced size is thought to improve tumour penetration (204), leading to the development of various smaller antibody derivatives that maintain their specific affinity, including the most commonly used formats such as the antigen-binding fragment (Fab), crystallizable fragment (Fc), and single-chain variable fragment (scFv) as shown in **Figure 5** (205) (206).

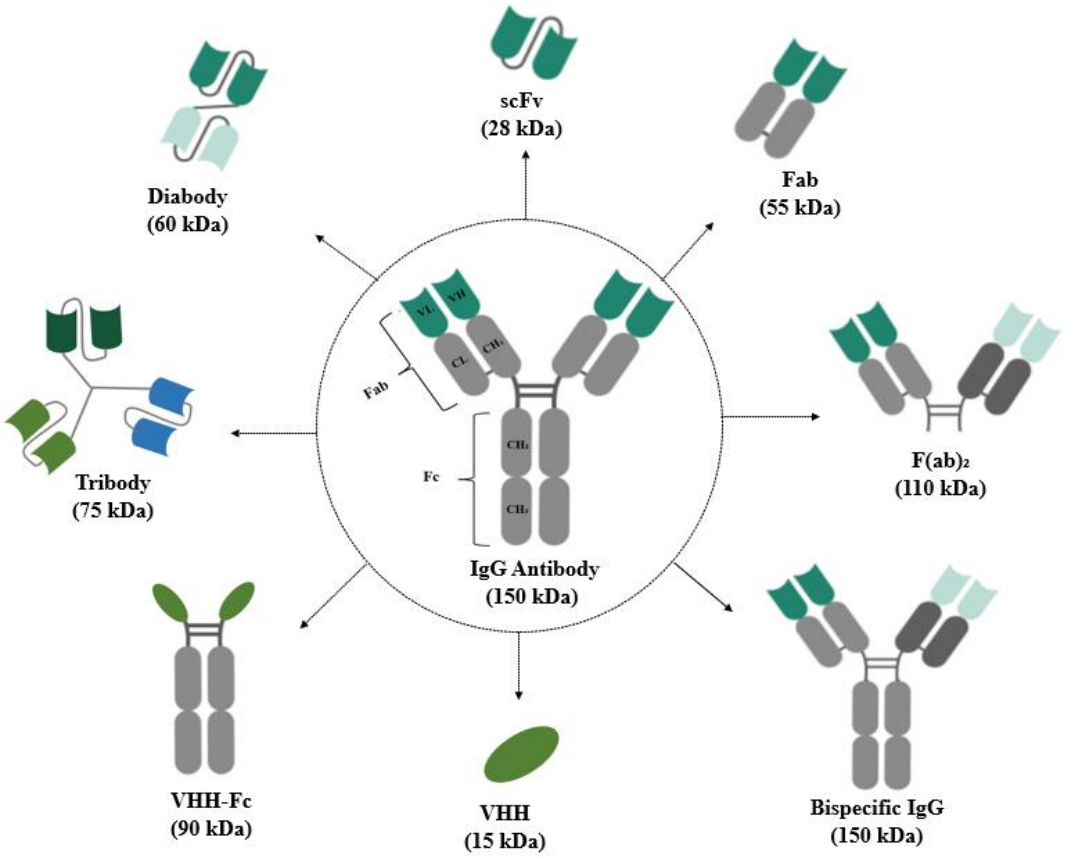

Figure 5. Schematic diagram showing the structure of the IgG molecule and the various antibody formats constructed. The scFv is formed by joining the variable heavy and light chains with a flexible short peptide linker. A diabody fragment is formed by joining two different single chain variable fragments by a short peptide linker and the tribody fragment is also formed by joining three separate single chain variable fragments. The Fab fragment contains the variable domains of an antibody but lacks the Fc region which is responsible for the antibody's effector functions. The $F(ab)_2$ contains two Fab fragments of an antibody joined together with disulphide bonds. A bispecific IgG antibody is an engineered format that has two different antigen binding sites and simultaneously binds to separate antigens. VHH are derived from heavy chain only antibodies and is approximately one-tenth the size of a conventional antibody and VHH-Fc is an engineered format that combines the two variable heavy chains of a nanobody joined to a human Fc domain for certain effector functions. The image was adapted from Jin *et al.* 2022 and altered using BioRender (206).

1.7.3 Engineered antibodies for therapeutic application

The first therapeutic applications of monoclonal antibodies utilized mouse-derived antibodies. While early studies with these monoclonal antibodies yielded remarkable results (207), immunogenicity (neutralisation by the body's natural immune response) limited the dosages of therapies that could be administered in a safe way (208). To overcome these limitations, researchers have utilized molecular engineering and humanization techniques to develop chimeric, humanized and fully human antibodies. These methods involve modifying the structure of antibodies to make them less immunogenic and more compatible with the human immune system **(Figure 6)** (209).

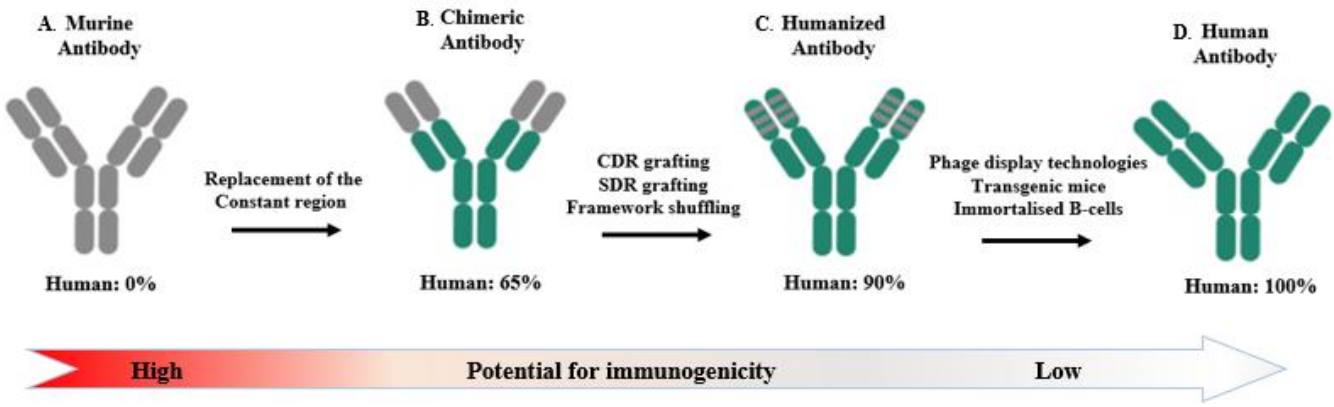

Figure 6. Developing chimeric, humanised derived from murine antibodies and fully human antibodies. (A) The grey parental murine monoclonal antibody with the variable and constant regions from mouse origins. **(B)** A chimeric monoclonal antibody with a variable region from mouse origins (grey) and a constant region of human origin in place of the murine constant region (blue). This was done by replacing the mouse constant region with the human constant region through the process of chimerization. **(C)** Humanized monoclonal antibody: merely the CDRs are of mouse origin, while the framework and constant regions are of human origin. This was done by incorporating the mouse CDRs into the human antibody scaffold by CDR grafting and SDR grafting. **(D)** Human monoclonal antibody: Fully human antibody produced by phage display, transgenic mice, or immortalised B-cells. The image was adapted from Shepard *et al*. 2017 and modified using BioRender (210).

1.7.4 SNAP-tag technology as a novel approach for generating fluorescently tagged antibodies

SNAP-tag is an engineered mutant of 06-alkylguanine-DNA alkyltransferase (AGT) that specifically, rapidly, and irreversibly reacts with 06-benzylguanine (BG) derivatives by transferring the benzyl moiety to its active site through a nucleophilic substitution reaction with release of the free guanine as shown in **Figure 7** (211). This reaction occurs via the BG irreversible alkyl group transfer to a cysteine residue at position 145 on the SNAP-tag (211). This is the same cysteine residue that AGT uses to catalyse alkylated DNA repair (117) (212). Benzylguanine is structurally identical to guanine, one of the four nucleotides that make DNA. It nevertheless happens to have a benzyl group attached to it, making it more reactive than guanine (117). SNAP-tag exhibits increased catalytic reactivity to BG-modified substrates, reduced binding to DNA, fewer amino acid residues and improved folding under oxidative conditions (213). SNAP-tag reacts with BG modified substrates in a 1:1 stoichiometry, which means that, each SNAP-tag protein may attach to one BG substrate molecule (117) (214).

SNAP-tag was later further modified to SNAPf a faster labelling variant, when compared to the original SNAP-tag, SNAPf has considerably higher reactivity to BG substrates. This increase in reactivity enables more efficient and quick protein labelling using BG-modified substrates (215) (214). The SNAP-tag can be used as an efficient tool for the site-specific labelling of recombinant antibody fragments (213).

The potential applications of antibody SNAP-tag fusion proteins include in vitro cellular imaging, the investigation of protein functionality, live-animal imaging, single-molecule tracking, and the analysis of protein-protein interactions using commercially available BG-modified fluorophores (216). In recent years, SNAP-tag proteins have been genetically fused to ligands and recombinant antibodies including scFvs that specifically bind or target tumours associated antigens (217) (218). These studies have shown that SNAP-tag fusion proteins can be expressed effectively in mammalian systems while maintaining their capability to bind to their specific antigens. Specificity, folding stability, and binding

affinity are all parameters that contribute to the diagnostic value of antibody fragments (117) (219). The ability to visualise binding with SNAP-tag-based antibody fusion proteins labelled with BG-modified fluorophores offers a promising approach for AML diagnosis.

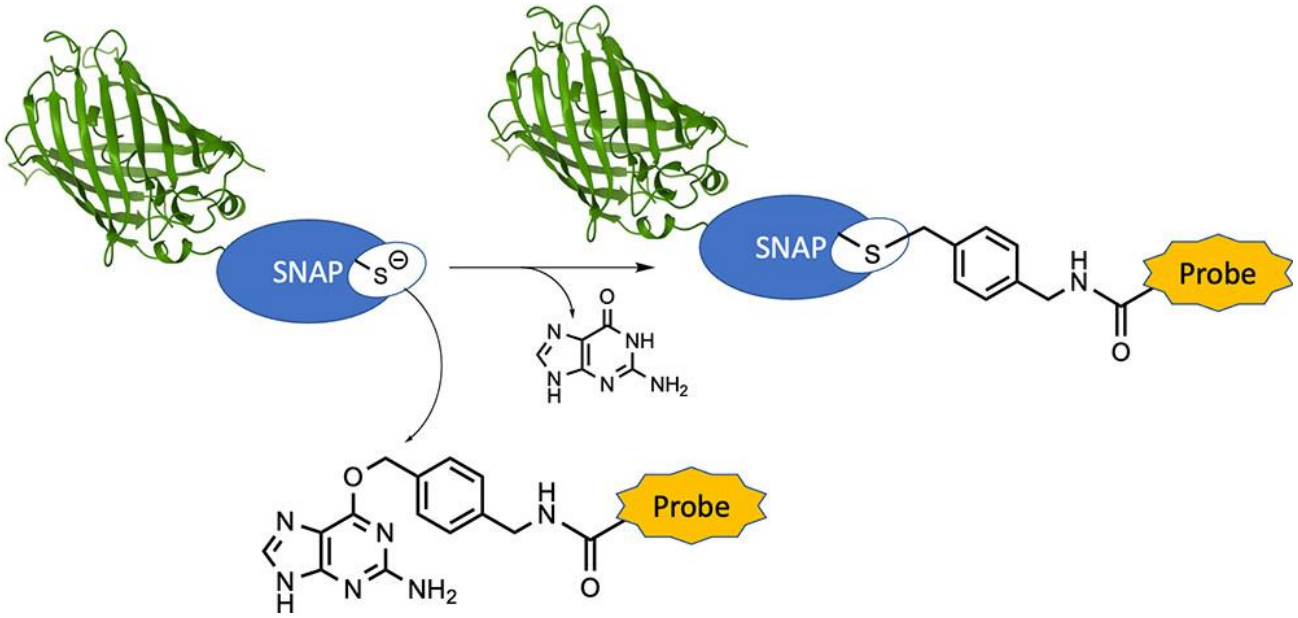

Figure 7. Schematic of SNAP-tag fusion proteins conjugated to O6 -benzylguanine (BG) modified fluorophores. When BG is incorporated into a solution containing SNAP-tag proteins, it triggers a nucleophilic substitution process with the SNAP-tag, involving a cysteine residue. The cysteine residue of the SNAP-tag attaches to the benzyl group of the benzyl guanine molecule, forming a covalent bond between the two molecules. As this covalent bond is stable and irreversible, the SNAP-tag and benzyl guanine cannot be separated after they have reacted. Adapted from Dreyer *et al*. 2023 (211).

1.8 Aims and objectives

Aute myeloid leukemia is a malignant blood disorder that arises due to genetic abnormalities in the bone marrow or lymphoid organs. It is categorized into various subtypes by the FAB and WHO classification systems, which consider the morphologic, genetic, molecular, and immunophenotypic characteristics of AML blast cells. Understanding these AML blast cell characteristics is crucial in aiding clinicians to achieve accurate diagnosis, determine suitable treatment options, and monitor prognosis effectively. In high-income countries, the landscape of acute leukemia, particularly AML, has witnessed a remarkable transformation over the past few decades. Advances in diagnostic approaches, therapeutic interventions, and supportive care have led to a substantial improvement in the survival rates associated with AML. On the other hand, in lower income countries particularly those in Africa, most countries lack up to date statistics of different leukemia sub-types prevalence's due to poor registry and limited diagnostic tools. Leukemic cells or blast morphology is mostly utilized in diagnosis of acute leukemia in many parts of Africa, and this has serious limitations in making accurate and timely diagnoses. The use of morphological examination for leukemia diagnosis is not able to detect a small number of leukemia cells during the disease's early stages or that remain in the bone marrow after treatment [15].

Since timely diagnosis has great influence on overall treatment outcomes and prognosis monitoring, the use of advanced technologies like flow-cytometric immunophenotyping and immunofluorescence microscopy imaging would allow to timely diagnose and clearly define each subtype of acute leukemia. Technological advancements in immunophenotyping have allowed successful development of highly sensitive monoclonal antibodies for selective diagnosis of diseased cell populations (tumour cells) in patients. However, the current costs of antibodies are likely to limit their availability and applicability in already strained developing countries' economies.

To overcome this challenge, an alternative approach is to use smaller antibody fragments such as scFvs coupled with a self-labelling protein tag (SNAP-tag). This can be done recombinantly under cost-controlling conditions, making it a more cost-effective method of AML diagnosis in resource-limited settings. Despite the potential of scFv fragments for diagnostic purposes, more research needs to be done to fully understand their capabilities and limitations. Nonetheless, this approach shows promise as a more accessible and cost-effective way of diagnosing various diseases in developing countries.

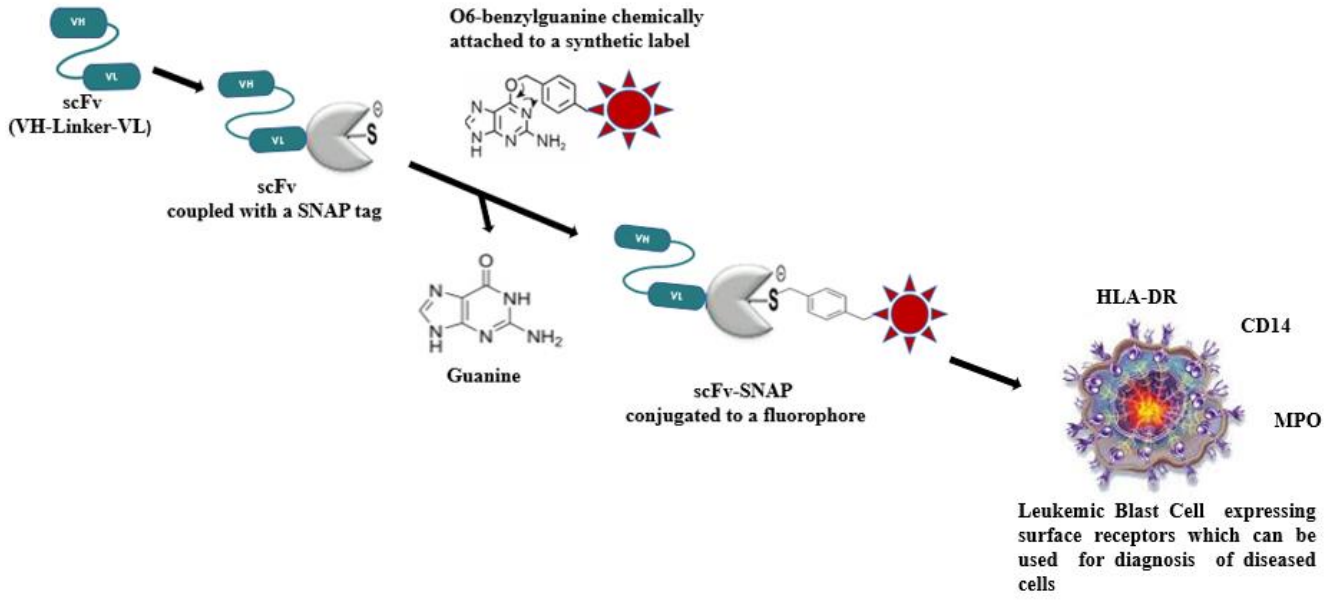

Figure 8. The scFv-SNAP fusion protein selectively targeting unique markers overexpressed on acute myeloid leukemia cells. The variable heavy and light chains are joined together with a linker to form an scFv. The scFv is coupled to a SNAP-Tag enzyme which is then conjugated to 06-benzylguanine chemically attached to a fluorophore. The labelled scFv-SNAP fusion protein is used to target specific antigens upregulated in acute myeloid leukemia blast cells. Diagram created using BioRender.

This study aimed to explore SNAP-tag-based antibody fusion proteins as supplementary or companion diagnostic tools for acute leukemia and the targets of interest included the following antigens overexpressed on leukemic cells: cluster of differentiation antigen 14 (CD14), myeloperoxidase (MPO) and the human leukocyte antigen DR (HLA-DR). Exposure to molecular cloning, recombinant antibody technologies, protein engineering and protein expression promotes local development and invention of next generation immunodiagnostics and therapeutics in Africa, and this could be

considered as a cost-containment strategy for cancer remedies that are being priced for the first-world markets. The research specific objectives included:

a) Performing in-silico design and engineering of single chain antibody fragments (scFv)- SNAP fusion constructs.

b) Generating CD14, MPO and HLA-DR specific (scFv)-SNAP fusion proteins.

c) Conjugation of purified SNAP fusion proteins from b) to BG-modified fluorophores.

d) Establishing a method for multiparameter flow cytometry and immunofluorescence microscopy imaging to confirm in vitro proof of binding on leukemic cell lines.

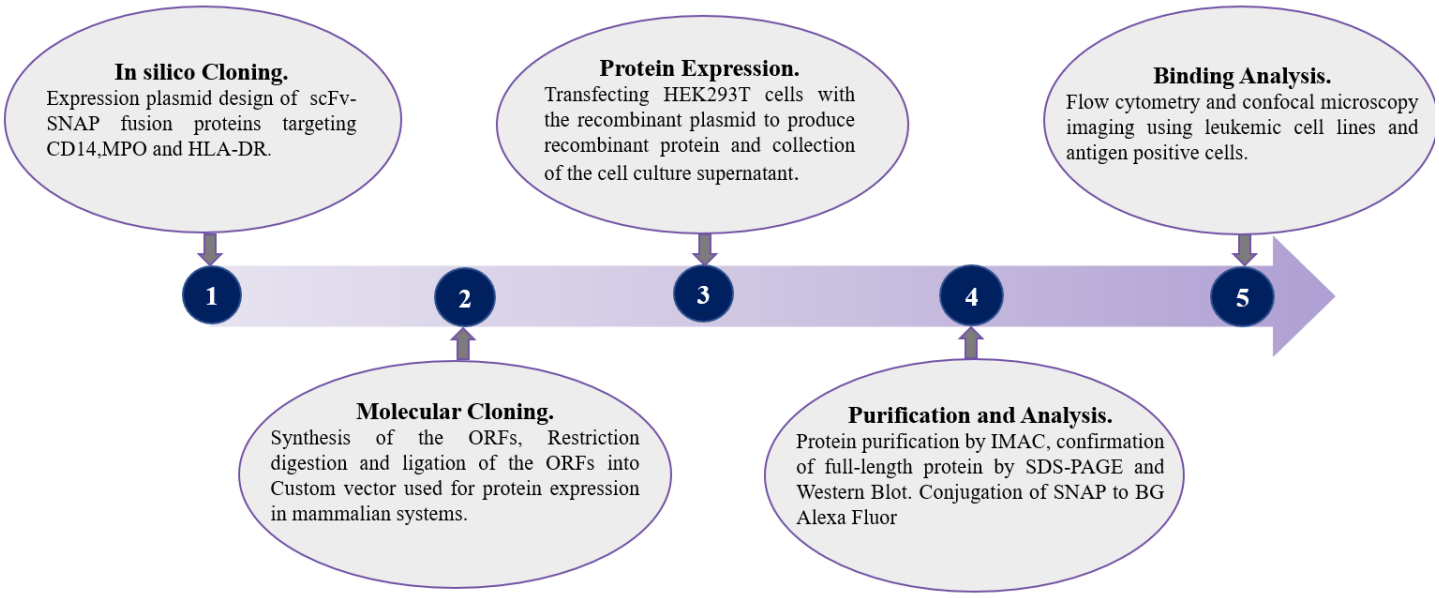

Figure 9. Flow chart illustrating the project workflow. The first step is Insilico engineering and design of expression plasmids using publicly available antibody sequences, followed by molecular cloning, protein expression in mammalian, protein purification by IMAC, conjugation of SNAP fusion proteins to Benzyl guanine (BG)-modified fluorophores and binding analysis using flow cytometry and confocal microscopy.

Chapter 2: Methods

This chapter provides information on the materials and devices used to develop and establish methods, protocols, and standard operating procedures at the Medical Biotechnology and Immunotherapy Research Unit (MB&I). The methodology described is used by members of the MB&I and is thus representative of MB&I background and know-how as documented by standard operation procedures, student's theses, and original publications.

2.1 *In silico* engineering and design of mammalian expression plasmids

To procure new monoclonal antibody sequences, a combination of literature search, software tools, and publicly available resources was used to identify and analyse potential monoclonal antibody amino acid sequences. Publicly accessible variable gene (V-gene) sequences were attained from a variety of sources including patents, journals, and antibody databases. The amino acid V-gene sequences obtained from these sources were then reverse translated into their corresponding nucleotide sequences using the Gene Infinity Back Translation Tool, which is a software tool developed by Gene Infinity LLC, San Diego, CA (http://www.geneinfinity.org/sms/sms_backtranslation.html). To analyse the obtained nucleotide sequences and compare them to existing germline V-gene sequences of immunoglobulins that are homologous to the obtained sequences, the IgBLAST tool was used and this is accessible through the National Centre for Biotechnology Information (NCBI) (available at: https://www.ncbi.nlm.nih.gov/igblast/). Once the framework regions (FR) and complementarity determining regions (CDRs) were identified for each using IgBLAST, all variable heavy (VH) and variable Light (VL) sequences were codon optimised for mammalian expression using the IDT codon optimisation tool (available at: https://eu.idtdna.com/pages/tools/codon-optimization-tool). To confirm if there were alterations in the corresponding amino acid sequencies after optimisation, the nucleotide sequences were translated into amino acid sequences using the ExPasy Translate Tool (available at https://web.ExPasy.org/translate/). The amino acid sequences were then aligned to their parental antibody sequences using EMBL-EBI Clustal Omega a multiple sequence alignment tool

(available at: https://www.ebi.ac.uk/) and this was done for quality control purposes. To assemble the confirmed codon optimised V-gene nucleotide sequences into a single chain variable fragment (scFv), the variable heavy and variable light nucleotide sequences were joined together with a short peptide glycine-serine linker $(G_4S)_3$ (sequence: 5'-GGTGGCGGTGGATCC-3') and flanked with *Sfi*1 and *Not*1 restriction sites. SnapGene software (version 3.1.1, GSL Biotech, Chicago) (available at www.snapgene.com) was used for designing of the mammalian plasmid vector system for transient expression as well as incorporating the newly designed single chain variable fragments into the custom vector backbone simulating molecular cloning (section **3.1**). Once the integrity of the open reading frames (ORFs) was confirmed, the scFv sequences including the *Sfi*I and *Not*I restriction sites, were sent for synthesis in a pUC-57 plasmid (GenScript; New Jersey, USA).

2.2 Molecular cloning

2.2.1 Liquid transformation of competent cells

The plasmid DNA of interest synthesized in pUC-57 from GenScript, along with the pCB-Annexin V-SNAP plasmid (plasmid backbone housing SNAP), which was already available at MB&I, were introduced into chemically competent DH5α *Escherichia coli* (*E. coli*) cells (these cells are of the K12 strain and have the genotype fhuA2 (argF-lacZ) U169 phoA glnV44 80 (lacZ)M15 gyrA96 recA1 relA1 endA1 thi-1 hsdR17) (New England Biolabs, MA USA). To initiate the transformation process, DH5α competent *E. coli* cells were thawed on ice for 10 minutes. Plasmid DNA was then diluted to a final concentration of 100n g/µl, and 5 µl of the diluted plasmid DNA was added to 50 µl of competent DH5α *E. coli* cells. The mixture was then thoroughly mixed by flicking the tube and incubated on ice for 30 minutes. After incubation, the *E. coli* cells were then subjected to a heat shock treatment using a heating block (Benchmark Scientific, USA) at 42°C for 60 seconds, followed by a 5-minute cooling period on ice. Subsequently, 950 µl of Super Optimal Broth (SOC) with catabolite repression was added to the mixture and incubated for 60 minutes at 37°C. The entire content was then transferred

into conical flasks containing 50 ml of Luria-Bertani (LB) broth plus 200 µg/ml ampicillin antibiotic (Sigma-Aldrich, USA) and incubated at 37°C on a shaker for 16 hours to promote bacterial growth (section **3.2.1**).

2.2.2 Purification of plasmid DNA from DH5α *E. coli* cells

The plasmid DNA was isolated from *E. coli* cultures and purified using the NucleoBond® plasmid purification kit (Product number: 740573, Macherey-Nagel, United Kingdom) according to the manufacturer's instructions with some minor modifications (220). The principle of this assay relies on the alkaline lysis of bacterial cells for the extraction of plasmid DNA. The DNA is bound to an anion-exchange resin in the NucleoBond® column, from where it is eluted off and precipitated using isopropanol. In the last step, 30 µl of molecular grade water (pre-heated at 50°C for 10 minutes) was used to resuspend the DNA pellet instead of TE buffer. This step was done because the presence of chemicals in TE buffer (EDTA and Tris) can affect the quality of the DNA samples that are meant to be used in downstream applications. The amount of DNA recovered was then quantified using a spectrophotometer Denovix NanoDrop™ ND-2000 (Thermo Fisher Scientific, USA) (section **3.2.1**). During quantification, the purity of the bulk-prepped plasmid DNA was evaluated using absorbance values obtained from the spectrophotometer. The nucleic acid to protein concentration, 260/280 ratios which signifies the ratio of nucleic acid to protein absorbance and a value of approximately 1.8 shows that the DNA is pure and uncontaminated with substances such as phenol, protein or other contaminants that strongly absorb at or near 280 nm. As well as the 260/230 ratio which shows the presence of contaminants that absorb at 230 nm, such as EDTA and a ratio of approximately 2.0-2.2 shows that the nucleic acids are not contaminated. These values were used to confirm the suitability of the purified DNA samples for downstream applications.

2.2.3 Restriction enzyme digestion

The New England Biolabs (NEB) double digest protocol and materials were used to perform restriction enzyme digests. Plasmid DNA, which was isolated and purified from *E. coli* using the NucleoBond Plasmid Purification Kit, was initially diluted to a concentration of 1000ng/µl. One microliter of the diluted plasmid DNA equates to one microgram. To carry out the double digest, plasmid DNA samples in pUC-57 (housing the sequences encoding for the scFv) and pCB-AnnexinV-SNAP (pCB vector backbone housing SNAP) were digested sequentially with *Sfi*I for 4 hours at 50°C, followed by *Not*I overnight incubation (16 hours) at 37°C on a heating block. The digests were performed using a reaction mixture illustrated in **Table 4** below. Following incubation with restriction enzymes, the reaction was rendered inactive by incubating it at 65°C for 20 minutes and this was done to denature the enzymes. Subsequently, the samples were left to cool at room temperature on the bench before being subjected to separation via agarose gel electrophoresis.

Table 4. Restriction enzymes digest reaction mixture

Component	**Amount**
10x NEB cutsmart buffer	5 µl
Sample DNA	2 µg (2 µl)
*Not*1 (37°C overnight)	1 µl
*Sfi*1 (50°C for 4 hours)	1 µl
Nuclease free water	41 µl
Total Volume	**50 µl**

2.2.4 Agarose gel electrophoresis

The agarose gel electrophoresis method was employed to separate the DNA fragments after the restriction digest. A 1.2% (w/v) agarose gel was prepared according to the manufacturer's instructions by dissolving 1.2g agarose powder in 100 ml of 1x TAE buffer with a pH of 8.5 (40 mM Tris, 20 mM

acetic acid, and 1 mM EDTA). A 1:10000 dilution of SYBR® Safe DNA gel stain (Thermo Fisher Scientific, South Africa) was added to the agarose gel to enable visualization and tracking of the DNA bands. As a reference, 5 µl of Quick-Load 1kb DNA ladder (New England Biolabs) was used. The digested DNA samples and controls were mixed with 2 µl of 6x Purple Gel Loading Dye (Thermo Fisher Scientific, USA). Electrophoresis was conducted at 100 volts for 60 minutes using Wide Mini Sub-Cell systems (Bio-Rad, USA). The gels were visualised and images were captured using the Gel Doc™ XR System (Bio-Rad, USA) which uses Image Lab (v6.1.0) software (section **3.2.2**).

2.2.5 Recovery of DNA fragments from agarose gels

To purify the DNA fragments of interest from the agarose gel, the QIAquick Gel Extraction Kit (QIAgen, Hilden, Germany) was used according to the manufacturer's instructions with some modifications. First, the bands were excised using a sterile sharp scalpel from the agarose gel and then pooled or placed in 1.5 ml microcentrifuge tubes. To solubilize the agarose gel, three volumes of Buffer QG (calculated based on the size of the excised DNA fragments) were added fully submerging the excised agarose gel slices containing the DNA. The tubes were incubated at 50°C for 10 minutes, ensuring that the gel was completely dissolved. Vortexing was periodically performed to aid dissolution. One volume of isopropanol was added, and the solution was placed in a spin column inside a collection tube. The column was centrifuged for 60 seconds at 15000 rcf, and the flowthrough was discarded. To wash the column, 750 µl Buffer PE was added, and the column was centrifuged for 60 seconds at 15000 rcf. The columns were placed in clean microcentrifuge tubes and 50 µl preheated nuclease-free water at 50°C was added to the centre of the filter. The tubes were then incubated at 50°C for 5 minutes to facilitate solubilization of the DNA before being centrifuged for 60 seconds at 15000 rcf to elute the DNA.

2.2.6 T4 DNA Ligation

The digested pCB vector backbone and the insert were ligated using the T4 DNA Ligase kit (New England Biolabs, USA) according to the manufacturer's instructions (221). Reactions were set up as indicated in **Table A3** and incubated overnight at 16°C. The amount of insert required for a 1:1 and 1:5 (vector: insert) ratio was calculated using the NEBioCalculator (https://nebiocalculator.neb.com/ligation) (section **3.2.3**). Vector-only (no insert) controls were included to determine vector self-ligation. After the overnight incubation, the T4 DNA ligase was then inactivated at 65°C for 10 min and chilled on ice for 5 minutes.

2.2.7 Bacterial transformation of ligated recombinant plasmids

Plasmid DNA was introduced into calcium competent DH5α *E. coli* cells through transformation as described in section **2.2.1**. Here, 1 µl of the ligated plasmids were added to 50 µl of competent DH5α *E. coli* cells. Thereafter, 950µl of room temperature SOC was added to the mixture, which was then incubated shaking in a 37°C incubator for 60 minutes. After the incubation period, the cells were mixed thoroughly by gently flicking and inverting the tube. A small volume (50 µl) of the mixture was plated on an LB agar plate containing 200 ng/µl ampicillin and incubated overnight at 37°C. Controls consisting of vector-only and bacteria-only were also included (section **3.2.3**). After incubation, transformation efficiencies were calculated by dividing the number of transformants (colonies that grew on the selective medium) by the amount of DNA used for the transformation using the following formular:

Transformation efficiencies = (Number of colonies / Mass of plasmid DNA) x Dilution factor

2.2.8 Miniprep (Small-Scale) DNA isolation

Three individual colonies were selected from each plate from section **2.2.7** above and each colony was transferred to separate 2 ml of LB broth medium in 10 ml conical tubes. The tubes were placed on a shaker and incubated overnight at 37°C**.** After incubation, recombinant plasmids were isolated from

the DH5α *E. coli* cells using the Zyppy Plasmid Miniprep Kit (Zymo Research, CA USA) on a small scale (10 ml cultures) according to the manufacturer's instructions with slight modifications (222). To avoid contamination of plasmid DNA with chemicals present in the Zyppy Elution Buffer, elution was performed using 30 µl of sterile nuclease-free water preheated to 50°C. Following that, the columns were incubated at 50°C for 5 minutes to aid in the solubilization of the DNA, rather than allowing them to stand at room temperature for 60 seconds. Subsequently, the concentration of the eluted DNA was measured using a spectrophotometer (Denovix NanoDrop™ ND-2000, Thermo Fisher Scientific).

2.2.9 Restriction mapping

Restriction mapping was done to distinguish between colonies that had been successfully transformed with the desired ligated plasmids of interest from section **2.2.7** and those containing products of vector self-ligation or products of partial digestion from section **2.2.3**. In this experiment, SnapGene software (version 3.1.1, GSL Biotech, Chicago) was used to predict the cutting patterns of *Pme*1 and *Blp*1 enzymes on the pCB-AnnexinV-SNAP and the ligated plasmids from section **2.2.6**. To verify the accuracy of the predictions, 50 µl reactions were set up using 2 µg DNA, 5 µl CutSmart Buffer and 1 µl of the enzyme (*Pme*1 and *Blp*1). The reactions were then incubated at 37°C for 16 hours (overnight). After incubation, agarose gel electrophoresis was performed to separate the DNA fragments based on their sizes (section **3.2.4**). The gels were then analysed to confirm the correct ligation of recombinant plasmids, as predicted by the simulations. The gels were visualised and images were captured using the Gel Doc™ XR System (Bio-Rad, USA)

2.2.10 DNA sequencing

Recombinant clones that had been confirmed via restriction mapping were subjected to bulk preparation and purification using the NucleoBond Plasmid Purification miniprep protocol, as previously described in section **2.2.2**. To confirm the accuracy of the restriction mapping open reading frame (ORF) sequence, samples were sent to Inqaba Biotec™ (South Africa). The universal T7

promoter forward primer (5'-TAATACGACTCACTATAGGG-3'), universal SNAP internal forward primer (5'-CAAGGACTGCGAGATGAAGAGAACCACCC-3'), and the universal SNAP reverse primer (5'-GAACGCCAGCACATGGACA-3') were used in this experiment. These primers facilitated the amplification of the ORF sequence from the T7 promoter up to a region after SNAP-tag and this includes the Igκ leader, 10His-tag, Enterokinase site and scFv which are in between the two regions. The resulting sequencing data were analysed using SnapGene software (version 3.1.1, GSL Biotech, Chicago). Open Reading Frames (ORF) sequences generated *in silico* (section **2.1**) were used as the reference sequence (section **3.2.5**).

2.3 Cell Culture

2.3.1 Seeding HEK 293T cells

The experiment involved producing recombinant proteins using a eukaryotic expression system, specifically mammalian human embryonic kidney T-cells (HEK 293T; ATCC: CRL-3216). This was performed in a Biosafety Level 2 (BSL2) facility in a strictly sterile biosafety cabinet. HEK 293T cells were cultured in Roswell Park Memorial Institute (RPMI) 1640 medium (Gibco, USA) supplemented with 10% foetal bovine serum (FBS; Gibco, USA) and 100 µl/ml penicillin-streptomycin (Gibco, USA) at 37 °C with 95% humidity and 5% CO_2. The ZOE™ Fluorescent Cell Imager (Bio-Rad, USA) was used to visualize cells and check cell confluence. The medium was changed every four days, and cells were passaged (split 1:5) when they reached 90% confluency.

2.3.2 Transfection and protein expression in HEK293T cells

Transfection refers to the artificial method of introducing DNA into cultured mammalian cells, typically achieved through chemical or physical techniques (223). In this context, chemical-aided transfection was carried out using the sequenced DNA plasmids from section **2.2.10.** To initiate this process, HEK293T cells were plated at 70% confluency two days prior in 35 mm x 10 mm round cell culture dishes (Sigma-Aldrich, USA) and grown in supplemented RPMI-1640 medium. The

XtremeGENE HP DNA Transfection Reagent Quick Protocol (Sigma-Aldrich, USA) was used following the manufacturer's instructions with some modifications (224). The transfection master mix, consisting of 188 µl of unsupplemented RPMI media, 9µl of transfection reagent, and 3 µg of DNA in 1:3 ratio (v/v) was prepared and evenly distributed in the seeded HEK 293T cells in a dropwise manner. A negative control was also included, consisting of cells that were not transfected. The transfected cells were then incubated at 37°C with 95% humidity and 5% CO_2. 72 hours post-transfection, eGFP expression was detected by examining the cells on a ZOE™ Fluorescent Cell Imager (Bio-Rad, USA).

2.3.3 Determination of transfection efficiencies, Zeocin selection and cell culture supernatant collection

Transfection efficiencies of the cells were evaluated through both qualitative and quantitative methods. Qualitative assessment was performed through microscopic visualization of enhanced green fluorescent protein (eGFP) expressed by the transfected cells using a ZOE™ Fluorescence Cell Imager (Bio-Rad, USA) at a magnification of 175x (section **3.3**). For quantitative determination, 1 ml of successfully transfected cells and non-transfected controls were taken from 35mm dishes in culture for flow cytometry analysis using the BD LSRFortessa™ Cell Analyzer (BD Biosciences, USA). After flow cytometry acquisition, data was analysed using FlowJo software (version 10.9.0; BD Biosciences, USA) as described in section **2.7.3.5**. Transfection efficiencies were calculated as the proportion of eGFP-positive cells in the total cell population. Thereafter, 4 days post-transfection cells were transferred to a T25 cell culture flask (SPL Life Sciences, USA). To enrich the eGFP-expressing population, the cells were first treated with a lower concentration of Zeocin (100 mg/ml) for a period of four weeks before being subjected to a higher concentration of 150 mg/ml for two weeks. This was done until over 90% the cells were expressing the eGFP and the assessment was performed through microscopic visualization using a ZOE™ Fluorescence Cell Imager (Bio-Rad, USA). Following that, cells were then transferred from T25 flasks to T175 flasks and this was done to increase protein production. These cells were then grown at 90% confluency and the cell culture supernatant containing

the secreted protein of interest, was harvested every 4 days until 1 litre of the CCSN (Cell Culture Supernatant) was collected. The collected supernatant was pooled, centrifuged at 4500 x g for 5 minutes to remove cellular debris, and then stored at 4°C until protein purification.

2.4 Protein purification

2.4.1 Immobilised metal affinity chromatography

Immobilised metal affinity chromatography (IMAC) was used for the enrichment of his-tagged SNAP fusion proteins using the ÄKTA Avant protein purification system (GE Healthcare, USA). The secreted 10 his-tagged fusion proteins in cell culture supernatant were mixed with 4x incubation buffer (200 mM NaH_2PO_4, 1.2 M NaCl and 10 mM $C_3N_2H_4$, pH 8.0). The mixture was then filtered using the Nalgene™ vacuum filtration system (Sigma-Aldrich, South Africa) containing a 0.45 µm Durapore® membrane filter (Millipore, USA) to exclude any microcellular debris, before being loaded into the ÄKTA Avant protein purification system. IMAC was carried out by using a Ni^{2+} Sepharose affinity resin (with in a HisTrap™ Excel column, GE Healthcare, USA) following the steps illustrated on **Table 5**. In the process, His-tagged recombinant SNAP fusion proteins bound to the HisTrap™ Excel column during the loading step. To prevent contaminating proteins with lower nickel affinity from binding to the column, a low concentration of 10mM imidazole ($C_3N_2H_4$) was used, this however still allowed SNAP fusion proteins to the interact with the column. Subsequently, during the column wash, a slightly higher concentration of 40 mM imidazole was used to wash away contaminating proteins that had lower affinity for nickel. Following this, elution of the SNAP fusion proteins was carried out using an elution buffer with a higher concentration of 250 mM imidazole. Since imidazole has a higher affinity for nickel compared to the His-tagged recombinant SNAP fusion protein. This higher concentration of imidazole was used to displace the recombinant SNAP fusion proteins by interacting with the nickel present on the column (section **3.4**). Throughout the IMAC process, 2 ml fractions were collected from the elutes, allowing for the identification and isolation of the desired SNAP fusion proteins.

Table 5. IMAC purification of SNAP fusion proteins from mammalian cell culture supernatant

Step	Composition	Flow rate	Volume
Step 1: Equilibration:	**Equilibration Buffer**: 50 mM NaH_2PO_4, 300 mM NaCl	5 ml/min	5 CV (25 ml)
Step 2: Loading:	750 ml **cell culture supernatant** and 250 ml **incubation buffer:** 200 mM (NaH_2PO_4), 1.2 M (NaCl), 10 mM ($C_3N_2H_4$).	1 ml/min	I litre
Step 3: Column Wash	**Wash Buffer:** 50 mM (NaH_2PO_4), 300 mM (NaCl), 40 mM ($C_3N_2H_4$).	1 ml/min	20 CV (100 ml)
Step 4: Elution	**Elution Buffer:** 50 mM (NaH_2PO_4), 300 mM (NaCl), 250 mM ($C_3N_2H_4$).	1 ml/min	5 CV (25 ml)
Step 5: Equilibration:	**Equilibration Buffer**: 50 mM (NaH_2PO_4), 300 mM (NaCl).	5 ml/min	10 CV (50 ml)

Abbreviations and molecular formulars: CV (Column Volume), Sodium Phosphate Monobasic (NaH_2PO_4), Sodium Chloride (NaCl), Immidazole ($C_3N_2H_4$).

2.4.2 Examining IMAC fractions for the presence of SNAP fusion protein.

The eluted IMAC fractions were analysed for the presence of SNAP fusion proteins by sodium dodecyl-sulfate polyacrylamide gel electrophoresis (SDS-PAGE). This technique utilizes electrophoresis to separate proteins based on their size under reducing conditions (225). Firstly, the theoretical molecular weight of SNAP fusion proteins was determined using the conversion calculator (available at https://www.aatbio.com/tools/calculate-peptide-and-protein-molecular-weight-mw). For sample preparation, 5 µl of 4x Laemmli protein-loading dye (Bio-Rad Laboratories, USA) supplemented with 10% (v/v) 2-mercaptoethanol (Sigma-Aldrich, South Africa) was mixed with 15

µl of the recombinant SNAP fusion protein samples from the eluted fractions making a final volume of 20 µl. Thereafter, all samples were heated at 95°C for 5 minutes and allowed to cool for 10 minutes at room temperature. A 10% SDS gel was prepared and protein samples were loaded onto the gel alongside 5 µl of protein molecular weight ladder (P7719S New England Biolabs). The gel was then run for 90 minutes at 150 volts using the Mini Protein Tetra Cell System (Bio-Rad, USA). Thereafter, protein bands were visualized by staining gel with Aqua Staining Solution (Vacutec, South Africa) and the Gel Doc™ XR System (Bio-Rad, USA) was used for image capture (section **3.4.1**).

2.5 Protein Analysis

2.5.1 Quantification of purified protein

Firstly, an Amicon column with a 100 kDa molecular weight cut off (MWCO) (Sigma-Aldrich, USA) was used to remove contaminating proteins which had a molecular weight above of 100 kDa from the eluted IMAC fraction. This was done by centrifugation at 4500 x g for 20 minutes at 4°C. Following that, the purified proteins were then concentrated using a second Amicon column with a 10 kDa MWCO (Sigma-Aldrich, USA) by centrifugation at 4500 x g for 20 minutes at 4°C. This was repeated until all the selected fractions had been concentrated into ~500 µl. Thereafter, buffer exchange (removal of residual imidazole from IMAC elution buffer which interferes with the enzymatic activity of the SNAP-tag) was carried out by adding 5 ml of 1x PBS (pH 7.4) into the Amicon column and washing down to a concentrated volume of ~500 µl. Quantification of the concentrated protein samples was done using a Denovix NanoDrop™ ND-2000 (Thermo Fisher Scientific, USA) by UV spectrophotometry, and further quantification was done by densitometry analysis (section **3.4.2**).

For densitometry quantification, 5 µl of the concentrated protein samples were diluted with 15 µl of 1x PBS making a final volume of 20 µl. Thereafter, 5 µl of 4x Laemmli protein-loading dye (Bio-Rad Laboratories, USA) supplemented with 10% (v/v) 2-mercaptoethanol (Sigma-Aldrich, South Africa) was mixed with the 20 µl of the diluted protein samples making a final volume of 25 µl. A two-fold

serial dilution of BSA standard protein (Thermo Fisher Scientific, South Africa) was also prepared in parallel as shown in **Table 6**. Following that, all samples were heated at 95°C for 5 minutes and allowed to cool for 10 minutes at room temperature. A 10% SDS gel was prepared and all protein samples were loaded onto the gel alongside 5 µl of protein molecular weight ladder (P7719S New England Biolabs). The gel was then run using the same equipment and conditions as described in section **2.4.2**.

Table 6. Amount (ug) of BSA standard and SNAP fusion proteins used for densitometry analysis.

Sample Lane	Volume	1x PBS	4x loading dye	Total Volume
1. Molecular weight ladder	5 µl	0 µl	0 µl	5 µl
2. SNAP fusion protein	5 µl	15 µl	5 µl	25 µl
3. BSA (16 µg)	16 µl	4 µl	5 µl	25 µl
4. BSA (8 µg)	8 µl	12 µl	5 µl	25 µl
5. BSA (4 µg)	4 µl	16 µl	5 µl	25 µl
6. BSA (1 µg)	1 µl	19 µl	5 µl	25 µl

To determine the quantity, yield and percentage purity of the SNAP fusion proteins, densitometry measurements were performed using ImageJ software (https://imagej.nih.gov/ij/download.html). This software compared the optical densities of SNAP fusion protein bands with the corresponding positive control Bovine Serum Albumin (BSA) bands on the same gel. As a result, Microsoft Excel software was used to plot a standard curve of optical colour intensity against the quantity of protein (µg) using BSA standards. This standard curve allowed for the calculation of the concentration of SNAP fusion proteins in each sample (section **3.4.3**).

2.5.2 Western blot.

To confirm for the integrity of the N-terminal poly-Histidine tag of SNAP fusion proteins, a western blot analysis was used. Two duplicate 10% SDS gels were prepared, and 5 µg of protein samples were

loaded onto each gel, following the procedure described in section **2.4.2**. However, it's worth noting that one of the gels was not stained and was used for immunoblotting, while the other gel was stained with AcquaStain. This allowed for a precise comparison between the results obtained from the immunoblot and the denaturing polyacrylamide gel. For immunoblotting, protein bands were transferred from the unstained SDS gel to a nitrocellulose membrane (PVDF transfer membrane, Roche, Switzerland) using a Mini Trans-Blot Cell system (Bio-Rad, USA), set at 25V for 7 minutes. The membrane was then blocked with fat-free milk for 60 minutes at room temperature, followed by incubation with a 1:1000 dilution of an anti-his rabbit primary antibody (Qiagen, Hilden, Germany) at 4°C overnight. The following morning, the membrane was rinsed 3 times with TBS-T at 5 minutes intervals. Thereafter, the membrane was incubated with a goat anti-rabbit horseradish peroxidase (HRP)-conjugated secondary antibody (Bio-Rad, USA) dissolved in fat-free milk (1:5000) for 60 min at room temperature, and then washed 3 times with TBS-T at 5 minutes intervals. To detect the HRP-bound proteins, 4 ml of TMB-Blotting Solution substrate (Bio-Rad, USA) was added to the nitrocellulose membrane for 1 minute, followed by washing with Type 1 dH_2O and this was done to stop the reaction. Thereafter, image capture was done using the Gel Doc™ XR System (Bio-Rad, USA) (section **3.5.1**).

2.6 Labelling of SNAP fusion proteins with BG derivatives

Conjugation reactions with benzyl guanine (BG) derivatives were conducted to verify the functionality of the enzymatic SNAP-tag component on the C-terminus of SNAP fusion proteins. Firstly, the micromolar concentrations of the SNAP fusion protein were calculated using an online conversion tool (available at https://www.bioline.com/media/calculator/0104.html) which converts mg/ml to µM. Following that, SNAP fusion proteins (5 µM) were mixed with 10 µM of SNAP-Surface® Alexa Fluor® 488 (BG-Alexa Fluor) from New England Biolabs (MA, USA), 1mM dithiothreitol (DTT, a reducing agent that improves the stability of SNAP-tag) (Sigma-Aldrich, South Africa) and 1x PBS buffer to a final volume of 20 µl **(Table A6)**. The mixture was incubated in the dark at 37°C for 60

minutes. The fluorescently labelled proteins were then run on an SDS-PAGE gel as described in **2.4.2**, and the fluorescent signal was visualized using a Dark Reader Transilluminator (Clare Chemical Research, USA) upon exposure to blue light excitation **(3.5.2)**.

2.7 Binding studies

2.7.1 Leukemic cell line culture

In this experiment, leukemic cell lines (THP-1 and HL60), along with HEK 293T cells, were seeded in a T25 flask (SPL Life Sciences, USA). The cells were incubated in RPMI-1640 medium (Gibco, USA) supplemented with 10% foetal bovine serum (Gibco, USA) and 100 µl/ml penicillin-streptomycin (Gibco, USA) at 37 °C with 95% humidity and 5% CO_2. The medium was changed after every 4 days and it is important to note that, THP-1 and HL60 cell lines are suspension cells. Consequently, upon reaching 90% confluency, cells were passaged by removing 4 ml of the old medium, retaining 1 ml, and replacing the discarded 4 ml with fresh supplemented RPMI medium.

2.7.2 Confocal microscopy

Live cell imaging using confocal microscopy was conducted on tumour cell lines to assess the binding abilities of the newly generated SNAP fusion proteins (section **3.6.1**). This method allowed for high-resolution imaging of cells and target antigens, revealing details about the antigen location, distribution, and expression levels. SNAP fusion proteins were first labelled SNAP-Surface® Alexa Fluor® 647 **(Table A7)** using the same procedure as described in section **2.6**. Thereafter, unconjugated fluorophore was removed by centrifugation at 1500 rcf for 2 minutes using Zeba™ Spin desalting columns (Thermo Fisher Scientific, SA) with a 7 kDa molecular weight cut off. Thereafter, the labelled SNAP fusion proteins were stored at 4°C until they were used for staining cells.

2.7.2.1 Staining cell surface antigens (CD14)

Approximately 1x10⁴ THP-1 cells (CD14+) and HEK 293T cell (CD14-) in cell culture medium were aliquoted into the FACs tubes (Fluorescence-activated cell sorting tubes; Sigma-Aldrich, USA) and centrifuged at 932 x g (Beckman Coulter Allegra™ X-12R) for 5 minutes at 4°C. Thereafter, the supernatant was discarded and cells were washed with 2 ml of 1x PBS by centrifugation at 932 x g for 5 minutes at 4°C. The cell pellet was resuspended in 200 µl of 1:5000 dilution of Hoechst nuclei stain (Thermo Fisher Scientific, South Africa) and incubated for 10 minutes at room temperature in dark. After incubation, excess dye was removed by washing the cells with 2 ml of FACs buffer (containing 2% (v/v) FBS and 0.1% (v/v) sodium azide in 1x PBS). Thereafter, cells were then incubated with 50 µl (containing 20 µg) of SNAP fusion proteins conjugated to Alexa Flour 647 for 60 minutes at 4°C in the dark. After incubation, cells were washed twice with 1 ml of 1x PBS before being resuspended in 250 µl of 1x PBS. Cells were then transferred to live cell imaging dishes (SPL Life Sciences, USA) and kept on ice until taken for live cell imaging using the Zeiss LSM880 Airyscan (Oberkochen, Germany).

2.7.2.2 Staining intracellular antigens (MPO)

Approximately, 1x10⁴ HL60 (MPO+) and HEK 293T (MPO-) cells were aliquoted into the FACs tubes, centrifuged at 932 x g for 5 minutes at room temperature. Thereafter, the supernatant was discarded and cells were washed with 2 ml 1x PBS by centrifugation at 932 x g for 5 minutes at 4°C. For intracellular MPO staining, cells were first fixed by incubation with 100 µl of Fix/Perm buffer (BD Biosciences, USA) and mixed thoroughly by vortexing for approximately 10 seconds before being incubated for 20 minutes at room temperature in the dark. Following that, cells were washed with 2 ml 1x Perm/Wash buffer (BD Biosciences, USA) by centrifugation at 932 x g for 5 minutes at room temperature. Thereafter, Cells were then incubated with 50 µl (containing 20 µg) of SNAP fusion proteins conjugated to Alexa Flour 647 for 60 minutes at 4°C in the dark. Unbound conjugated fusion proteins were removed by washing with 2 ml of 1x Perm/Wash buffer for 5 minutes at room

temperature. Following that, cells were then incubated with 200 µl of 1:5000 Hoechst nuclei stain (Thermo Fisher Scientific, South Africa) for 10 minutes in the dark at room temperature. Excess dye was removed by washing the cells twice 1 ml of 1x PBS before being resuspended in 250 µl of 1x PBS. Cells were then transferred to live cell imaging dishes (SPL Life Sciences, USA) and kept on ice until taken for live cell imaging using the Zeiss LSM880 Airyscan (Oberkochen, Germany).

2.7.3 Flow cytometry

Flow cytometry was used to further confirm the binding abilities of the newly generated recombinant SNAP fusion proteins and this also allows for the relative quantitation of receptor expression status in a population of tumour cells (section **3.6.2**). This procedure facilitated the examination of different antigens and the differentiation of different cell populations based on their surface markers or intracellular antigens. In these studies, SNAP fusion proteins were first labelled SNAP-Surface® Alexa Fluor® 488 **(Table A7)** using the same procedure as described in section **2.7.2.**

2.7.3.1 Antibody titration

Antibody titration was used to determine the optimal antibody concentration that yields the highest signal from the positive population while minimizing the background signal from the negative population (226). Background fluorescence typically arises from cell autofluorescence, spectral overlap, and undesirable antibody binding due to the use of high antibody concentrations. In this study, antibody titrations were performed using different serial dilutions of the SNAP fusion proteins conjugated to BG Alexa Flour 488 as shown in **Figure 10**. At first, 8 microcentrifuge tubes were loaded with 50 µl of 1x PBS. In the first tube, 50 µl (containing 100 µg of labelled SNAP fusion proteins) were added and the tube was vortexed for approximately 10 seconds. Subsequently, 50µl of diluted proteins were drawn from the first tube and titrated into the remaining seven tubes, each containing 50 µl of 1x PBS, resulting in the final concentrations used for staining as illustrated in **Table 7**.

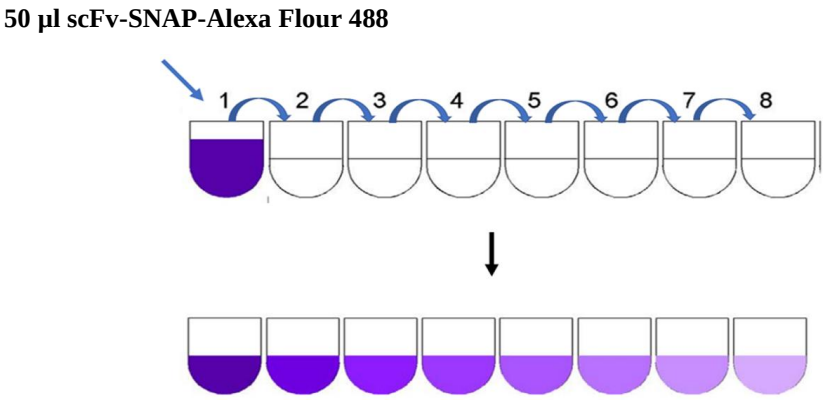

Figure 10. Antibody 2-fold dilution series for titration. This method is used to determine antibody concentration in solution. Every tube having half concentration of antibody from the previous tube. The ideal concentration is the one that generates the brightest and most precise staining while reducing non-specific binding, as this can cause increased background noise signal and affect the accuracy of the analysis.

Table 7. Example of antibody titration concentrations used for staining

SAMPLE	scFv-SNAP Alexa Flour 488	Cells
Tube 1	500 µg/ml	5 x 10^5
Tube 2	250 µg/ml	5 x 10^5
Tube 3	125 µg/ml	5 x 10^5
Tube 4	62.5 µg/ml	5 x 10^5
Tube 5	31.25 µg/ml	5 x 10^5
Tube 6	15.6 µg/ml	5 x 10^5
Tube 7	7.8 µg/ml	5 x 10^5
Tube 8	3.9 µg/ml	5 x 10^5

2.7.3.2 Preparation of compensation controls

Compensation in flow cytometry studies was done to correct for spectral overlap between fluorochromes or dyes used in the experiments (227). This was done since more than two different dyes were used in every flow cytometry session. Firstly, the compensation beads were vortexed thoroughly before use (to avoid clumping) and thereafter, 1 drop of negative control compensation particles and another 1 drop of anti-mouse IgK compensation particles (BD Biosciences, USA) were

added to each tube. The corresponding stain (1 µl of fluorescently tagged commercial antibodies) was added directly onto the compensation particles as illustrated in **Figure 11.** The samples were then incubated for 30 minutes in the dark at 4°C before being washed with 2 ml 1x PBS by centrifugation at 932 x g for 5 minutes at 4°C. The supernatant was discarded and the beads were then resuspended in 200 µl of 1x PBS and kept in the dark at 4°C until data acquisition.

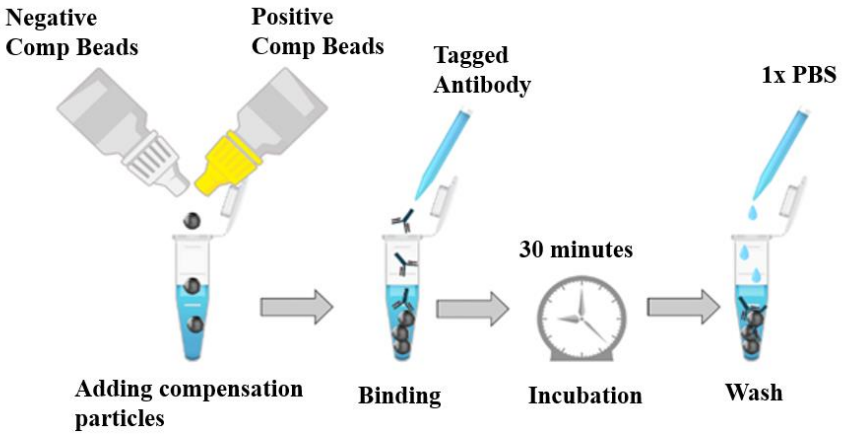

Figure 11. Preparation of compensation controls for a multicolour flow cytometry. Compensation beads were used to set spectral unmixing parameters on flow instruments, additionally adjust flow cytometers and setting up voltages. The anti-mouse IgK compensation particles (positive comp beads) binds to the Fc chain of fluorescently tagged mouse antibodies and these are combined with non-antibody binding beads (negative comp beads). This allows to create simulated positive and negative populations that are comparable to the heterogeneous populations of cells in a sample that are negative or positive for a particular antigen.

2.7.3.3 Staining cell surface antigens (CD14 and HLA-DR).

Regarding the staining of cell surface antigens, approximately $5x10^5$ cells in RPMI-1640 medium (Gibco, USA) supplemented with 10% foetal bovine serum (Gibco, USA) and 100 µl/ml penicillin-streptomycin (Gibco, USA) were aliquoted into FACs tubes and centrifuged at 932 x g for 5 minutes at 4ºC. Thereafter, the supernatant was discarded, and the cells were washed with 2 ml of 1x PBS. After decanting the supernatant, the cell pellet was resuspended in 50 µl of a 1:1000 dilution of LIVE/DEAD™ Fixable Violet Dead Cell Stain (Product number: L34963, Thermo Fisher Scientific, South Africa) and incubated at room temperature for 20 minutes in the dark. Cells were then washed with 2 ml of FACs buffer (containing 2% (v/v) FBS and 0.1% (v/v) sodium azide in 1x PBS) and

centrifuged at 932 x g for 5 minutes at 4ºC. The cell pellets were then resuspended in the dead volume and incubated with 50 µl of Alexa Flour 488 conjugated scFv-SNAP fusion proteins for 60 minutes at 4°C. After incubation, cells were then washed twice with 1 ml FACs buffer. Subsequently, to fix the cells, each cell pellet was resuspended in 300 µl of 1% (v/v) Paraformaldehyde (PFA) solution and incubated for 10 minutes at room temperature in the dark. The cells were then washed twice with 2 ml of 1x PBS, resuspended in 200 µl of 1x PBS and kept in the dark at 4ºC until data acquisition using the BD LSRFortessa™ Cell Analyzer (BD Biosciences, USA).

2.7.3.4 Staining intracellular antigens (MPO)

Similarly, for staining intracellular antigens, approximately 5 x 10^5 cells in RPMI-1640 medium (Gibco, USA) supplemented with 10% foetal bovine serum (Gibco, USA) and 100 µl/ml penicillin-streptomycin (Gibco, USA) were aliquoted into FACs tubes and centrifuged at 932 x g for 5 minutes at room temperature. Thereafter, the supernatant was discarded, and the cells were washed with 2 ml of 1x PBS by centrifugation at 932 x g for 5 minutes at room temperature. Following that, cell pellets were then resuspended in 50 µl of a 1:1000 dilution of LIVE/DEADTM Fixable Violet Dead Cell Stain (Thermo Fisher Scientific, South Africa) and incubated at room temperature for 20 minutes in the dark. After incubation, excess dye was removed by washing the cells with 2 ml of 1x PBS. For staining intracellular MPO, cells were resuspended in 100 µl of Fix/Perm buffer (BD Biosciences, USA) and mixed thoroughly by vortexing for approximately 10 seconds before being incubated for 20 minutes at room temperature in the dark. This was done to fix the cells thereby avoiding leakage of the antigens upon permeabilization of the cell membrane which allows for the passage of labelled SNAP fusion proteins into the cell. After incubation with Fix/Perm buffer, cells were then washed with 2 ml 1x Perm/Wash buffer (BD Biosciences, USA) and centrifuged at 932 x g (Beckman Coulter Allegra™ X-12R) at 932 x g for 5 minutes at room temperature. The supernatant was discarded and 50 µl of the labelled Snap fusion proteins were added into the tubes and incubated for 60 minutes at in the dark at 4°C. After incubation, stained cells were washed with 2 ml Perm/Wash buffer (BD Biosciences, USA)

before being, resuspended in 200 µl of 1x PBS and keep in the dark at 4°C until data acquisition using the BD LSRFortessa™ Cell Analyzer (BD Biosciences, USA).

2.7.3.5 Flow cytometry data analysis

Data analysis was conducted using FlowJo software (version 10.9.0) from BD Biosciences in the USA. This involved creating pseudocolor plots with a specific gating strategy employed. Statistical analysis was performed to generate antibody titration curves for signal-to-noise ratio, staining index, and median fluorescence intensity (MFI) of the stained cells. The signal-to-noise ratio measures the difference in fluorescence between positive and negative cell populations, while the staining index assesses the relative brightness of the fluorochrome detected by the flow cytometer. The following equations were used to calculate the signal to noise ratio and staining index:

Signal-to-noise ratio = MFI (positive population) / MFI (negative population)

Staining index = MFI (positive population) – MFI (negative population) / 2*x Robust standard deviation (negative population)

Thereafter calculation, bar graphs were generated to compare the distribution of antigens across target cell lines. Statistical analyses were performed using Student's t-tests relative to the negative and positive populations to identify any statistically significant differences.

Chapter 3: Results

This study aimed to generate innovative molecules in the form of SNAP-tag fusion proteins, specifically L243(scFv)-SNAP, 2F9(scFv)-SNAP, and 8E2(scFv)-SNAP, designed for the selective diagnosis of AML. This chapter, therefore, describes the design and generation of these SNAP fusion proteins in human embryonic kidney cells (HEK293T), their functional characterisation and in vitro assessment. This chapter is structured as follows: The first two sections (sections **3.1–3.2**) explain the *in silico* expression plasmid design and molecular cloning strategies employed, the next 3 sections (sections **3.3–3.5**) provide a summary of the generation and characterization of these SNAP fusion proteins. The final section (section **3.6**) presents the comparative binding to leukemic cell lines and PBMCs.

3.1 *In silico* engineering and expression plasmid design

During this experiment, new anti-CD14 (2F9), anti-HLA-DR (L243) and anti-MPO (8E2) antibody sequences, were extracted from: HLA-DR (AU2006218454B2), CD14 (CN102260350A), and MPO (Journal PMID:11034396) (228) (229) (230) (231). Afterwards, for evaluation of their heavy and light chain variable region sequences, Ig-BLAST analysis of the sequences, against preexisting immunoglobulin germline variable region gene sequences was carried out using both the IMGT/V-QUEST tool and GenBank for quality control purposes as described in section **2.1**. The results of the analysis indicated a high degree of similarity which was above 95%, between the extracted sequences and the known germline variable region gene sequences as exemplified for the HLA-DR light chain sequence shown in **Figure 12**. Also, this Ig-BLAST analysis confirmed the existence of intact and complete CDRs and FR regions for all the attained v-gene sequences. Subsequently, the homology of their CDR sequences was confirmed by aligning them with their parental sequences using EMBL Clustal Omega tool (available at http://www.ebi.ac.uk) and ExPasy (accessible at https://www.expasy.org).

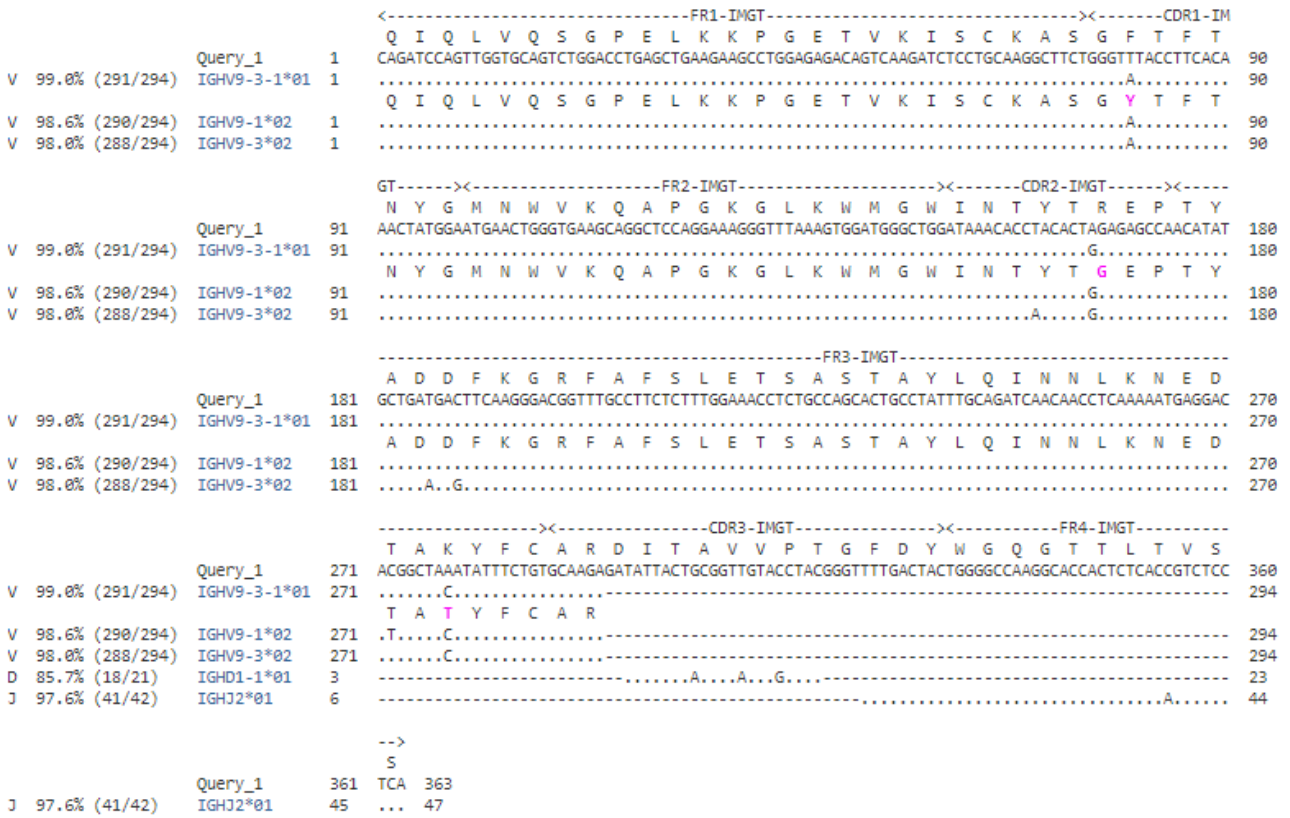

Figure 12. illustrates the results of the IgBLAST analysis performed on the variable heavy chain of anti-HLA-DR antibody (L243) sequences: The extracted v-gene sequences were compared to pre-existing immunoglobulin germline variable region gene sequences. The analysis enabled the identification of both intact CDRs, FR regions and overall sequence homology greater than 95%. Any variations from the germline sequence were highlighted in pink.

The variable heavy chains (VH) of all antibody sequences identified were paired with their corresponding variable light chains (VL) by using a linker sequence, resulting in assembled scFv constructs. These were flanked by *Sfi*1 and *Not*1 restriction sites at their 3'- and 5'-prime ends for molecular cloning purposes. The newly designed scFv(L243), scFv(2F9), and scFv(8E2) sequences were then each inserted into the pCB expression plasmid vector (initially housing AnnexinV-SNAP) through *in silico* restriction enzyme digestions with *Sfi*I and *Not*I. These sequences were subsequently ligated into the pCB-AnnexinV-SNAP digested plasmid yielding the desired pCB-L243(scFv)-SNAP, pCB-2F9(scFv)-SNAP, and pCB-8E2(scFv)-SNAP plasmids (after replacement of the AnnexinV with sequences encoding for the scFv) using SnapGene software (version 3.1.1, GSL Biotech, Chicago) as shown in **Figure 13**.

A. L243 (scFv)-SNAP plasmid map.

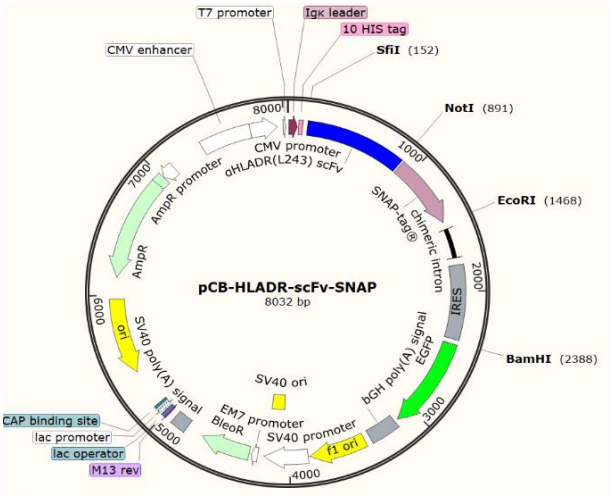

B. 2F9 (scFv)-SNAP plasmid map.

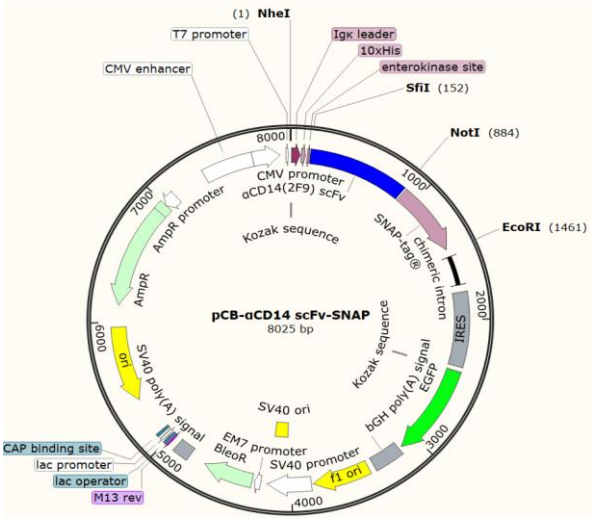

C. 8E2 (scFv)-SNAP plasmid map

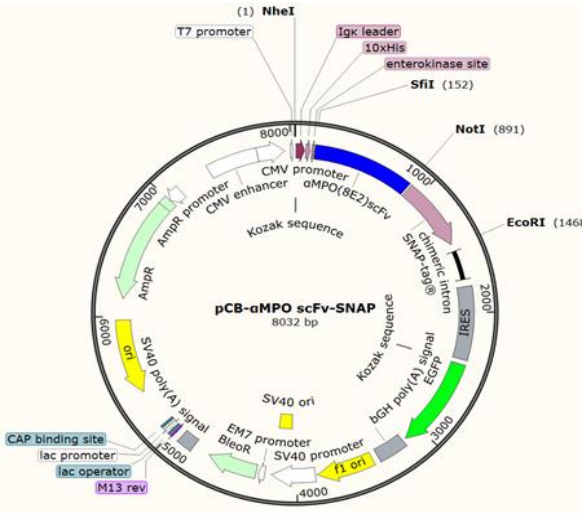

D. Open reading frames (ORFs)

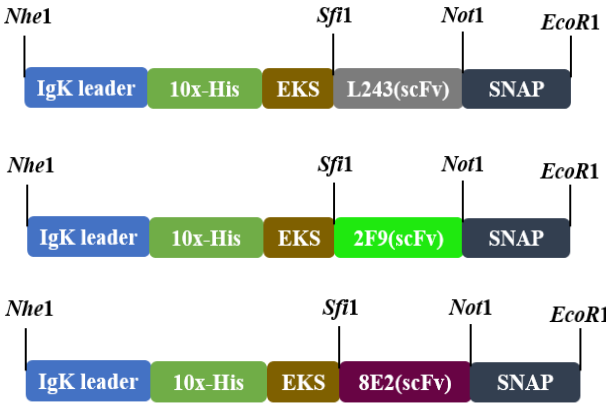

Figure 13. A schematic representation of mammalian expression vectors used in the generation of antibody scFv-SNAP fusion proteins and their corresponding open reading frames (ORFs). The figure includes: **(A)** plasmid map for pCB-L243(scFv)-SNAP, which targets HLA-DR. **(B)** plasmid map for pCB-2F9(scFv)-SNAP, which targets CD14. **(C)** plasmid map for pCB-8E2(scFv)-SNAP, which targets MPO. **(D)** shows the ORFs of the scFv-SNAP fusion proteins.

Table 8. pCB-Antibody (scFv)-SNAP fusion proteins expression plasmid components

Component	Description
1. **Igκ leader:**	A signal peptide that facilitates secretion of the fusion protein into the cell culture supernatant (232).
2. **10His-tag:**	Enables high-affinity binding to Ni^{2+}-chelating resin for purification purposes (233).
3. **Enterokinase site:**	Encodes for cleavage site DDDDK for recognition with specific cleavage proteins (234).
4. **scFv- SNAP-tag®:**	Single-chain variable fragment which binds to specific antigens and is fused to a C-terminal self-labelling SNAP-tag protein (213).
5. **Chimeric intron:**	Efficient and rapid export of mRNA out of the nucleus significantly enhancing transgene expression (235).
6. **IRES:**	Enables the initiation of translation (236).
7. **eGFP:**	Enables the recognition of the translated protein in HEK293T cell (237).
8. **bGH Poly(A) signal:**	Ensures efficient transcription termination and polyadenylation of mRNA (238).
9. **F1 origin:**	Facilitates rescue of single-stranded DNA (239).
10. **SV40 promoter:**	Facilitates high-level expression of the hygromycin resistance gene and allows for episomal replication specifically in cells expressing the SV40 large T antigen (240).
11. **EM7 promoter:**	A promoter of bacterial origin that allows for constant expression of the antibiotic resistance gene in *Escherichia coli* (241).
12. **bleO:**	Bleomycin resistance gene for selection of transfected HEK293T cells (242).
13. **SV40 Poly(A): signal**	Ensures efficient transcription termination and polyadenylation of mRNA (243).
14. **M13 rev:**	A single-stranded oligonucleotide that has 5′-hydroxyl and 3′-hydroxyl ends, along with a selection of four fluorescent labels, and it is commonly used in polymerase chain reaction (PCR) protocols. Another term used for M13 rev is 5′-CAG GAA ACA GCT ATG ACC-3′ (244).
15. **lac operator**	A DNA sequence that binds to the Lac repressor protein, controlling the expression of genes downstream in the lac operon (245).
16. **lac promoter**	Controls transcription of lac operon genes (245).
17. **AmpR:**	The gene providing resistance to the antibiotic ampicillin in *E. coli* used for selection of transformed bacteria (246).
18. **CMV promoter**	DNA regulatory element used for efficient and high-level expression of recombinant protein (247).
19. **T7 promoter**	Allows for in vitro transcription in the sense orientation and sequencing through the insert (248).

3.2 Molecular cloning

3.2.1 Liquid transformation, NucleoBond Midi prep DNA isolation and purification of plasmids from *E. coli*

Plasmids received from GenScript (pUC57-L243(scFv), pUC57-2F9(scFv), and pUC57-8E2(scFv) carrying the open reading frames that encode for all the single chain variable fragments were effectively introduced into competent *E. coli* cells **(**described in section **2.2.1)**. After the plasmids were extracted and purified using the NucleoBond midi prep kit, **Table 9** shows quantification of all pUC57 plasmids following the resuspension of the 4 µg DNA pellets from GenScript, recorded as initial concentration and quantification after bulk-prep which was recorded as final concentration.

Table 9. Quantification of pUC57-scFv plasmids following bulk-prep

Construct	Nuclease-Free Water	Initial Concentration	Final Concentration
pUC57-L243 (scFv)	40 µl	207 ng/µl	2823 ng/µl
pUC57-2F9 (scFv)	40 µl	188 ng/µl	3286 ng/µl
pUC57-8E2 (scFv)	40 µl	229 ng/µl	2317 ng/µl

During quantification, the purity of the bulk-prepped plasmid DNA was evaluated using absorbance values obtained from a spectrophotometer. **Table 10** displays the nucleic acid to protein concentration, 260/280 ratio and 260/230 ratio. All the purified plasmid samples fell within the acceptable ranges between 1.80-1.90 for 260/280 ratio and 2.0-2.2 for 260/230 ratio, confirming that the DNA was pure and suitable for downstream applications **(**section **2.2.2)**.

Table 10. Nucleic acid to protein absorbance ratio using the spectrophotometer

Construct	260/280	260/230
pUC57-L243 (scFv)	1.90	2.21
pUC57-2F9 (scFv)	1.83	2.22
pUC57-8E2 (scFv)	1.85	2.21

3.2.2 Restriction enzyme digestion and agarose Gel electrophoresis

The endonuclease digestion with *Sfi*I and *Not*I restriction enzymes for all the constructs in pUC57 as well as the pCB vector backbone was successfully performed (section **2.2.3**). The use of these enzymes for digestion resulted in sticky ends on both the enconding for the scFv and the pCB vector backbone which allowed for ligation. To separate scFv from the pUC57 backbone as well as, the pCB vector backbone from AnnexinV, an agarose gel electrophoresis was performed (section **2.2.4**). Clear bands of the expected sizes for the digested DNA fragments were observed under UV light, indicating successful digestion as shown in **Figure 14**. The resulting DNA fragments were then purified and subsequently used for ligation.

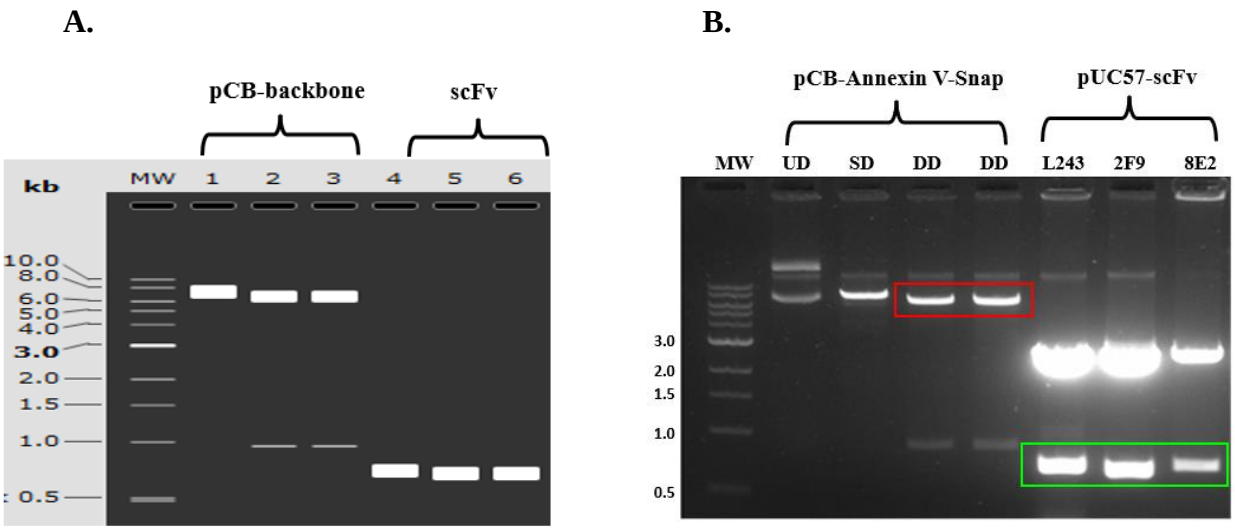

Figure 14. Displays the results of agarose gel electrophoresis after restriction enzyme digestion. (A) Shows a simulation of the expected gel results using SnapGene software. **(B)** Presents the actual gel with a 1 kb DNA ladder used as a molecular weight marker in lane labelled MW. The lanes labelled UD (undigested pCB-AnnexinV-SNAP backbone) with a size of 8234 bp, SD (single digested pCB-AnnexinV-SNAP backbone with *Sfi*1), and DD (double digested with *Sfi*1 and *Not*1) shows pCB vector backbone separated from AnnexinV highlighted in red with a size of 7272 bp. The last four lanes show double digested commercial pUC57 vectors with *Sfi*1 and *Not*1. The bands highlighted in green shows: L243 scFv (753 bp), 2F9 scFv (747 bp) and 8E2 scFv (756 bp).

3.2.3 Gel extraction, ligation, and transformation into *E. coli* cells

After DNA extraction from the agarose gel **(**section **2.2.5)**, ligation of pCB vector backbone with the insert DNA on a 1:1 and 1:5 (vector to insert) ratios (section **2.2.6**) and bacterial transformation into *E. coli* cells **(2.2.7)**. Positive colony growth was observed on ampicillin-supplemented plates, containing the ligated plasmids as illustrated in **Figure 15.** On the other hand, the digested pCB-backbone only and bacteria control showed no growth, confirming that the ligation was successful and bacterial growth was determined by the presence of ampicillin resistance in the ligated plasmids.

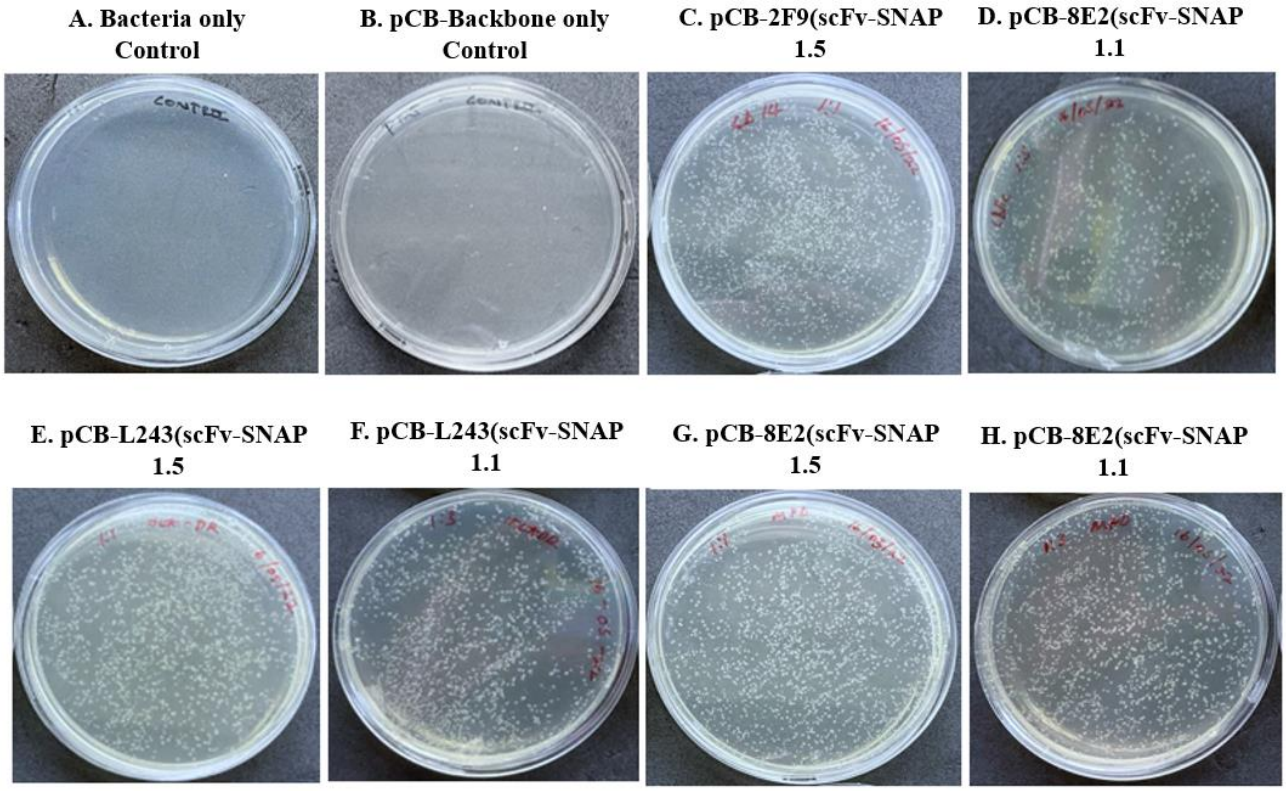

Figure 15. Shows the growth of *E. coli* cells transformed with potential recombinant plasmid DNA. Different ratios of vector to insert were used in the transformation: 1:1 and 1:5. **(A)** Bacteria only contamination control. **(B)** pCB-vector backbone-only control to evaluate the efficiency of restriction digestion and the presence of partial digestion. **(C and D)** Shows pCB-2F9(scFv)-SNAP vector to insert ligation ratios 1:1 and 1:5 respectively. **(E and F)** Shows pCB-L243(scFv)-SNAP ligation ratios vector to insert ligation 1:1 and 1:5 respectively. **(G and H)** Shows pCB-8E2(scFv)-SNAP ligation ratios vector to insert ligation 1:1 and 1:5 respectively.

Further analysis on transformation efficiencies showed that the lowest vector to higher insert DNA ratio resulted in the most successful ligation as shown in **Table 11**. This suggests that a lower ratio of vector to insert may be more efficient for ligation in this system.

Table 11. Ligation and total number of colonies after transformation

Ligation Product	Ligation Ratio	Backbone Mass (pCB-SNAP)	Insert Mass (scFv)	Transformation efficiencies (cfu/µg)
1. pCB-2F9-SNAP	1:1	50 ng	5.13 µg	1.97 x10^3
	1:5	50 ng	25.68 µg	2.36 x10^3
2. pCB-L243-SNAP	1:1	50 µg	5.18 µg	2.06 x10^3
	1:5	50 µg	25.93 µg	2.43 x10^3
3. pCB-8E2-SNAP	1:1	50 µg	5.19 µg	2.25 x10^3
	1:5	50 µg	25,9 µg	2.97 x10^3
4. pCB-Backbone Only Control	1:0	50 µg	0	0

3.2.4 Restriction Mapping

Because of these ideal results in comparison to the controls, a total of six colonies were picked per construct in each plate and used for restriction mapping (section **2.2.9**). The results of the restriction mapping analysis showed successful cloning of the recombinant plasmids. A combination of different restriction enzymes was used to map specific locations on the plasmids and the resulting fragments were separated using agarose gel electrophoresis. The pattern of fragments and band sizes observed on the gel matched the expected pattern based on the simulated agarose gel image generated using the SnapGene software, confirming the successful incorporation of inserts into the pCB-backbone (**Figure 16).**

.

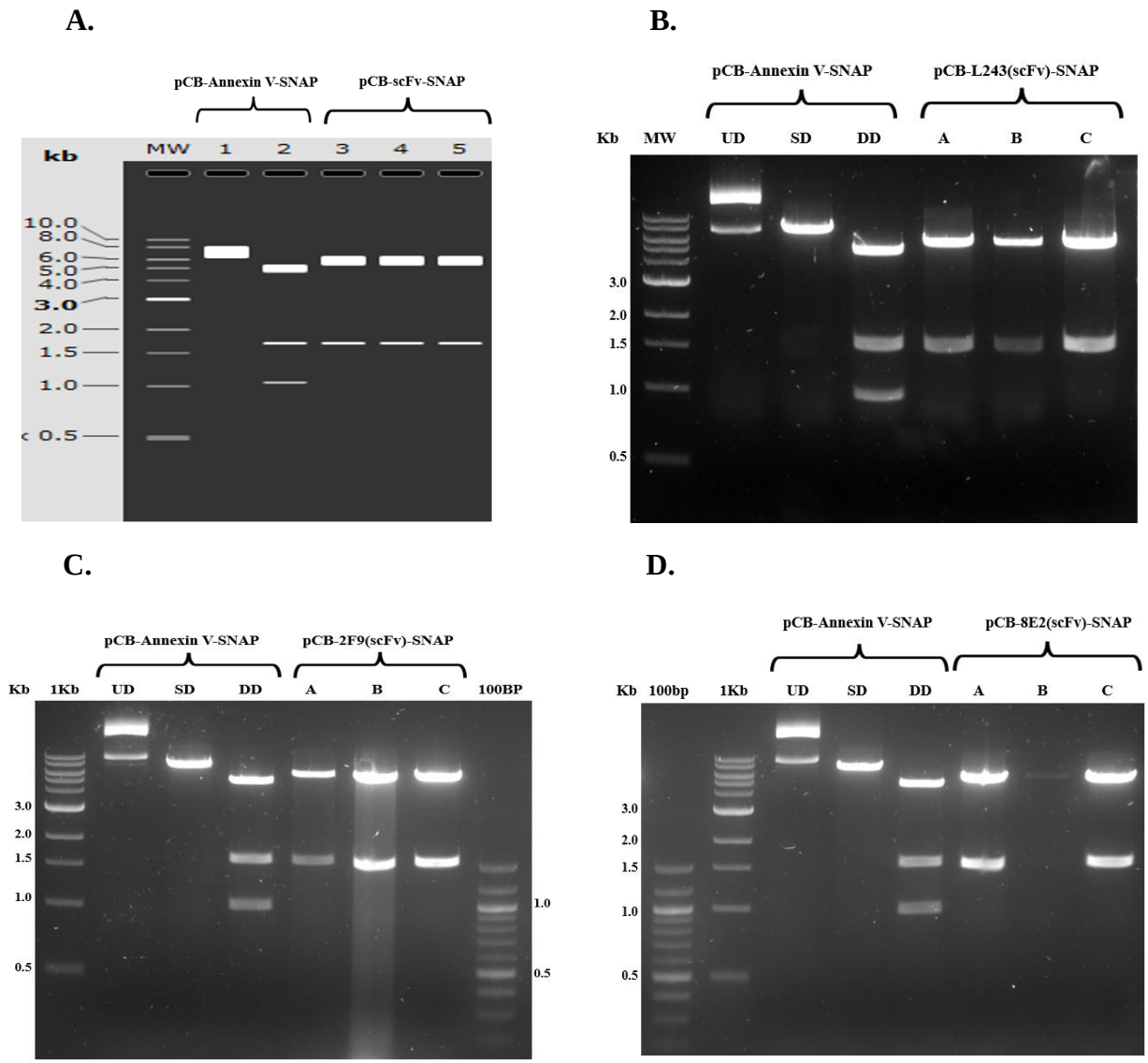

Figure 16. Comparison between a simulated agarose gel image generated using the SnapGene software and actual 1.2% agarose gel images. (A) Shows a simulated agarose gel image indicating what was expected from the actual gel. **(B, C** and **D**) Shows the actual 1.2% agarose gel images of pCB-Annexin V-SNAP, pCB-L243-SNAP, pCB-2F9-SNAP, and pCB-8E2-SNAP obtained after restriction endonuclease digestion using *Blp*1 and *Pme*1 enzymes respectively. The lanes labelled UD (undigested pCB-AnnexinV-SNAP backbone) with a size of 8032bp, SD (single digested pCB-AnnexinV-SNAP backbone with *Pme*1), and DD shows double digested pCB-Annexin V-SNAP plasmid with *Pme*1 and *Blp*1, this produced three bands of sizes 5312 bp, 1675 bp, and 1045 bp. For the pCB-L243-SNAP plasmid, the expected band sizes after digestion with *Pme*1 and *Blp*1 were 6357 bp and 1675 bp, as shown in lanes A-C of the gel on **B**. Secondly, The expected sizes of pCB-2F9-SNAP digested with *Pme*1 and *Blp*1 were 6357 bp and 1675 bp, as shown on **C**. Lastly, the expected sizes of pCB-8E2-SNAP digested with *Pme*1 and *Blp*1 were 6357 bp and 1675 bp, as shown on **D**.

3.2.5 Plasmid DNA sequencing.

The positive clones from restriction mapping were sent to Inqaba Biotechnical Industries for Sanger sequencing of recombinant plasmid DNA (section **2.2.10**). To aid in the sequencing of the cloned product the universal SNAP reverse primer, universal T7 promoter and universal SNAP internal forward primers were used for sequencing and the resulting sequences were analysed using SnapGene software (version 3.1.1, GSL Biotech, Chicago). **Figure 17** depicts the plasmid maps that were created. All clones were nearly identical (approximately 100% homology) to their *in silico* ORF sequences, confirming correct ligations for all constructs generated (section **3.1**).

A. pCB-L243(scFv)-SNAP

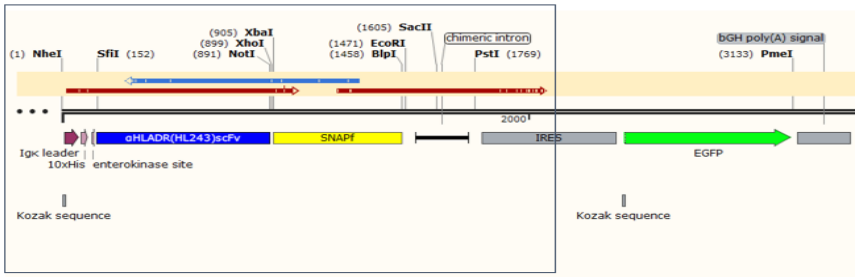

B. pCB-2F9(scFv)-SNAP

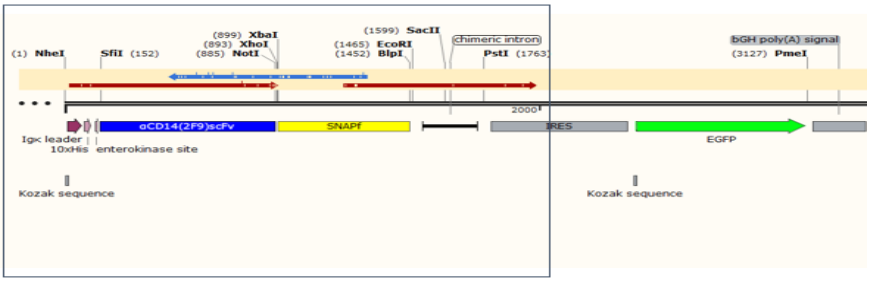

C. pCB-8E2(scFv)-SNAP.

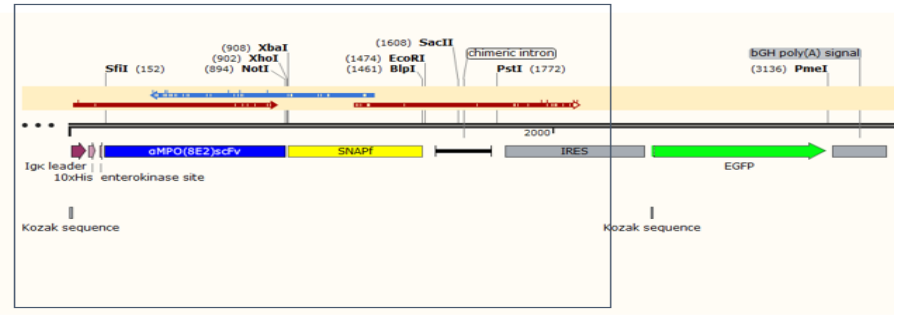

Figure 17. Plasmid maps produced after aligning sequences received from Sanger sequencing with the corresponding *in silico* sequences. (A) pCB-L243(scFv)-SNAP plasmid map, **(B)** pCB-2F9(scFv)-SNAP plasmid map and **(C)** pCB-8E2(scFv)-SNAP map. The red arrows indicate the forward primers and the blue arrows indicate the reverse primers.

3.3 Expression of the fusion proteins in HEK 293T cells

Following confirmation of the ORF sequence, recombinant plasmids (pCB-L243(scFv)-SNAP, pCB- and pCB-8E2(scFv)-SNAP) were transfected into HEK 293T cells as described in **2.3.2**. Positively transfected cells were identified by visualisation of cytosolic enhanced green fluorescent protein (eGFP) expression using a ZOE™ Fluorescence Cell Imager (Bio-Rad, USA). Flow cytometry was then used to quantitatively assess the transfection efficiencies of recombinant plasmids into HEK293T cells (section **2.3.3**). As shown in **Figure 18** the transfection efficiencies after analysing the frequencies of eGFP positive cells were: pCB-L243(scFv)-SNAP (68.8%), 2F9(scFv)-SNAP (70.6%), and pCB-8E2(scFv)-SNAP (67.2%).

A. 2F9(scFv)-SNAP **B. L243(scFv)-SNAP** **C. 8E2(scFv)-SNAP** **D. Non-transfected control**

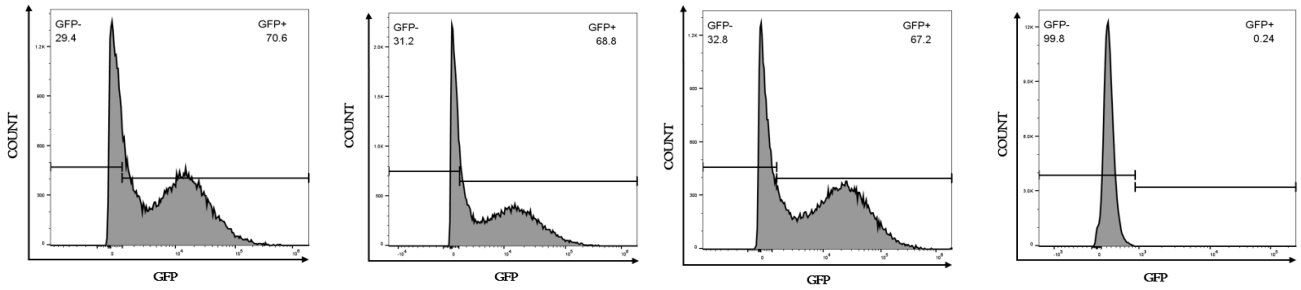

Figure 18. Flow cytometry plots depicting the eGFP expression profiles of transfected HEK293T cells. (A) Represents the eGFP expression profile for L243(scFv)-SNAP, **(B)** Represents the eGFP expression profile for 2F9(scFv)-SNAP, **(C)** Represents the eGFP expression profile for 8E2(scFv)-SNAP and **(D)** Represents the eGFP expression profile of HEK293T cells non-transfected control.

To enrich the transfected eGFP-positive cell population carrying the bleomycin resistance gene, zeocin selection was used. The first round of zeocin selection was carried out with a 100 µg/ml concentration of the antibiotic for a period of four weeks, followed by a one-week break. After the break, a second round of zeocin was added at a concentration of 150 µg/ml for two weeks. As a result, the eGFP expression was enhanced and the cells were grown until the cell culture supernatant containing the target fusion proteins was ready for collection four days after the last round of zeocin and 8 weeks post transfection (**Figure 19**).

A. L243(scFv)-SNAP

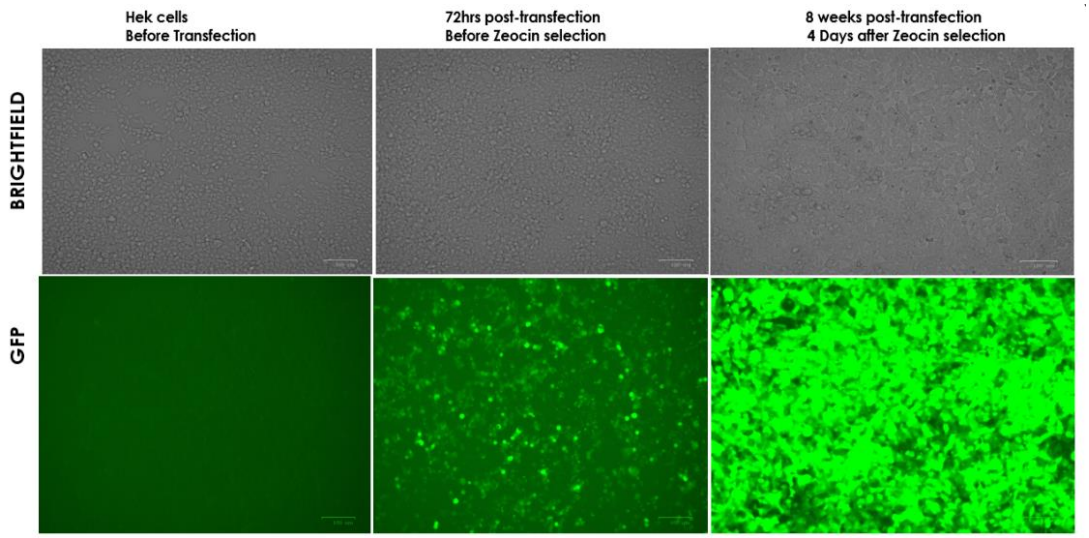

B. 2F9(scFv)-SNAP.

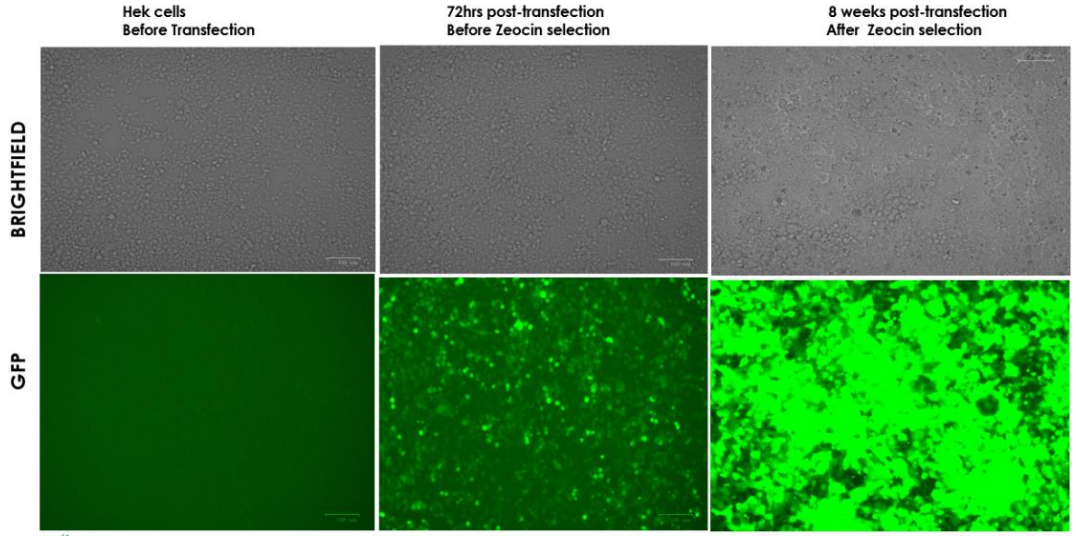

C. 8E2(scFv)-SNAP.

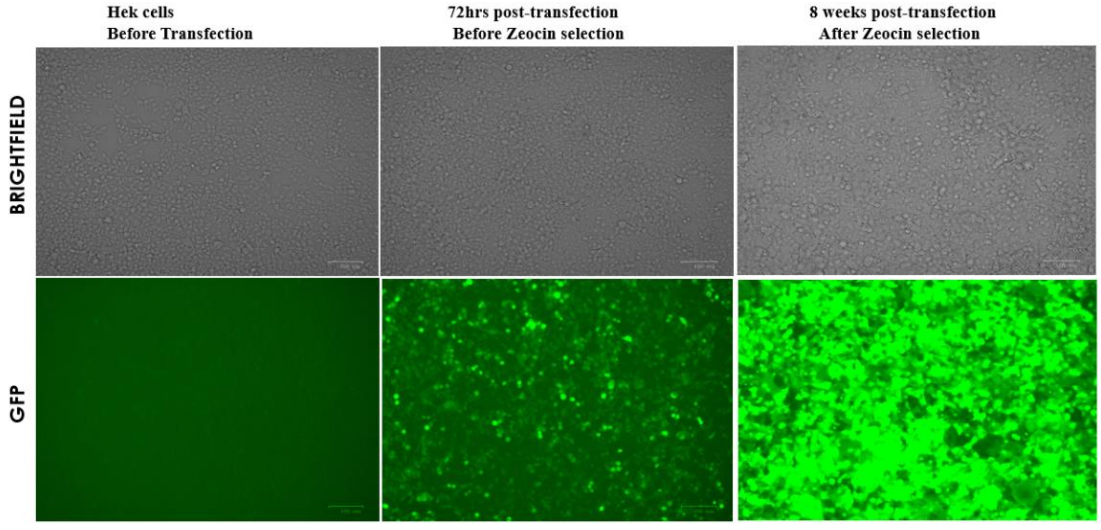

Figure 19. eGFP expression in HEK293T cells transfected with the recombinant plasmids. (A) pCB-L243 (scFv)-SNAP, **(B)** pCB-2F9(scFv)-SNAP and **(C)** pCB-8E2(scFv)-SNAP. Images were captured in both brightfield (no green florescence) and greenfield (eGFP expression). The images were taken at varying stages of cell culture: before transfection (without eGFP expression on the green field), 72 hours post-transfection with the recombinant plasmids before zeocin selection (with the green fluorescence on the green field) and 8 weeks post-transfection and 4 days after zeocin selection (with enhanced green fluorescence).

3.4 Purification of scFv-SNAP recombinant fusion proteins

After collecting a total of 1 litre cell of culture supernatant for all the constructs, immobilised affinity chromatography (using the N-terminal 10His-tag) was used to enrich fusion proteins from cell culture supernatant (section **2.4.1**). This method utilizes the use of immobilised metal ion (Nickel ion: Ni^{2+}) affinity beads and the SNAP fusion proteins have the N-terminal 10 His-tag which has affinity for Ni^{2+}. Because of this reason, recombinant proteins specifically bound to the column (Ni^{2+}). Following that, the elution of recombinant SNAP fusion proteins from the column was achieved by using imidazole, which has a higher affinity for Ni^{2+} than the 10 His-tag. This led to a competitive binding scenario between SNAP fusion proteins and imidazole, resulting in the displacement of SNAP fusion proteins from the column during the elution process. The collection of eluted fractions containing the SNAP fusion proteins was continuously monitored at a wavelength of 280 nm (**Figure 20**).

A. L243(scFv)-SNAP IMAC Chromatogram.

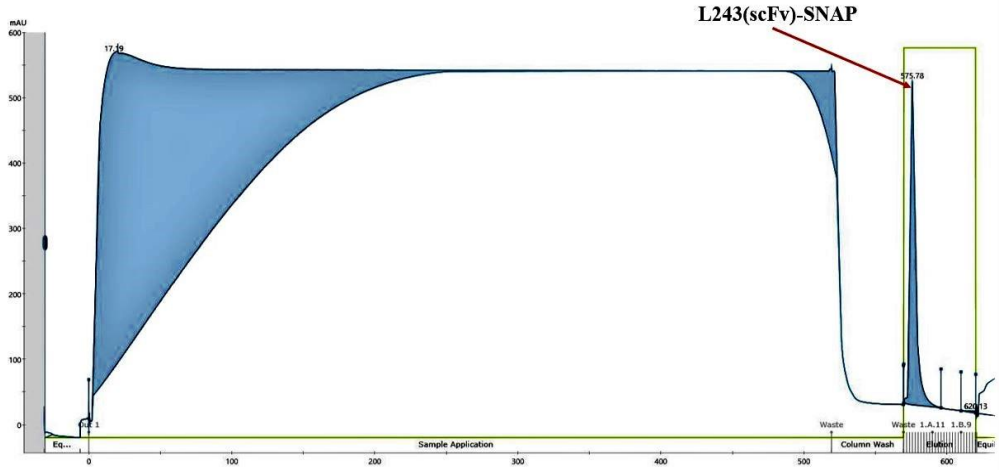

B. 2F9(scFv)-SNAP IMAC Chromatogram.

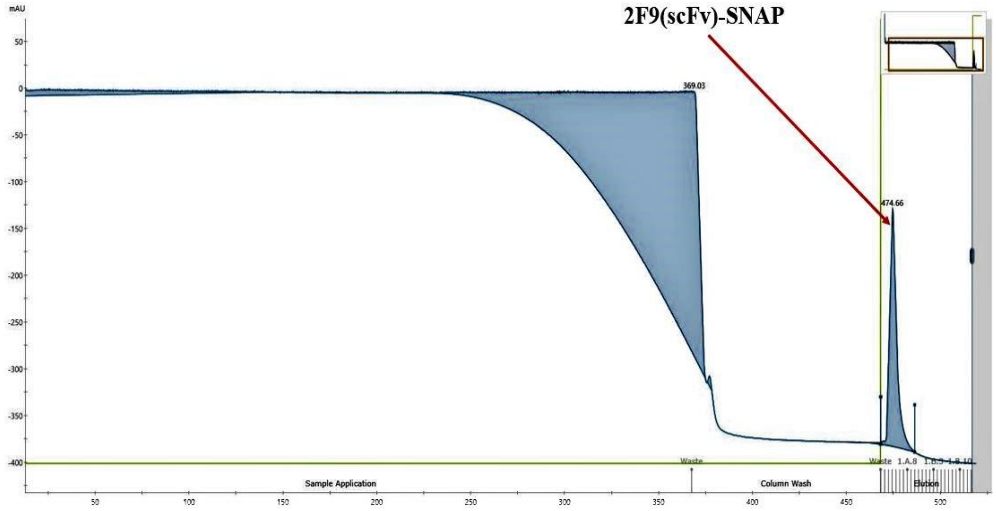

C. 8E2(scFv)-SNAP IMAC Chromatogram.

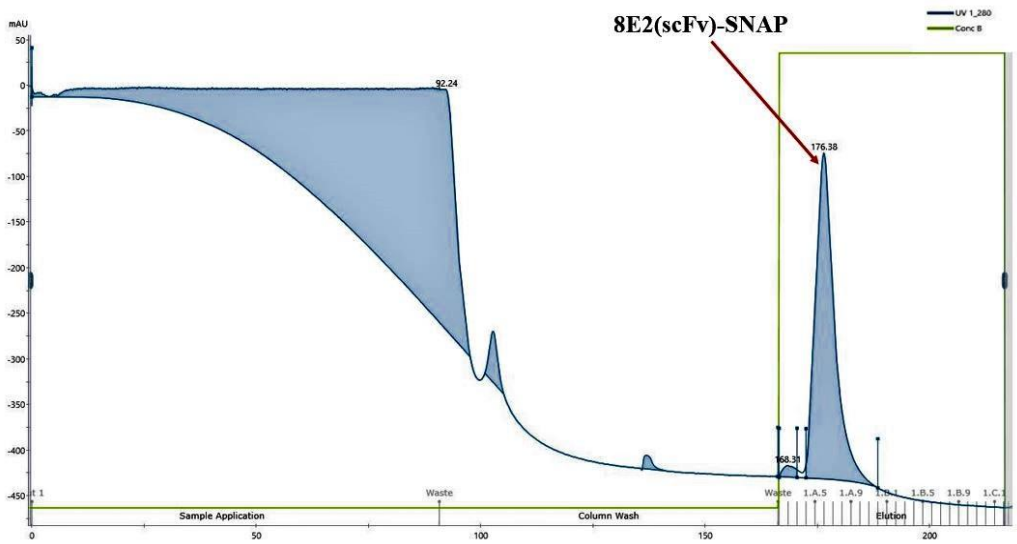

Figure 20. IMAC-purified chromatograms of three different fusion proteins. (A)L243(scFv)-SNAP, **(B)** 2F9(scFv)-SNAP and **(C)** 8E2(scFv)-SNAP. The y-axis represents the elution buffer percentage, indicating the strength of the elution buffer used. On the x-axis, we have the AKTA flow-through volume, which corresponds to the progression of time during the purification process. The blue line in each chromatogram represents the elution profile of the respective fusion protein, indicating its release from the column. The green line represents the imidazole concentration gradient applied during the purification process. The initial peaks seen in blue in each chromatogram represent the removal of contaminating proteins during the sample application stage using 10 mM imidazole, followed by a column washing step with 4 0mM imidazole and the red arrows indicate the elution peaks of the SNAP fusion proteins. The final elution step was performed using 250 mM imidazole which allowed for the specific release of the target fusion proteins from the column.

3.4.1 SDS-PAGE analysis of IMAC fractions

The fractions corresponding to each individual peak on the chromatogram were subjected to sodium dodecyl sulphate polyacrylamide gel electrophoresis (SDS-PAGE) to identify protein bands corresponding to the theoretical sizes of L243(scFv)-SNAP (51.26 kDa), 2F9(scFv)-SNAP (51.18 kDa) and 8E2(scFv)-SNAP (51.92 kDa) (section **2.4.2**). Using the protein molecular weight ladder, the thick bands observed at around 55 kDa of the 10% SDS gel were predicted to be our protein of interest (**Figure 21)**.

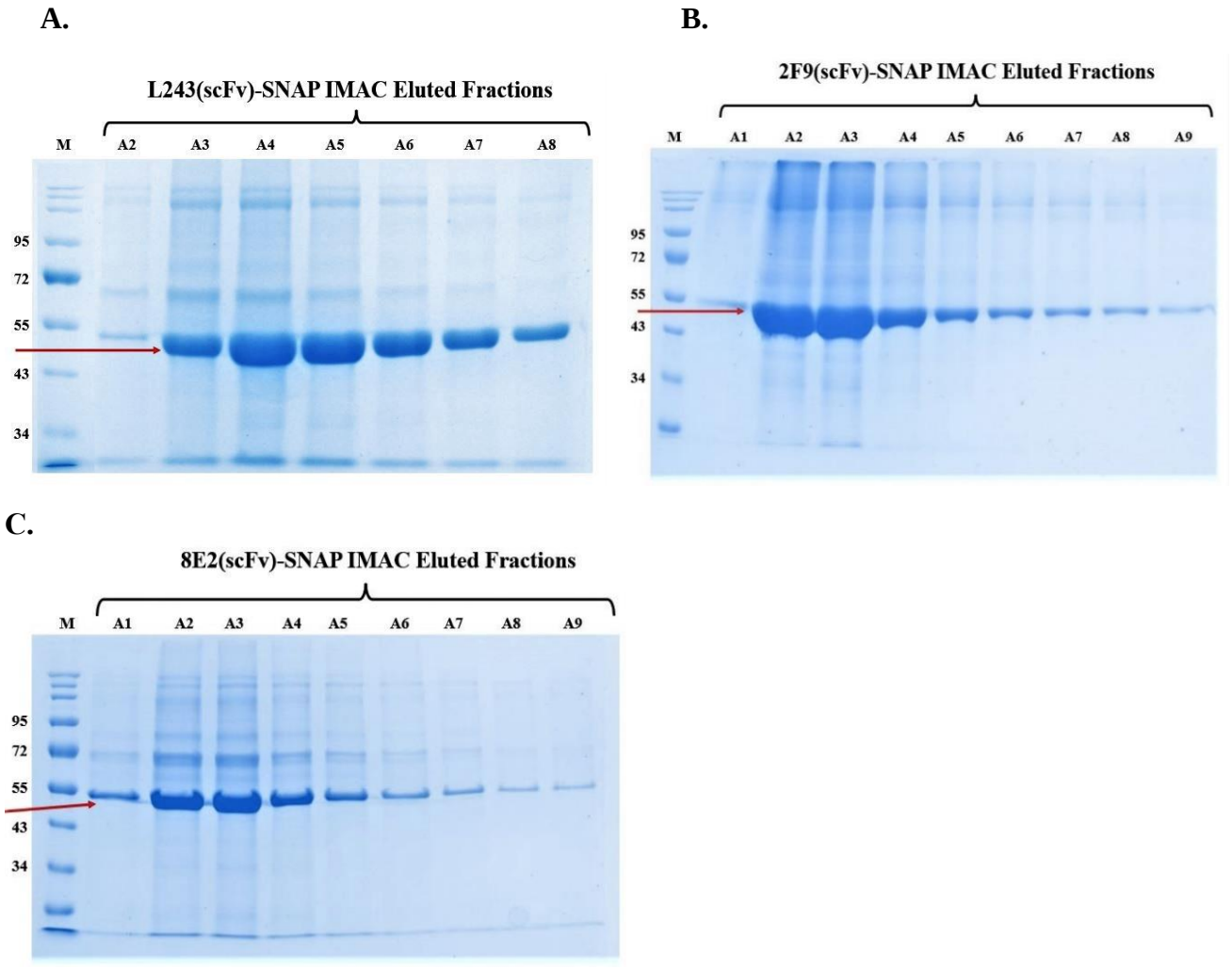

Figure 21. SDS-PAGE analysis of scFv-SNAP protein fractions from pre-concentrated IMAC eluates. (A) L243(scFv)-SNAP (51.26 kDa), **(B)** 2F9(scFv)-SNAP (51.18 kDa) and **(C)** 8E2(scFv)-SNAP (51.92 kDa). The molecular weight of the protein in each band was determined using a protein ladder (M). The red arrows indicate SNAP fusion proteins with a molecular weight around 55 kDa and the black arrows indicate fractions of elution peaks screened for the presence of the proteins of interest.

3.4.2 Densitometric quantification of concentrated purified protein fractions

Firstly**,** contaminating proteins that had a molecular weight above 100 kDa were removed using an Amicon column with a 100 kDa MWCO as described in section **2.5.1**. Following that, protein fractions from IMAC elution were then concentrated using an Amicon column with a 10 kDa molecular weight cut-off. Subsequently, concentrated proteins were first quantified using a Denovix NanoDrop™ ND-2000 (Thermo Fisher Scientific, USA), which measures the total protein content within the sample including contaminating proteins. As a second quantification step specific to SNAP fusion proteins, densitometry was used to determine the actual amount of SNAP fusion proteins in a sample and this also allowed for the calculation of percentage purity **(Table 12**). For this purpose, a two-fold serial dilution of the BSA standard protein was prepared and alongside with 5 µl of the concentrated proteins were loaded and run on a 10% SDS-PAGE gel **(Figure 22)**.

A. L243(scFv)-SNAP

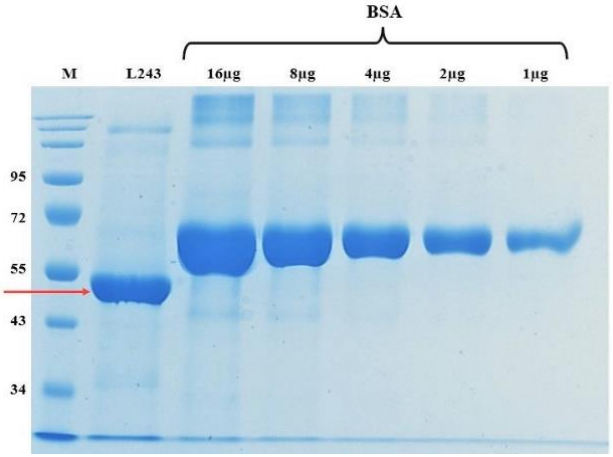

B. 2F9(scFv)-SNAP

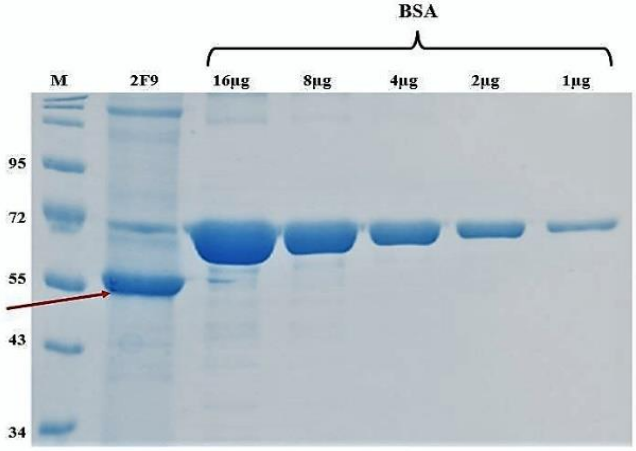

C. 8E2(scFv)-SNAP

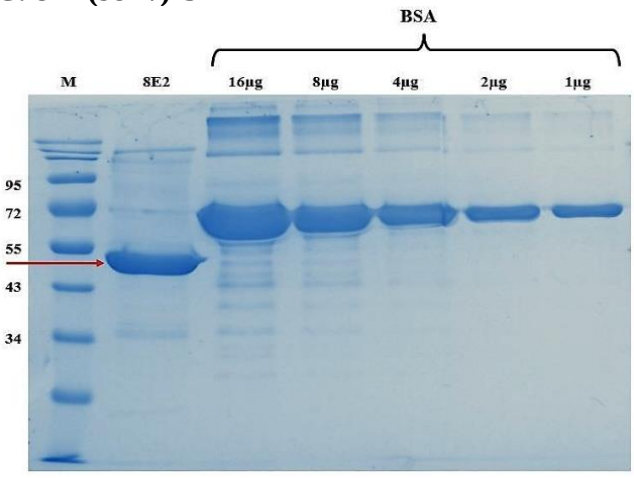

Figure 22. Estimation of protein concentration from an SDS-PAGE gel using densitometry. (A) L243(scFv)-SNAP, **(B)** 2F9(scFv)-SNAP and **(C)** 8E2(scFv)-SNAP. The red arrows indicate SNAP fusion proteins and the black arrows indicate the BSA standard protein with a twofold serial dilution.

3.4.3 Generation of a BSA standard curve for determining the protein concentration

Aqua stained SDS-PAGE gel images were analysed using ImageJ (NIH) software, a public domain program from the National Institutes of Health that allows image processing. This software was used to measure the optical colour intensity for BSA standard protein bands and as a result, a BSA standard curve was generated using Microsoft Excel **(Figure 23).**

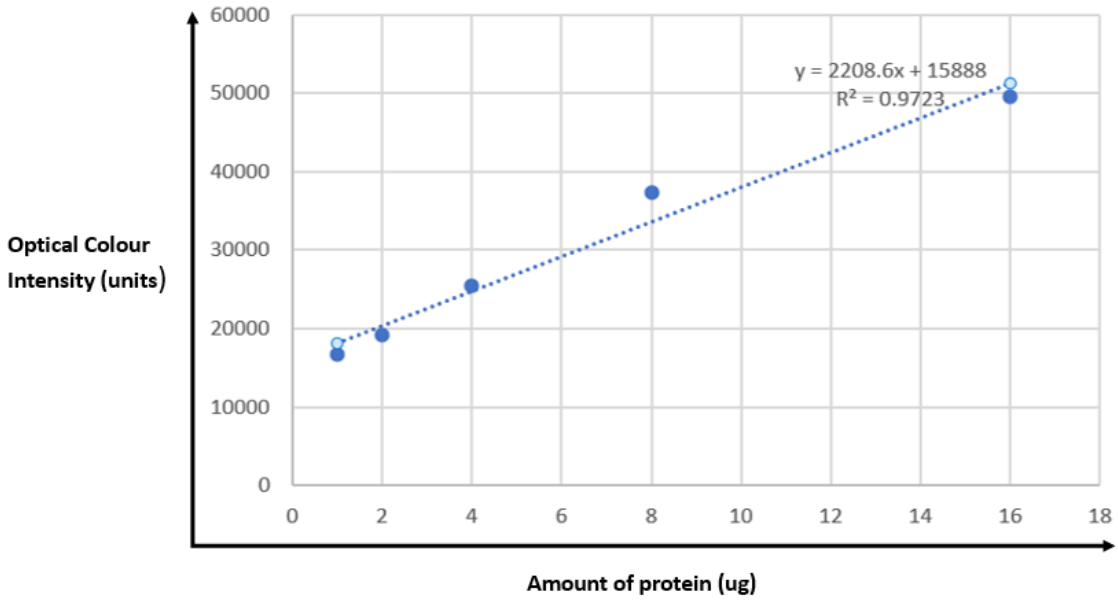

Figure 23. Development of a BSA standard curve for determining the protein concentrations. Following the measurement of optical colour intensity for the BSA standard bands (using ImageJ software), a graph of optical colour intensity (in units) versus the corresponding amount of protein (in µg) was created. The amount of SNAP fusion proteins in the total protein sample was estimated using the resulting graphical equation, allowing determination of the protein yield and percentage purity **(Table 12).**

The protein yield and percentage purity determined by densitometry data varied across constructs as shown in **Table 12**. L243(scFv)-SNAP had the highest yield with 16.1 mg/l, followed by 2F9(scFv)-SNAP with 12.4 mg/l and lastly 8E2(scFv)-SNAP with 8.9 mg/l of purified cell culture supernatant, suggesting that the cells producing L243(scFv)-SNAP were more confluent and efficient in protein production compared to others.

Table 12. Determination of the percentage purity and total full length protein yield

Sample volume	Peak Area	Densitometry Concentration	Denovix NanoDrop Concentration	%Purity	Total Protein Purified
5 µl L243(scFv)-SNAP	25467.43	4.3 µg/µl	6.7 µg/µl	61	16,1 mg/l
5 µl 2F9(scFv)-SNAP	24698.78	4.0 µg/µl	7.1 µg/µl	56.3	12.4 mg/l
5 µl 8E2(scFv)-SNAP	22765.57	3.1 µg/µl	5.6 µg/µl	55.4	8.9 mg/l

3.5 Confirmation of full-length protein by Western blot analysis and conjugation

3.5.1 Western blot analysis

Following protein quantification, western blot analysis was used to confirm the presence of a functional 10 His-tag on the N-terminus of scFv-SNAP fusion proteins as described in section **2.5.2**. The His-tag protein was detected by chemiluminescence using an anti-His-tag antibody conjugated to HRP. As shown in **Figure 24**, two identical SDS PAGE gels were run and the first one was stained with aqua stain, whereas the second one was transferred onto the PVDF membrane for western blot analysis and all SNAP fusion proteins were confirmed to have the 10 his-tag.

A. L243(scFv)-SNAP **B. 2F9(scFv)-SNAP**

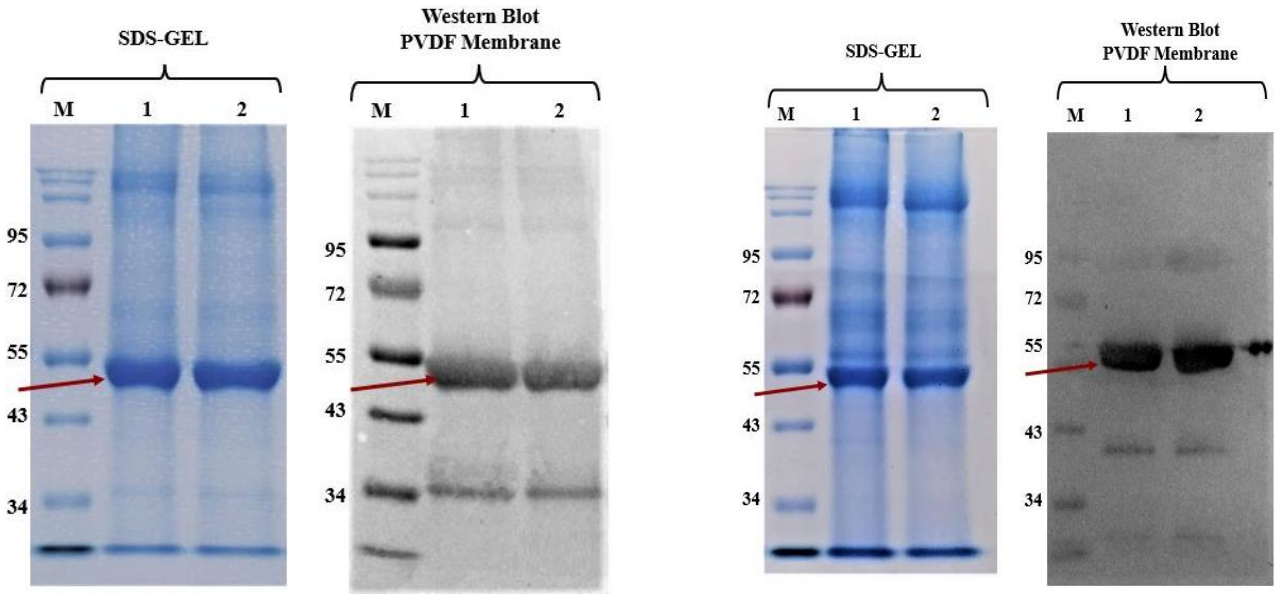

C. 8E2(scFv)SNAP

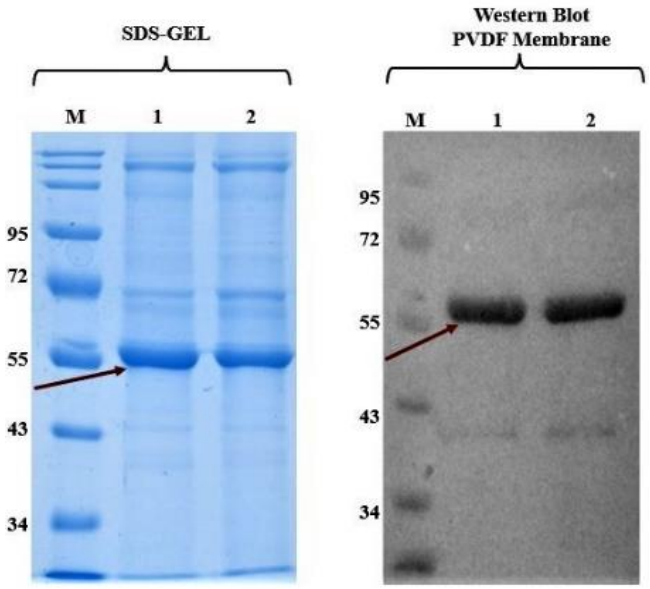

Figure 24. Confirmation and analysis of a functional 10 His-tag on the N-terminus of scFv-SNAP fusion proteins. (**A**) Anti-HLA-DR antibody L243(scFv)-SNAP, (**B)** Anti-CD14 antibody 2F9(scFv)-SNAP and (**C**) Anti-MPO antibody 8E2(scFv)-SNAP. Proteins were analysed using western blot by using an anti-His antibody and a secondary anti-Goat-Rabbit HRP antibody. These were used to detect the proteins after they had been successfully transferred onto the PVDF membrane. On both the SDS-GEL and the membrane lane (M) is the molecular weight ladder, Lane 1 and 2 contains the tested scFv-SNAP fusion proteins in two replicas. The red arrows indicate the scFv-SNAP fusion proteins.

3.5.2 Conjugation of the generated SNAP fusion proteins to BG-modified substrates

After confirmation of the 10His-tag by western blot on the N-terminus of the SNAP fusion proteins, conjugation with BG-Alexa Fluor 488 was used to confirm for the presence of functional SNAP-tag enzyme on the C-terminus (section **2.6**). The conjugated proteins were run on an SDS gel and exposed to blue light (380-500nm wavelength). Since Alexa Fluor 488 is excitable at a 488nm wavelength, which falls within the blue light spectrum. All the generated SNAP fusion proteins were successfully conjugated with Alexa Fluor 488 as shown in **Figure 25.**

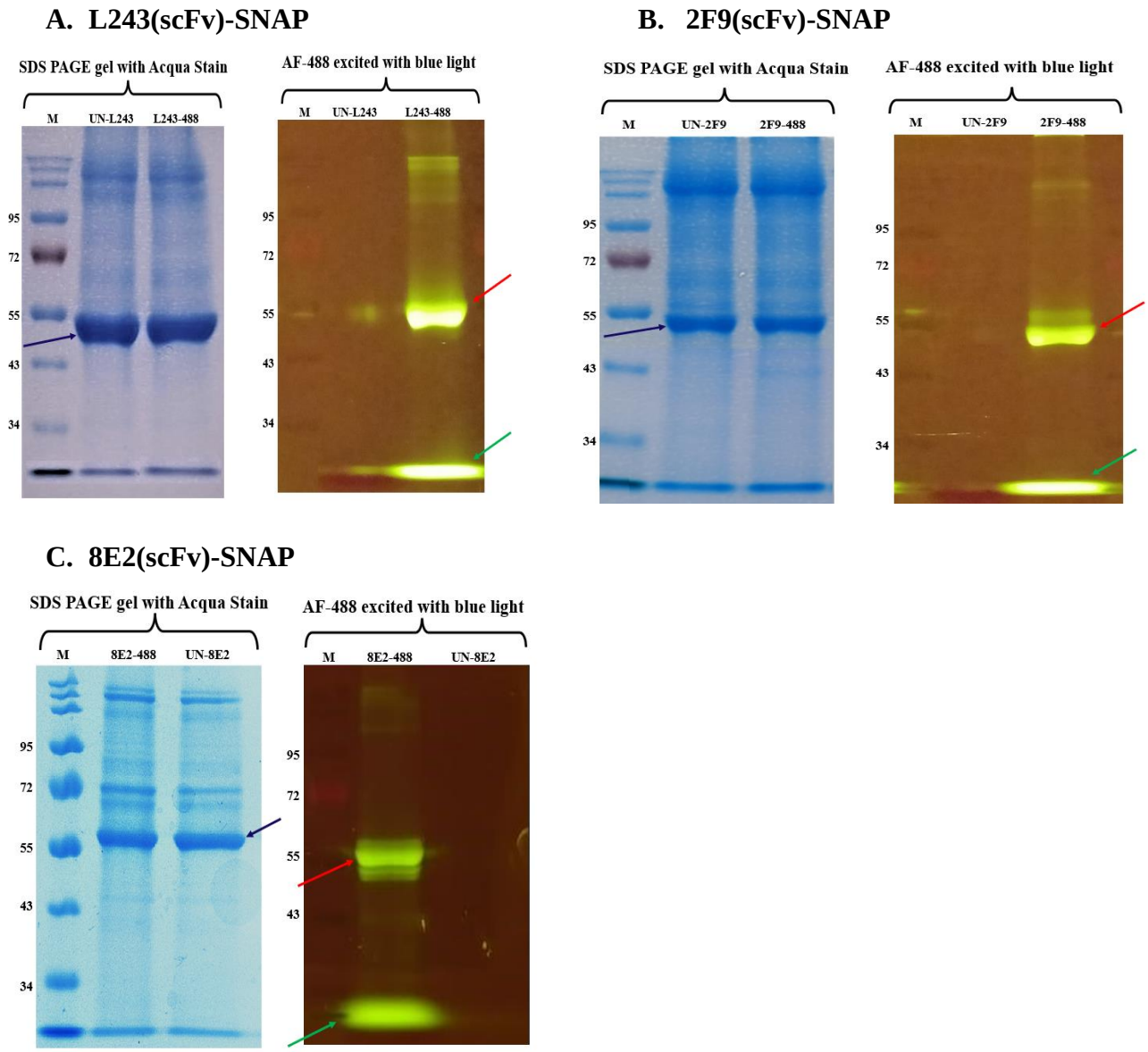

Figure 25. Conjunction of the SNAP fusion proteins to BG-Alexa Flour 488. (A) L243(scFv)-SNAP, **(B)** 2F9(scFv)-SNAP, and **(C)** 8E2(scFv)-SNAP. The lanes labelled (M) indicate the molecular weight ladder. The blue arrows indicate the unconjugated scFv-SNAP fusion proteins used as controls (UN-L243, UN-2F9 and UN-8E2). The red arrows indicate the BG Alexa Four 488 conjugated scFv-SNAP fusion proteins exposed to blue light, enabling the excitation of the fluorophore at a 488nm wavelength. The green arrows indicate excess BG-Alexa Flour 488 showing complete saturation of the SNAP enzyme with the substrate.

3.6 Analysing the binding abilities of SNAP fusion proteins conjugated to BG-Alexa Fluor 488 and BG-Alexa Fluor 647 to antigen positive cells

3.6.1 Confocal microscopy

Confocal microscopy imaging was used to test for the binding abilities of the newly generated anti-CD14 antibody 2F9(scFv)-SNAP conjugated to Alexa Flour 647 using THP-1 cell line (section **2.7.2.1**). The antibody specifically bound to CD14 on the surface of antigen-positive cells (THP-1 cell line) in a punctate pattern since the antigen was expressed on the THP-1 cells in a clustered or patchy manner. On the other hand, there was no binding observed on HEK 293T cells, which do not express the CD14 antigen as shown in **Figure 26A**. Similarly, HL60 cells were used to test for the binding abilities of anti-MPO antibody 8E2(scFv)-SNAP conjugated to Alexa Flour 647 (section **2.7.2.2**). The antibody specifically bound to MPO in the cytoplasm of HL60 cells in a granular pattern corelating to the packaging of MPO in lysosomes. HEK 293T cells, which are MPO negative did not show any signal when incubated with the antibody (**Figure 26B)**.

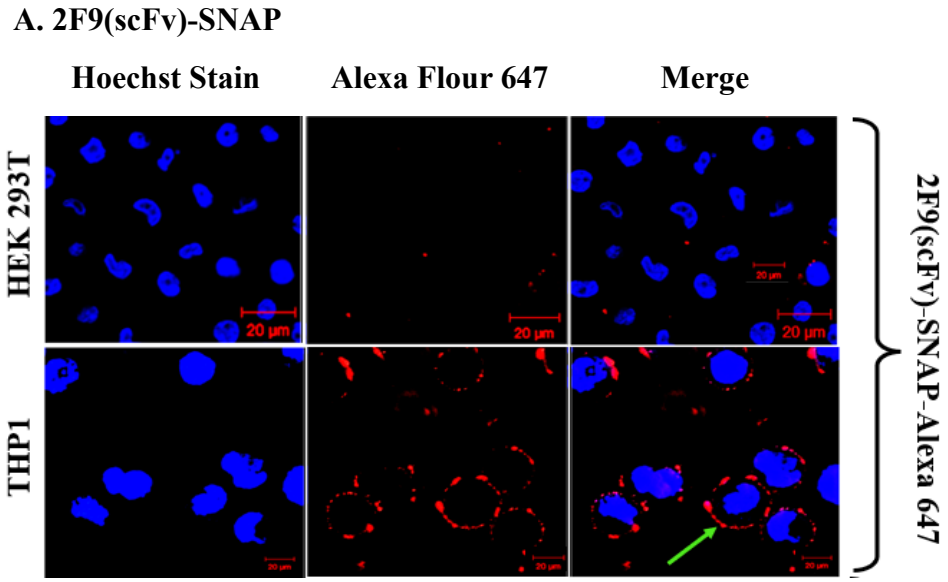

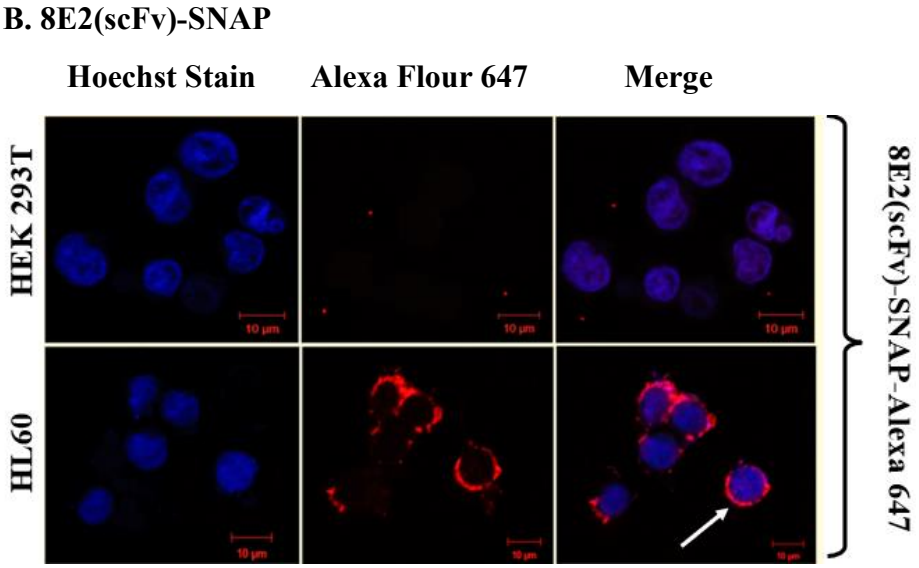

Figure 26. Confocal microscopy imaging of cell surface CD14 positive and intracellular MPO. (A) shows HEK 293T cells which are CD14 negative and THP-1 cells expressing CD14 incubated with 2F9(scFv)-SNAP conjugated to Alexa Flour 647. The blue signal indicates the Hoechst nuclei stain (1:5000 dilution in media) and the red signal indicated by the green arrow indicates the surface binding of 2F9(scFv)-SNAP-Alexa Flour 647 to CD14 on the surfaces of THP-1 cells. **(B)** HEK 293T cells which are MPO negative and HL60 cells expressing MPO were incubated with 8E2(scFv)-SNAP conjugated to Alexa Flour 647. The blue signal indicates the Hoechst nuclei stain and the red signal indicated by the white arrow shows the binding activity of 8E2(scFv)-SNAP-Alexa Flour 647 on MPO. All the images were captured using a Zeiss confocal-scanner microscope (LSM880) with Airyscan at magnifications of 20 µm and 10 µm.

3.6.2 Flow cytometry

To further confirm the binding activity and the signal observed from confocal imaging, the newly generated anti-CD14 antibody 2F9(scFv)-SNAP, anti-MPO antibody 8E2(scFv)-SNAP and anti-HLA-DR antibody L243(scFv)-SNAP were conjugated to Alexa Fluor 488 and used for flow cytometry staining. THP-1 cells (CD14+) were stained for CD14 using 2F9(scFv)-SNAP and HL60 cells were stained for MPO using 8E2(scFv)-SNAP. An anti-CD33 hP67.6(scFv)-SNAP antibody conjugated to BG Alexa Fluor 488 (already available at MB&I) was used as a positive control for both THP-1 cells and HL60 cells since they express the CD33 cell surface receptor (249) (250) while HEK 293T cells served as the negative control for CD14 and MPO since they lack the target antigens. PBMCs were stained for HLA-DR using the L243(scFv)-SNAP antibody, with a focus on B cells, which are HLA-

DR positive but CD4 negative. The parental murine version of anti-HLA-DR L243 antibody (Biolegend, USA) was used as a positive control and the anti-CD4 antibody SK3 (Biolegend, USA) was used as a B cells negative control (251).

3.6.2.1 Determining the ideal concentrations of 2F9(scFv)-SNAP-AF 488 for CD14 staining

Following a twofold antibody titration as described in section **2.7.3.1**, ideal antibody concentrations for staining CD14 on THP-1 cells and HEK 293T cells (CD14 negative cells) were determined by taking into consideration factors including: (i) the MFI values indicating the fluorescence intensity of the stained cells and higher values suggest stronger signal intensity, (ii) signal-to-noise ratio which measures the difference in fluorescence between the CD14 negative and positive cell populations, (iii) Staining Index which is a normalised measure of staining performance that considers both signal and background noise (usually from cell auto-florescence), and (iv) frequencies indicating the percentage of both the CD14 negative and positive cells. **Figure 27** shows the optimum antibody concentrations for HEK 293T cells were 62.5 µg/ml and THP-1 cells were 500 µg/ml.

HEK 293T

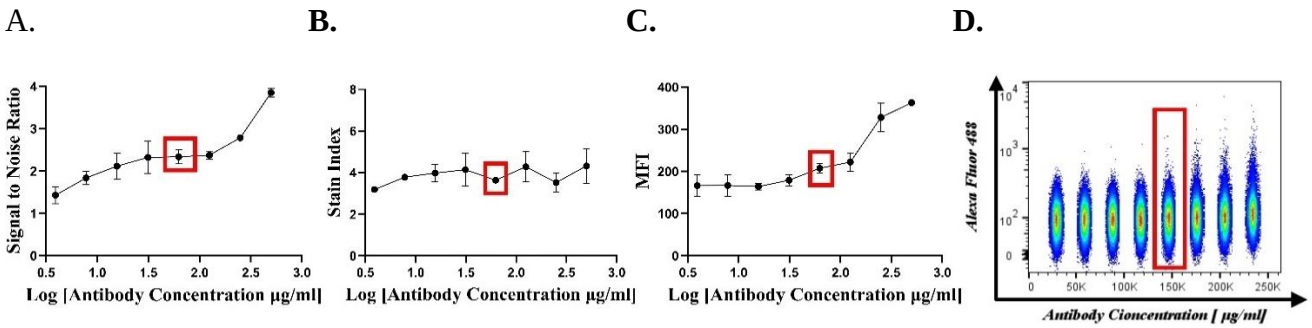

THP-1

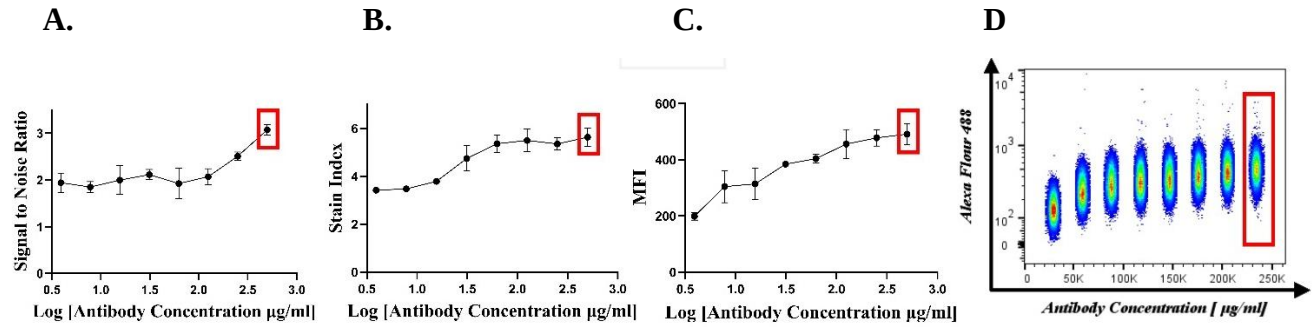

Figure 27. Titration of anti-CD14 antibody 2F9(scFv)-SNAP-Alexa Flour 488. THP-1 and HEK 293T cells were incubated with increasing concentrations of antibody ranging from 3.9 µg/ml to 500 µg/ml. The experiments were done in replicates **(A)** Shows the signal-to-noise ratio indicating the separation between the signal and the background noise. **(B)** Stain index showing the separation between positive and negative populations. **(C)** Median Fluorescence Intensity indicating the fluorescence strength of the stained population. **(D)** Concatenated pseudocolor plot showing combined multiple flow cytometry samples in a single plot. The red boxes indicate the chosen antibody concentrations for HEK 293T cells (62.5 µg/ml) and THP-1 cells (500 µg/ml).

3.6.2.2 CD14 staining on THP-1 cell line

After determining the ideal antibody concentration to achieve the best staining quality, a gating strategy employed prior allowed for calculation of the proportion of cells expressing the CD14 antigen. As illustrated in **Figure 28**, the first inclusion gate was used for selecting cells that met specific criteria based on SSC-A (Side Scatter Area) and FSC-A (Forward Scatter Area) parameters while excluding debris at the bottom of the scale. Secondly, a singlets gate was implemented to ensure that only single cells were analysed, excluding doublets or aggregates. Thirdly, using the Live Dead gate, dead cells were kept out of the analysis and cells that were positive for the live dead/ aqua stain were recognised and excluded. Lastly, the CD14 positive and negative gate was used to separate cells that were positive and negative for the target antigen and the threshold was determined on unstained cells. This gating strategy enabled us to quantify the distribution of receptors among antigen-positive and antigen-negative cell lines based on Median Fluorescence Intensity by calculating the proportion of cells expressing the antigen.

A. hP67.6(scFv)-SNAP-AF 488 binding to CD33 on THP-1 cells (positive control)

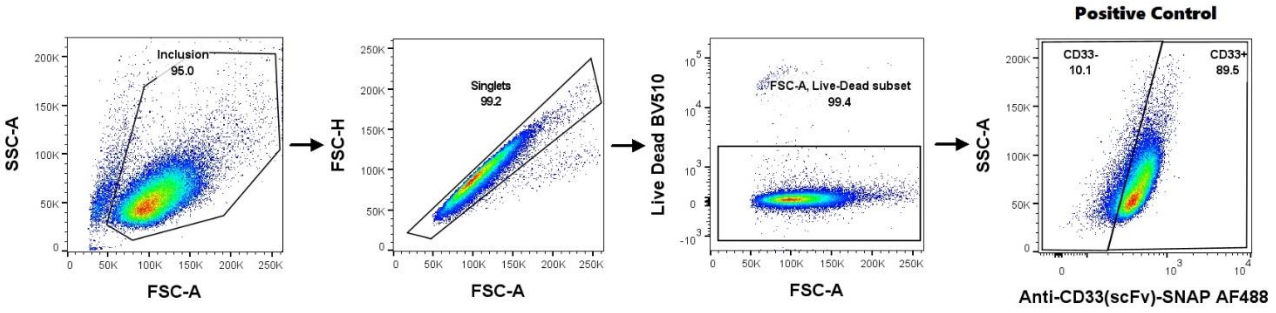

B. 2F9 (scFv)-SNAP binding to CD14 on THP-1 cells

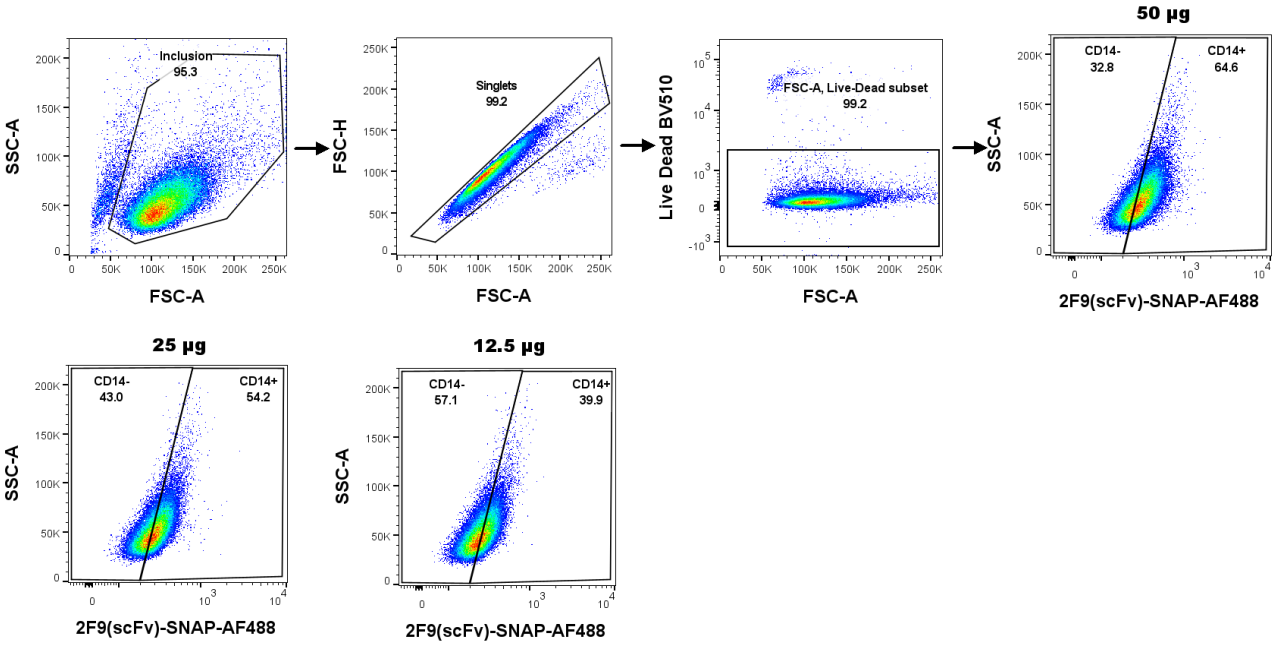

C. 2F9 (scFv)-SNAP staining HEK 293T cells CD14 negative control

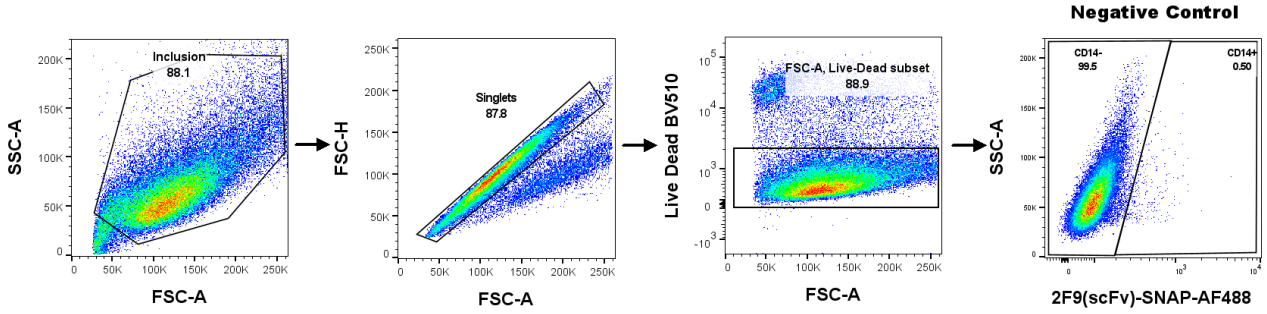

Figure 28. Representative flow cytometry plots depicting the gating strategy after staining THP-1 cells and HEK 293T cells. The first inclusion gate was used to incorporate cells that met the desired criteria based on the SSC-A (Side Scatter Area) and the FSC-A (Forward Scatter Area) excluding debris, a singlets gate was used to exclude doublets or aggregates and select only single cells for analysis based on the FSC-A and FSC-H (Forward Scatter Height), and the Live Dead gate was used to exclude dead cells population that were positive for the live dead aqua stain. **(A)** Shows the gating strategy for CD33 staining using hP67.6(scFv)-SNAP-AF

488. A concentration of 250 µg/ml had 89% binding to CD33 on THP-1 cells. of antibody and this was used as a positive control. **(B)** Show CD14 staining using 2F9(ScFv)-SNAP-AF 488 and the optimum staining concentration was determined to be 500 µg/ml (50 µg protein in 100 ml staining volume) which had 65% binding on THP-1 cells. Reducing the amount of antibody was corelating to the percentage binding. **(C)** No binding was observed on HEK 293T cells negative control.

Lastly, frequencies of the CD14 populations were calculated for THP-1 cells and HEK 293T as shown in **Figures 29A** and **B**. Histograms were generated showing the separation of CD14 negative and positive cells (**Figure 29 C**). Bar graphs were generated showing the comparisons of the negative HEK 293T cells and positive THP-1 cells in relation to frequencies of the positive cells and the MFI (**Figure 29D and E**).

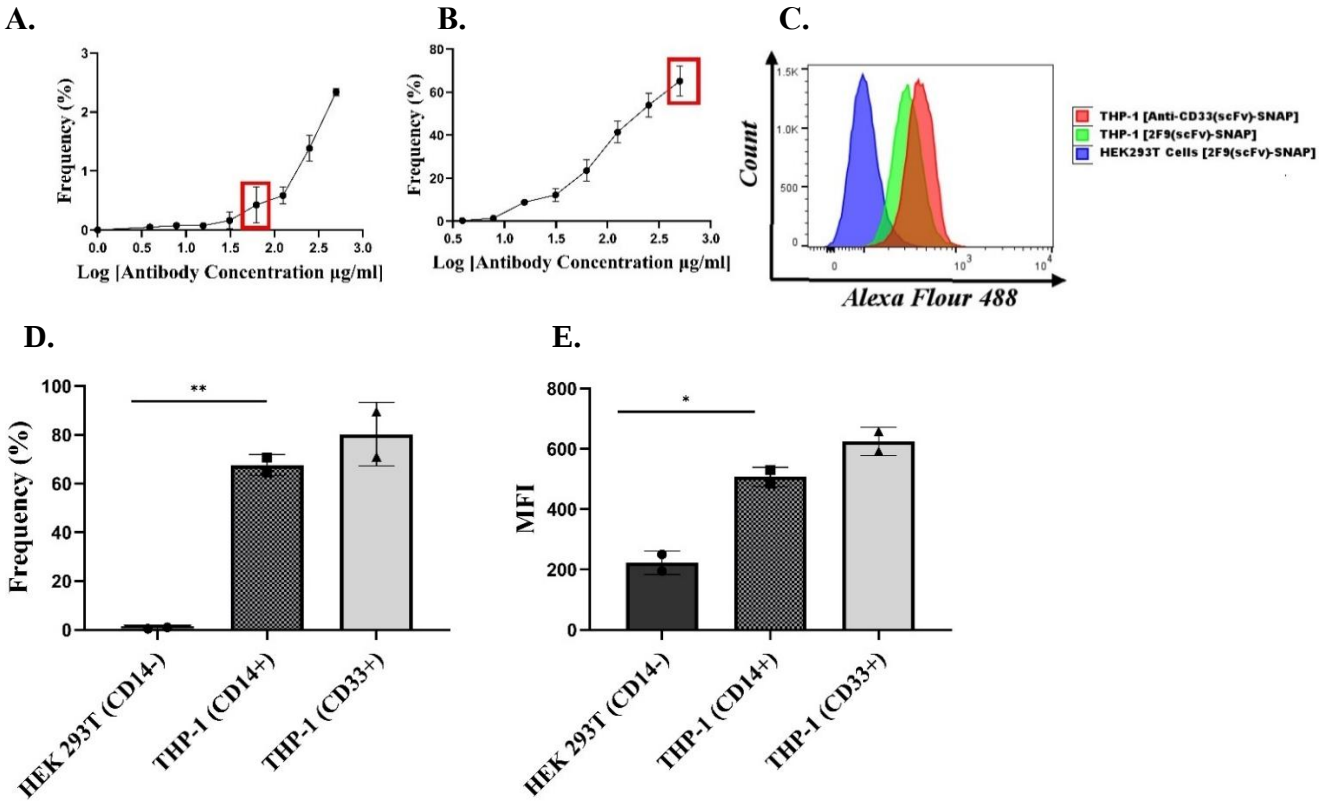

Figure 29. An illustration of a summary of CD14 expression on THP-1 cells and negative HEK 293T cells. (A and B) Antibody titration curves showing the frequency of the Alexa Flour 488-positive population at the optimal antibody concentration (indicated by the red box). © Histograms displaying the relative fluorescence of the Alexa Flour 488-positive and negative populations. **(D and E)** Bar graphs showing the frequency of the Alexa Flour 488-positive population and the median fluorescence intensity (MFI). Student's t-tests were used for statistical analysis (*p 0.05, **p 0.01, ***p 0.001, ns (not significant)).

3.6.2.3 MPO staining in HL60 cell line

Ideal antibody concentrations for 8E2(scFv)-SNAP-AF 488 were determined based on the same factors used for 2F9(scFv)-SNAP-Alexa Flour 488 as described above in section **3.6.2.1**. The optimum concentrations chosen for staining HL60 cells (250 µg/ml) and HEK 293T cells (62.5 µg) taking into consideration of the staining index, median fluorescence intensity, signal-to-noise ratio and frequencies of MPO positive and negative cells **(Figure A1)**. A similar gating strategy was also used which allowed quantitative analysis of the proportion of cells expressing the antigen and to examine receptor distribution across cells as described in **3.6.2.2.** As illustrated in **Figure 30,** the first gate was the inclusion gate, followed by the singlets, live cells, and antigen-positive and antigen-negative population gates.

A. hP67.6(scFv)-SNAP-Alexa Flour 488 binding to CD33 on HL60 cells (positive control)

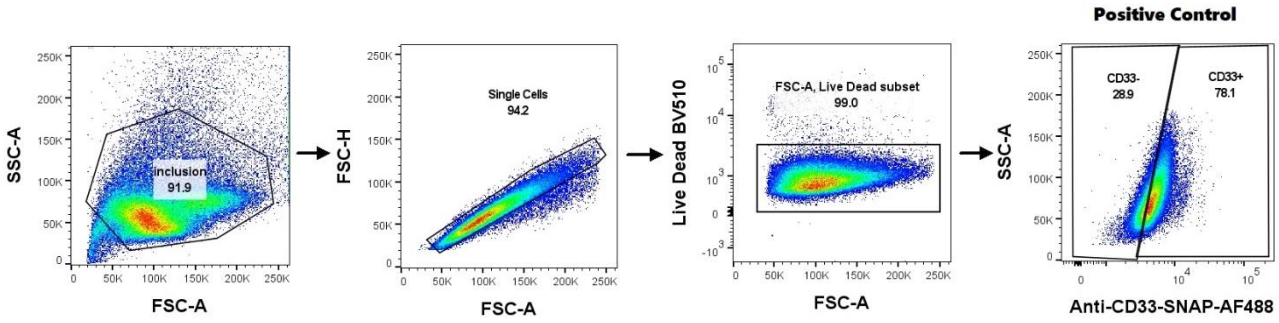

A. 8E2(scFv)-SNAP binding to MPO on HL60 cells

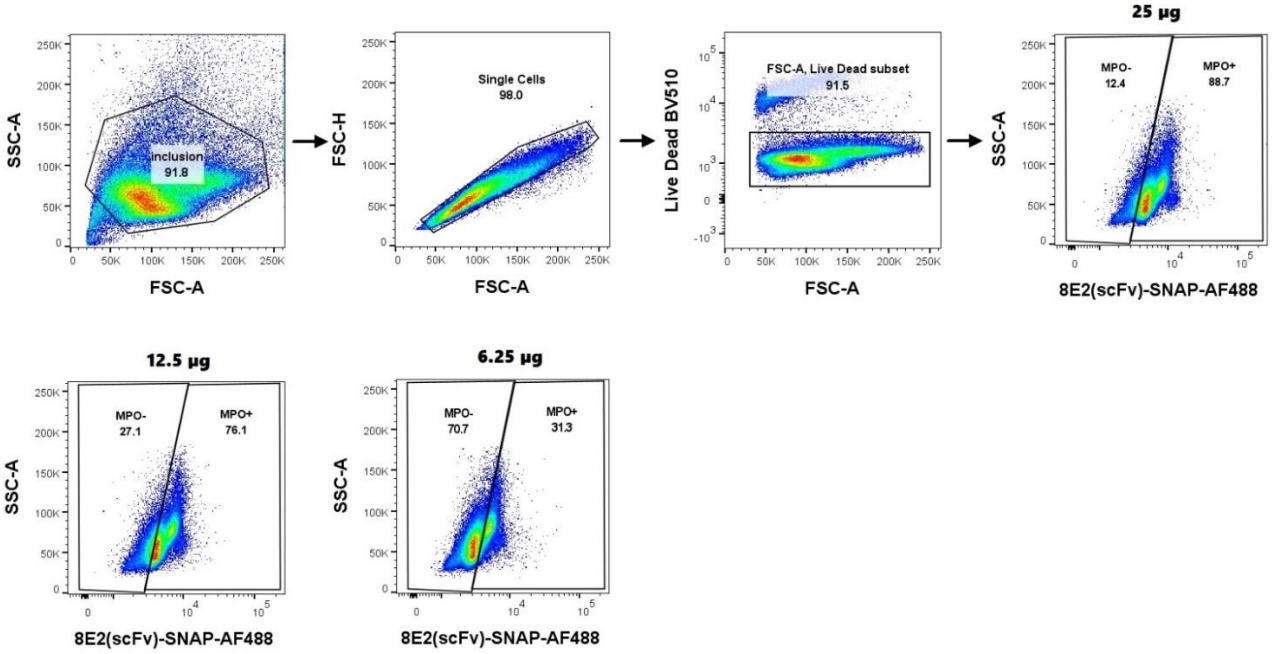

B. HEK 293T cells MPO negative control

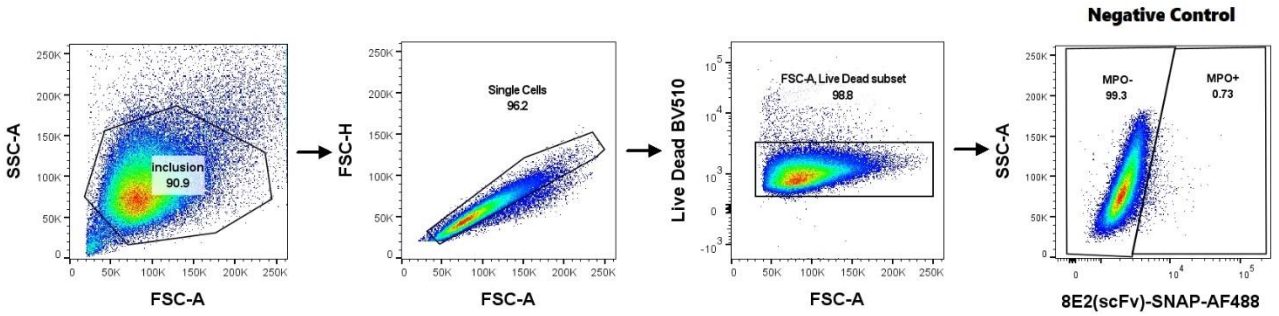

Figure 30. Representative flow cytometry plots depicting the gating strategy after staining HL60 cells and HEK 293T cells. The gates include the inclusion gate, a singlets gate, the Live Dead gate, and antigen positive and negative gates. **(A)** Anti-CD33 hP67.6(scFv)-SNAP-Alexa Flour 488 was used as a positive control and had a 78% binding on HL60 cells. **(B)** 8E2(ScFv)-SNAP-Alexa Flour 488 with the optimum staining concentration of 250 µg/ml (25 µg protein in 100 ml staining volume) having 88% binding and reducing the amount of antibody was corelating to binding. **(C)** No binding was observed on HEK 293T cells negative control.

Frequencies of the MPO positive cells were calculated using the MPO positive cell line, HL60, and the MPO negative cell line, HEK 293T as shown in **Figure 31A** and **B**. Histograms were used to show the separation of MPO negative and positive cells (**Figure 31C**). Bar graphs were used to compare the negative and positive cells in relation to frequencies of the positive population and MFI **(Figure 31D and E)**.

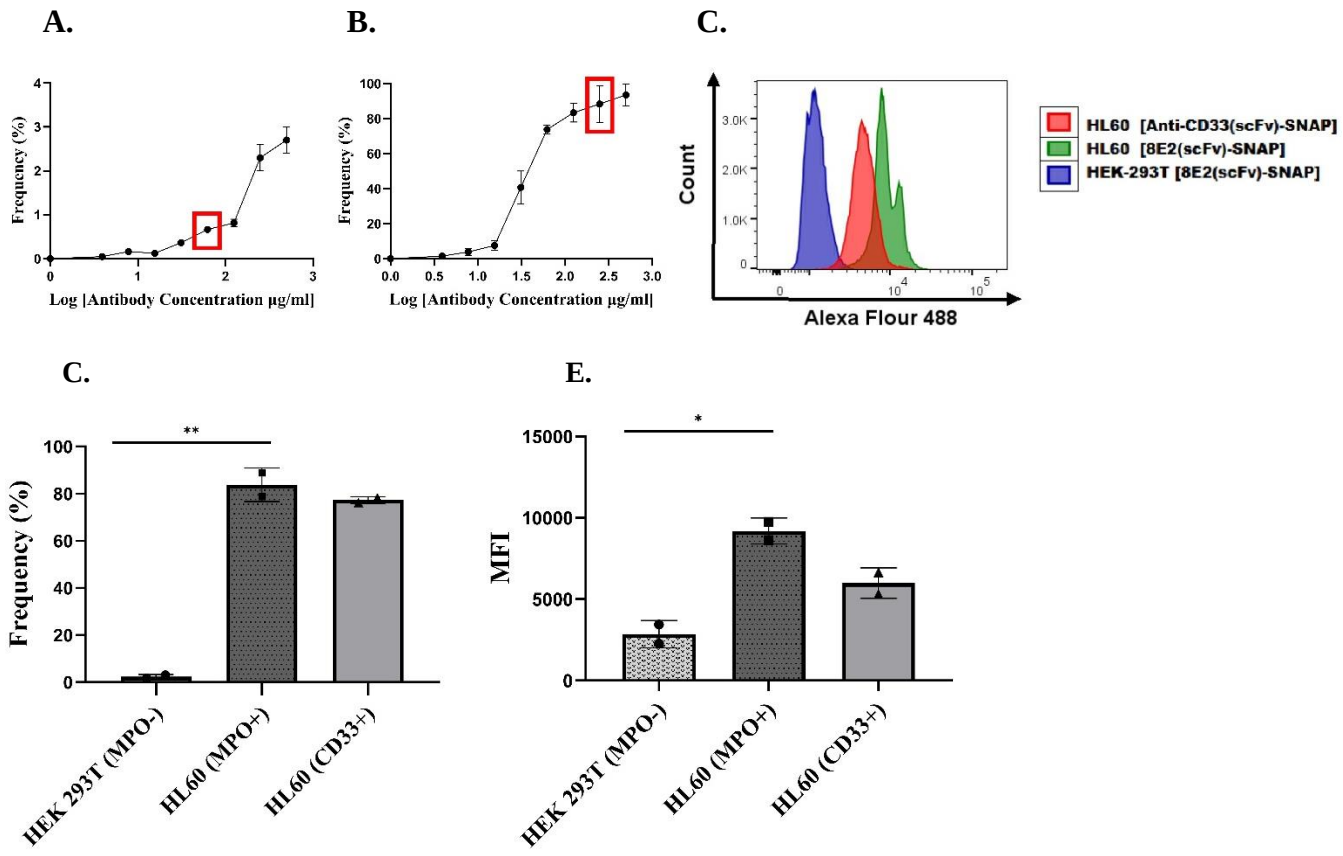

Figure 31. An illustration of a summary of MPO expression on HL60 cells and negative HEK 293T cells. (A and B) Antibody titration curves demonstrating the frequency of the Alexa Flour 488-positive population at the optimal antibody concentration (indicated by the red box). © Histograms displaying the relative fluorescence of the Alexa Flour 488-positive and -negative populations. **(D and E)** Bar graphs showing the frequency of the Alexa Flour 488-positive population and the median fluorescence intensity (MFI). Student's t-tests were used for statistical analysis (*p 0.05, **p 0.01, ***p 0.001, ns (not significant)).

3.6.2.4 HLA-DR staining on PBMCs (B cells)

Similarly, ideal antibody concentrations for L243(scFv)-SNAP-Alexa Flour 488 were determined based on the same factors used for 2F9(scFv)-SNAP-Alexa Flour 488 as described in section **3.6.2.1**. The optimum concentrations chosen for staining PBMCs were 50 µg/ml taking into consideration of the staining index, median fluorescence intensity and signal-to-noise ratio as shown in **Figure A2** and **Figure 32** is showing the gating strategy employed**.**

A. L243 commercial antibody binding to HLA-DR on B cells

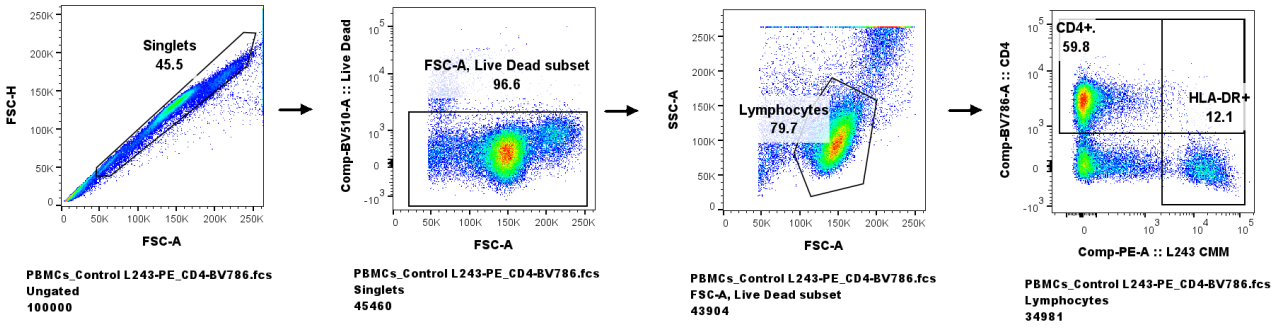

B. L243(scFv)-SNAP binding to HLA-DR on B cells

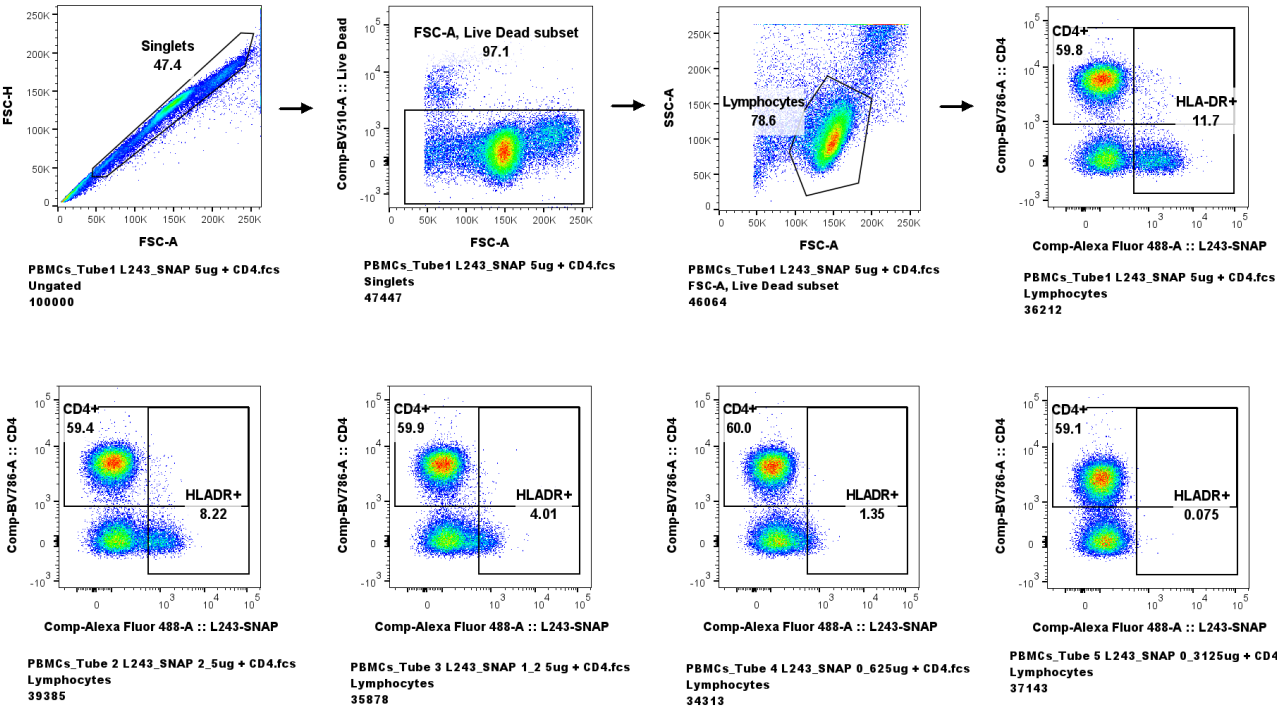

Figure 32. Representative flow cytometry plots depicting the gating strategy used after staining PBMCs. The gates include the singlets gate, the Live Dead gate, lymphocytes gate and the CD4 and HLA-DR positive gates. **(A)** Anti-HLA-DR L243 commercial antibody conjugated to Phycoerythrin (PE) was used as a positive control and anti-CD4 SK3 commercial antibody conjugated to BV786, was utilized for discriminating CD4+ lymphocytes and HLA-DR positive B cells. **(B)** The optimal concentration for staining HLA-DR with L243(scFv)-SNAP, conjugated to BG Alexa Fluor 488 was determined to be 50 µg/ml (5 µg of protein in a 10 0ml staining volume). It's worth noting that a reduction in antibody concentration correlated with decrease in binding. Importantly, no binding was detected on lymphocytes that were positive for CD4.

Similarly, frequencies of the HLA-DR positive B cells were calculated for newly generated L243(scFv)-SNAP conjugated to Alexa Flour 488 as shown in **Figure 33A**. Histograms were used to show the separation between HLA-DR negative and positive cells for both the commercial L243 antibody conjugated to PE and L243(scFv)-SNAP (**Figure 33B and C**). Bar graphs were used to compare the commercial L243 antibody and L243(scFv)-SNAP in relation to frequencies of the positive population and MFI **(Figure 31D and E)**.

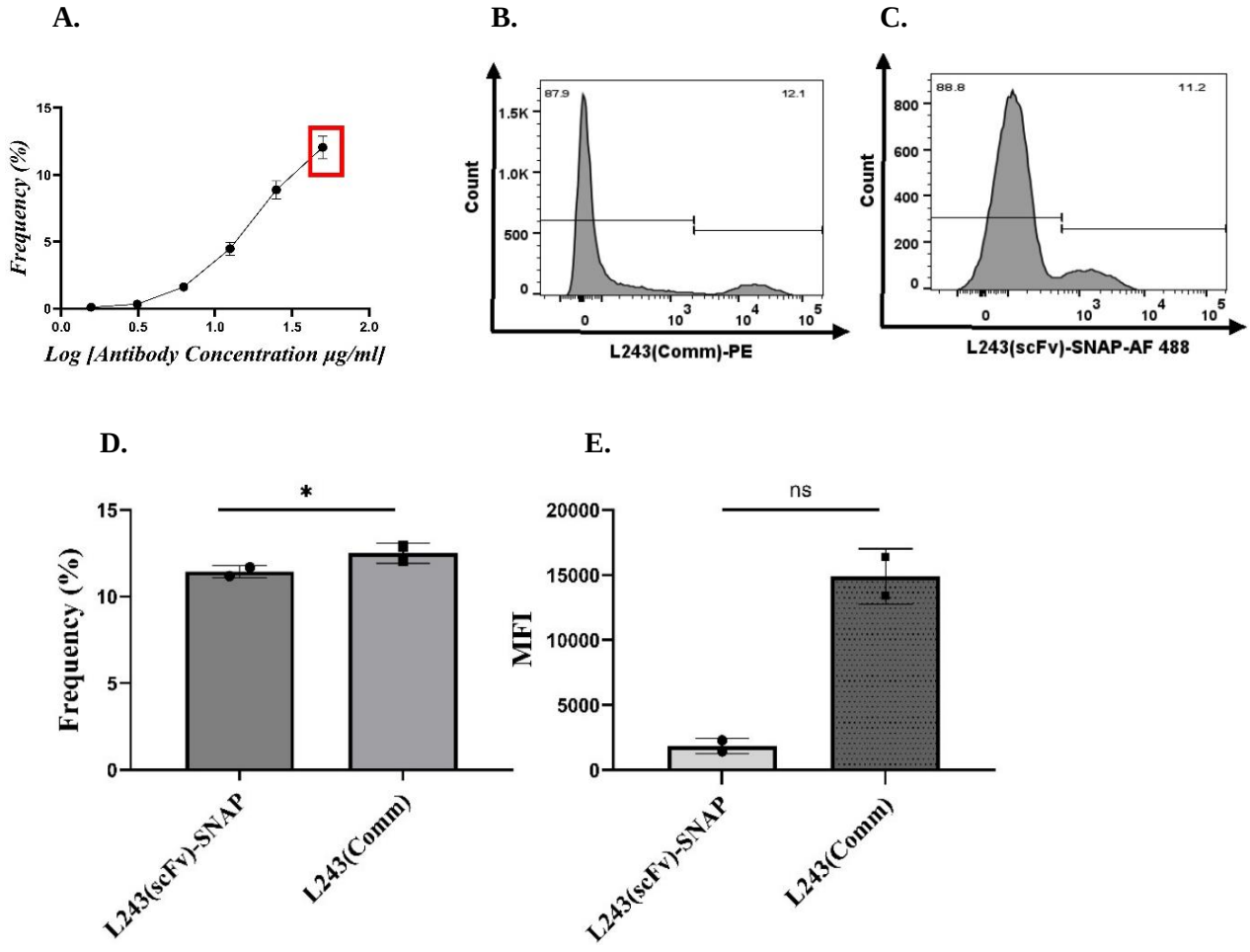

Figure 33. Summary of L243(scFv)-SNAP binding to HLA-DR on B cells in comparison to L243 commercial antibody. (A) Antibody titration curves demonstrating the frequency of the L243(scFv)-SNAP Alexa Flour 488-positive population and the optimal antibody concentration is indicated by the red box. **(B** and **C)** Display histograms illustrating the separation between HLA-DR positive and negative populations after staining with the commercial antibody clone L243 and newly generated L243(scFv)-SNAP. **(D and E)** Bar graphs showing the frequency of the Alexa Flour 488-positive population and the median fluorescence intensity (MFI). Student's t-tests were used for statistical analysis (*p 0.05, **p 0.01, ***p 0.001, ns (not significant)).

In summary, the outcomes of the flow cytometry data unequivocally validate the successful binding of 2F9(scFv)-SNAP to CD14 on the surfaces of THP-1 cells, as well as the binding of 8E2(scFv)-SNAP to intracellular MPO in HL60 cells. Notably, HEK 293T cells, serving as the negative control, exhibited minimal to negligible labelling, conclusively demonstrating the absence of nonspecific binding for both 2F9(scFv)-SNAP and 8E2(scFv)-SNAP, thus confirming the remarkable specificity of these fusion proteins. Furthermore, the effective binding of L243(scFv)-SNAP to HLA-DR positive B cells was also confirmed on PBMCs, further supporting the validity of the experimental results.

Chapter 4: Discussion

4.1 Antigens upregulated in AML necessitate the development of new, highly sensitive detection and quantitative analysis methods

AML is a highly heterogeneous disease with different subtypes characterized by the upregulation of leukemia associated antigens (LAA) (252). These antigens expression levels changes over time during the disease progression and treatment hence, highly sensitive methods are recommended for diagnosis and monitoring of the disease in order to detect even trace quantities of these LAAs in AML disease (163) (253). Flow cytometry and immunohistochemistry are among the highly sensitive diagnostic techniques used in AML diagnosis and they utilise the use of monoclonal antibodies conjugated to chromogenic or fluorescent labels (254) (255). Specifically, flow cytometry allows for quantitative assessment of antigen expression on individual cells and this provides detailed information about antigen profiles, including expression levels and patterns across different cell populations (256). On the other hand, IHC allows for visualisation of antigen expression at the cellular level as well as providing comprehensive information on the localization and quantification of antigen expression (257). These methods allow for timely and accurate detection, multiparametric and quantitative analysis of leukemic cells which enables a more comprehensive characterization of different AML subtypes (258). Additionally, they are capable of detecting minimal residual disease, aiding in the early detection of relapse (258). Accurate and early-stage diagnosis of AML is crucial for effective treatment and taking into consideration that the current novel passive immunotherapies (ADCs) target leukemia-specific or leukemia-associated antigens to induce apoptosis of cancer cells via various mechanisms (259). Flow cytometry and immunohistochemistry allow for precise identification of these antigens, which may be targeted and used for making personalised treatment plans for AML patients which improve therapeutic outcomes (260).

To date, CD33, CD123, CD14, CD11c, HLA-DR, MPO, CD89, and CD45 are amongst the identified potential diagnostic and therapeutic targets for AML (166) (261) (262) (263) (167) . Their differential expression on leukemic cells compared to normal hematopoietic cells holds promise for targeted therapies and accurate disease monitoring. This study specifically focused on CD14, MPO, and HLA-DR, which are differentially expressed biomarkers across AML subtypes. CD14, is a cell surface receptor expressed on neutrophils and monocytes, which is involved in recognizing bacterial lipopolysaccharides (264) (265). In primitive AML (M0, M1 and M2) characterised as the AML subtypes where the leukemic cells are less mature and have not undergone significant differentiation into specific myeloid cell types, CD14 expression is low due to the immature nature of the AML cells. On the other hand, in matured AML which is regarded as the AML subtype where by the leukemic cells have undergone further differentiation and maturation towards specific myeloid cell types including monocytes or macrophages the expression of CD14 increases (266). The AML-M4 and M5 subtypes exhibit the highest CD14 expression across the different subtypes (267). In a study conducted in 2016 by Lubna Alattia and her colleagues to assess the significance of CD14 expression in core biopsies for diagnosing the AML-M4 subtype using immunohistochemistry, their findings indicated that out of the 40 AML-M4 patients examined, 77% exhibited immunoreactivity for CD14 (268). Therefore, building upon the existing literature and considering the WHO and FAB classifications of AML which supports the use of CD14 as a marker for the diagnosis of AML-M4 and M5 subtypes (60) (166) (266) (269). In this study, we have generated an anti-CD14 antibody (2F9(scFv)-SNAP) and tested for its binding abilities on the THP-1 cell line. This cell line was derived from the peripheral blood of an acute monocytic leukemia patient (270). It is a well-established model for studying AML and resembles primary monocytes and macrophages with regards to morphology and differentiation properties, which is why the cells express the CD14 cell surface receptor (271–273).

Simillar to CD14, myeloperoxidase (MPO) is also a differentially expressed biomarker in different AML subtypes. This is an enzyme expressed on neutrophils that plays a role in generating reactive

oxygen species to combat bacterial infections (274). In AML (M1, M2 and M3 subtypes), it has been found that more than 80% of the blasts show MPO activity (275) and its expression varies across subtypes depending on the maturation levels of myeloid progenitors. For instance, in M1 and M2 AML subtypes, MPO expression is generally low, whereas the AML M3 subtype shows the highest levels of MPO expression (186). However, in a study conducted by Suchita Pant and Misra in 2020 to evaluate the role of immunohistochemistry in diagnosing and subtyping acute leukemia's, they observed that MPO was positive in M1 to M6 subtypes, with a 100% positivity in the M3 subtype (276). Although, blast morphology still remains the gold standard for MPO detection using paraffin embedded bone marrow trephines in countries with limited recourse settings, immunohistochemistry and flow cytometry staining have become an integral part of the diagnostic workup in cases of hematologic malignancies (276). Building upon the existing evidence in the literature and considering the WHO classification of AML which emphasizes the role of myeloperoxidase (MPO) detection as the only requirement for assigning myeloid lineage to a blast population in AML diagnosis (277) (278). For this reason, we generated an anti-MPO antibody (8E2(scFv)-SNAP) which holds promise for potential applications in the diagnosis of AML. The HL-60 cell line was used to test for the antibody's binding abilities to intracellular MPO. This is a human cell line derived from the peripheral blood lymphocytes of a 36-year-old woman suffering from acute promyelocytic leukaemia (279). It expresses MPO and has been used as a model to study the cellular and molecular events involved in the proliferation and differentiation of leukemic cells (280).

Similarly, HLA-DR is also highly expressed in AML cells derived from myeloid precursor cells, particularly myeloblasts and promyelocytes. Normally, HLA-DR is a cell surface receptor that is expressed on B cells and dendritic cells (281). It plays a crucial role in antigen presentation to the immune system. The differential expression of HLA-DR in AML has diagnostic and prognostic implications. High HLA-DR expression is associated with better prognosis, while low HLA-DR expression is linked to poor prognosis (171). The use of HLA-DR for AML diagnosis was supported

in the 2017 and 2022 European LeukemiaNet (ELN) recommendations from an international expert panel, both of which state that HLA-DR is a precursor marker for AML diagnosis (172) (173). However, more research still needs to be done to further confirm the use of HLA-DR in the clinical setting. Within the scope of this research, we generated an anti-HLA-DR antibody L243(scFv-SNAP and assessed its binding abilities to B cells using PBMCs. It's noteworthy that PBMCs constitute a heterogeneous population of immune cells, encompassing T cells, B cells, natural killer cells, monocytes, and dendritic cells. HLA-DR is primarily found on antigen-presenting cells (APCs), such as B cells among the lymphocytes (282) (283). In conclusion, the use of CD14, MPO, HLA-DR and other relevant markers represents a promising set of biomarkers for establishing a diagnostic panel for AML. Accurate identification and quantification of these upregulated antigens on leukemic cells using IHC and flow cytometry is crucial for precise diagnostic and disease monitoring (173).

4.2 SNAP-tag based fusion proteins conjugated to fluorophores as novel approach for AML diagnosis

Innovative ways to diagnose diseases such as AML are critical for early detection and effective treatment. New methods for diagnosing diseases involving linking antibodies with fluorophores are being developed. These antibody-fluorophore conjugates can be employed in the identification of diseased cells through techniques such as immunohistochemistry and flow cytometry, providing innovative pathways for disease diagnosis (284). Consequently, with the advances in protein engineering, several site-specific conjugation strategies have been developed, capitalizing on the introduction of unnatural amino acids into the antibody to drive the controlled chemical conjugation of compounds (285). This coupling process relies on precise interactions between functional groups present on both antibody and fluorophore components for example the amino-succinimide reaction, which involves reacting the primary amines on the antibody (typically lysine residues) with the NHS (N-hydroxysuccinimide) ester of the fluorophore (286). The reaction forms a stable amide bond between the antibody and the fluorophore. The most common NHS ester fluorophores include FITC

(fluorescein isothiocyanate) and cyanine dyes (287). Additionally, Thiol-Reactive coupling is also widely used for antibody conjugation. This approach utilises the thiol groups (sulfhydryl groups) on cysteine residues of the antibody to react with maleimide-functionalized fluorophores including Alexa Fluor dyes and DyLight dyes (288). Furthermore, the click chemistry is one of the most widely used bioconjugation reactions that are highly specific, fast, and efficient. This utilizes the use of copper-catalysed azide-alkyne cycloaddition (CuAAC), where an azide-functionalized fluorophore reacts with an alkyne-modified antibody in the presence of a copper catalyst (289). Once conjugated, these probes can be used for flow cytometry or immunocytochemistry, which are both powerful techniques for detecting and analysing cells (256). Nevertheless, self-labelling tags such as SNAP-tag, genetically fused to antibodies or their fragments, are gaining momentum in the development of recombinant immunodiagnostics (217) (290). SNAP-tag is a self-labelling engineered mutant of the human O(6)-alkylguanine-DNA alkyltransferase enzyme, capable of specifically and covalently reacting with any BG-substrates, in an irreversible manner to generate homogeneous conjugates in a 1:1 stoichiometric reaction (291). It offers advantages ranging from the simplicity of the reaction, the specificity and short duration of conjugation (reacts only with BG-modified substrates for 30 mins for fluorochromes) (213), no requirement for activating substrates, as well as a predictable 1:1 stoichiometric reaction with the generation of homogeneous products (292) (217). In addition to its application in a variety of experimental settings, the versatility of this technology is further validated through the emergence of recombinant SNAP-tag based fusion proteins (scFv-SNAP) bearing specificity towards tumour-associated antigens (293) (218). As such, this class of immunodiagnostics demonstrates cutting-edge advancements in various aspects: (1) they can be produced in different expression systems (bacteria and mammalian) with high yields, (2) antibody functionality is maintained (SNAP-tag provides distant conjugation away from the paratope, creating a spacer between the antibody and the effector molecule) (294) (295) (296). Taken together, the above arguments provide the rationale behind the stipulated aims and objectives of this study. The novelty in this research lies in genetically fusing SNAP-tag to

three different single chain variable fragments (targeting CD14, MPO and HLA-DR) for the development of immuno-diagnostic tools for AML.

4.3 Production of recombinant SNAP-tag based fusion proteins

Producing recombinant SNAP-tag-based fusion proteins involves genetic engineering techniques to generate a fusion between the SNAP-tag protein and an scFv or target protein of interest (213). In this study, recombinant proteins were generated by genetically fusing the SNAP-tag enzyme with the sequences encoding for anti-CD14, anti-MPO and anti-HLA-DR scFvs. Firstly, the sequences encoding for the scFvs were extracted and analyzed on Ig-BLAST for quality control purposes. Following that, codon optimization was done by exchanging codons which are rarely found in the mammalian host organism with more frequently observed codons. This was done to improve gene expression and increase the translational efficiency, which ultimately resulted in higher protein production (297). The optimized sequences were then attached to SNAP and cloned *in silico* using the pCB plasmid backbone, yielding an in-frame sequence free of stop codons that would interfere with DNA transcription **(Figures 12 and 13)**. As a result, the generated sequences were used to create the inserts ordered from GenScript, which were then used in molecular cloning.

During molecular cloning, restriction endonuclease digestion for both the pUC57 plasmid (housing the insert DNA) and pCB-SNAP plasmid backbone was done. The visualised agarose gels demonstrated the effectiveness of the restriction enzyme digests in this process (**Figure 14)**. Despite this accomplishment, we experienced several unanticipated hurdles throughout the process. One noticeable issue was partial digestion and vector re-ligation, as shown in **Figure 14**, where bands with lengths more than 8000 bp were present. It is anticipated that presence of the 5'-phosphate groups from vector molecules resulted in vector self-ligation (298) or that partial restriction digestion of the plasmid vectors by the restriction enzymes might have contributed to the observed result. We made certain modifications to solve this issue and improve the separation of DNA fragments on the gel.

First, we ran the agarose gel at a lower voltage during electrophoresis to minimise the heat generated during the run, which prevents DNA bands from diffusing and merging, we also increased the running time of the gel electrophoresis which increased time for DNA fragments to separate (299) (300). As a result, distinguishing between partially digested and fully digested fragments became easier, enabling the subsequent ligation reaction to proceed. After ligation, the existence of bacterial colonies on LB agar test plates, as well as the absence of colonies on the bacteria-only and vector-only control plates, gave strong evidence that the ligation step was successful, showing that all colonies carried the ligated pCB-scFv-SNAP plasmid vector **(Figure 15)**. Although, transformation efficiencies with highly competent DH5α *E. coli* cells are expected to be ranging from 1-3 x 10^9 cfu/g (301), the transformation efficiencies observed from the ligated plates varied from 1.97-2.97 x 10^3 cfu/g **(Figure 15 and Table 11)**. Variations in growing conditions, plasmid size, and purity are potential reasons for this variance, which may have affected our ligated plate's transformation efficiency (302).

The plasmid's validity was then confirmed through restriction mapping and DNA sequencing as the final step in the cloning procedure. Upon digestion with restriction enzymes, the ligated clones exhibited distinct fragment patterns compared to the original vector. The original pCB vector was initially housing Annexin-V, which was subsequently replaced with the inserts encoding the scFvs of interest. The observed band sizes on the agarose gel confirmed the successful integration of the inserts into the vector backbone **(Figure 16).** Additionally, DNA sequencing confirmed the validity of the plasmids **(Figure 17)**. The sequences generated by sanger sequencing aligned with the original sequences developed *in silico*, with a close to 100% homology as well as no missense, nonsense, or frameshift mutations were identified.

Following cloning, the recombinant plasmids were transfected into HEK293T cells, these cells were chosen for protein expression due to the multiple benefits they possess over other expression systems. Notably, their high transfection efficiency simplifies the introduction of new foreign DNA into the

cells (303) (304). In this study, transfection efficiencies were determined by qualitative evaluation of eGFP intracellular expression levels alongside quantitative flow cytometry and were found to be close to 70%. **(Figures 18 and 19)**. A colleague within our MB&I group Uslar, has also reported similar findings to these results (unpublished doctoral thesis). Similarly, Mungra *et al*, 2023 specifically documented transfection efficiencies of 70-80% when introducing recombinant anti-CSPG4-SNAP expression plasmids into HEK 293T cells (305). As an alternative to the lipid-based transfection approach using transfection reagents utilized in this study, electroporation has the potential to achieve significantly higher transfection efficiencies, potentially exceeding 80%. A different approach that could be utilised is calcium phosphate precipitation, which may produce transfection efficiencies close to 100% depending on the cell line used which is relatively higher compared to the 70% recorded in this study (306) (307). Consequently, occasional Zeocin selection was then used to improve the GFP-positive state by eliminating the non-transfected cells, resulting in a high percentage of cells expressing the recombinant proteins which allowed proceeding to collection of the cell culture supernatant containing the protein of interest.

After collection of the supernatant from the HEK293T cells, a protein purification process was carried out using IMAC. In this method, SNAP fusion proteins were specifically captured by their 10 His-tag, which is fused to the N-terminal peptide sequence. This 10 His-tag was chosen because of its modest size as well as its ability to facilitate successful purification without interfering with the folding, structure, and function of the proteins of interest (308). The decision to adopt this specific fusion tag was further strengthened by its higher affinity for Nickel in comparison to the previously used 6 His-tag at the MB&I. This is due to the fact that the 10 His-tag is longer in length and has a higher number of histidine residues compared to 6 His-tag thus contributing to its higher affinity for nickel during IMAC (309). Capitalising on the higher nickel affinity of the 10 His-tag, a lower concentration of imidazole was used in the washing steps of IMAC to eliminate loosely bound protein impurities from

the supernatant on the nickel column. Subsequently, a higher concentration of imidazole was used for the elution step, allowing for the efficient purification of SNAP fusion proteins (**Figure 20**).

SDS-PAGE and western blot analysis were utilized to verify the presence of SNAP fusion proteins after purification corresponding to the size of the construct using a protein molecular weight ladder. However, the findings from SDS-PAGE and western blot analysis of the recovered SNAP fusion proteins highlighted that relying solely on IMAC purification as the initial enrichment step was insufficient to achieve the desired high purity levels of greater than 90%. The main issue with IMAC purification was its tendency to bind and co-elute contaminants that had endogenous histidine residues or metal-binding motifs as illustrated on the bands at around 72 kDa and close to 100 kDa **(Figure 21)**. Amicon columns with a molecular weight cut-off were incorporated to improve the protein purity, although the desired protein purity was not reached. Densitometry analysis utilized for protein quantification and calculation of percentage purity, confirmed protein purity at close to 60% **(Figures 22 and 23)** Although the precise impact of the contaminants on protein binding and activity remained uncertain, it was speculated that the increasing amounts of contaminants, which might include degradation products containing a functional scFv portion without SNAP, could potentially interfere with the binding affinities of the fluorescently tagged recombinant antibodies through competitive binding (310). These contaminating proteins are shown on the SDS-PAGE gel with bands at around 34 kDa **(Figure 24A)** and 43 kDa **(Figures 24B and C)** on the western blot indicating his-tagged proteins. To address these challenges, it was suggested that an ideal purification process would involve multiple steps, starting with IMAC, followed by size exclusion chromatography (SEC) and incorporating ion exchange chromatography as the final purification step (311) (312). In a study conducted by Wang *et al.*, the combination of IMAC, ion exchange chromatography, and SEC achieved protein purities of up to 96% during the purification of his-tagged recombinant kinesin proteins produced in *E. coli* (313). Moreover, incorporation of protease inhibitors in the cell culture supernatant for storage as well as purified protein samples is a way to prevent protein degradation

(314). Recombinant protein purity is important because it can affect the outcome of subsequent experiments, as contaminants in purified proteins can interfere with in vitro and in vivo research, leading to misinterpretations of fusion protein functionality (310).

Following densitometry-based protein quantification, the absolute amount of purified fusion proteins was determined to be 8.9 mg, 12.4 mg, and 16.1 mg per 1 litre of supernatant for 8E2(scFv)-SNAP, 2F9(scFv)-SNAP, and L243(scFv)-SNAP, respectively **(Table 12)**. Previous studies conducted by Hussain *et al*, reported similar yields in the range of 10-20 mg/l when purifying cell culture supernatants using IMAC purification (296). Woitok *et al*, also conducted a study involving the production of SNAP-tag recombinant fusion proteins in mammalian systems, where they achieved an absolute protein yield of 30 mg/l (294). It's worth mentioning that typical yields for transient transfections typically fall between 10 to 30 mg/l. However, it's important to note that these yields can vary, sometimes reaching lower or higher values depending on the specific methodology used or the expression capabilities of the specific proteins (315). The variations in protein yield in our study are a result of the incomplete optimization of transient mammalian expression protocol. Hence, there's a clear requirement to develop approaches that can enhance protein production while being mindful of resource constraints. This improvement can be attained through, refining the environmental conditions during culture or exploring alternative production cell lines like Chinese hamster ovary cells, yeast, or insect cells (316) (317). In summary, the results of this study highlight that, despite lacking industrial production processes which increase protein yield and using IMAC for purification of SNAP-tag fusion proteins which does not reach the desired protein purity of greater 95%. Preliminary binding analysis of the newly generated SNAP fusion proteins could be used as proof-of-concept studies at university level.

4.4 scFv-SNAP based fluorophores selectively target antigen positive cells

Firstly, conjugation with the BG-Alexa 488 fluorophore was used to confirm the self-labelling capability of the SNAP-tag on the terminus of the generated fusion proteins. This step effectively confirmed that the SNAP-tag maintained its labelling capability after purification **(Figure 25)**. The SNAP-tag technology offers a distinct advantage in that it allows for conjugation at a remote location from the paratope (antigen binding site). By introducing a spacer between the antibody and the effector molecule, the potential drawbacks linked to direct conjugation are mitigated. These drawbacks often encompass adverse effects on the structure, function, and binding affinity of the antibodies (296) (217). Furthermore, the functionality of the Alexa Fluor 488 effector molecule remained intact throughout the conjugation process.

A comprehensive investigation into the binding capabilities of the newly developed antibodies: anti-CD14 2F9(scFv)-SNAP and the Anti-MPO antibody 8E2(scFv)-SNAP conjugated to Alexa Flour 647 was conducted using confocal microscopy. We aimed to elucidate their specific interactions with target antigens, shedding light on their potential diagnostic applications. The anti-HLA-DR L243(scFv)-SNAP was not included in the initial confocal experiments due to the absence of HLA-DR positive cell lines but was included in the flow cytometry analysis using PBMCs.

Our findings on the anti-CD14 antibody revealed specific binding of the antibody to the CD14 antigen present on the surface of THP-1 cells. Notably, this binding interaction was visibly absent on CD14 negative HEK 293T cells, confirming the specificity of the antibody (**Figure 26)**. A punctate binding pattern was observed on the surfaces of THP-1 cells, which corresponds with the similar patterns depicted in the studies by Carine *et al*, 1998 and Marie *et al*, 2015 this suggests that the CD14 antigen is expressed on these cells in a clustered or patchy manner (318) (319). The limited or absence of binding observed on other CD14 positive THP-1 cells in **Figure 26** was likely attributed to the low expression of the antigen on those cells. Therefore, it is worth contemplating the application of

Phorbol-12-myristate 13-acetate (PMA) treatment to enhance CD14 antigen expression in these cell lines (320).

In our investigation, we successfully extended our study to include the anti-MPO antibody 8E2(scFv)-SNAP conjugated to Alexa Flour 647, which demonstrated a specific binding to the myeloperoxidase antigen present in the cytoplasm of the HL60 cell line. This binding interaction was particularly evident in the form of a distinctive granular pattern, which corresponded to the localisation and packaging of MPO within the lysosomes as shown in **Figure 26** (321). This granular binding pattern validates the antibody's specificity to its target, as it aligns with the expected subcellular localization of MPO. Similar observations were observed by Nicchi S *et al*, 2022 when HL60 cells were stained using commercially available anti-myeloperoxidase antibodies clone 2C7 (322) (323). Comparatively, the lack of signal observed when incubating the antibody with MPO-negative HEK 293T cells further emphasizes its specificity. This specific lack of binding in MPO-negative cells serves as a crucial control, strengthening the credibility of the antibody's performance and substantiating its potential diagnostic relevance.

Subsequently, we employed flow cytometry as an additional method to validate the binding capacities of the generated SNAP fusion proteins. This approach also enabled the quantification of relative surface expression levels of target receptors within the live cell population. We examined the binding capabilities of 2F9(scFv)-SNAP on THP1 cells, 8E2(scFv)-SNAP on HL60 cells and the anti-HLA-DR L243(scFv)-SNAP on PBMCs targeting the B cells.

To account for potential effects arising from low protein purity and to optimize the separation between antigen-positive and negative cell populations, we performed antibody titrations which is a crucial step in development and optimisation of multicolour flow cytometry assays **(Figure 27).** This step was taken to mitigate the potential impact of protein purity on the binding potential of the scFv-SNAP fusion proteins. It also facilitated the determination of the optimum antibody concentration that would

yield maximal staining of the target receptor, while minimizing any background signal interference (324). Having determined the optimal concentrations of SNAP fusion proteins for staining, the Median Fluorescence Intensity (MFI) values were calculated. These values signify the average fluorescence intensity of a specific parameter (in this case, the Alexa Flour 488 channel). This was used to distinguish between cells that are positive for a particular marker and those that are negative (325). It's important to note that even negative control cell populations can generate MFI values, mainly due to background fluorescence. However, positive cells typically display higher MFI values compared to negative cells and therefore this could be used to differentiate them.

In the case of CD14, approximately 60% of the THP-1 cells exhibited the presence of the CD14 antigen validating the initial confocal microscopy results **(Figure 26),** which confirmed the binding of the newly developed anti-CD14 2F9(scFv)-SNAP to THP-1 CD14-positive cells. Importantly, these CD14-positive cells displayed Median Fluorescence Intensity (MFI) values of 507 that exceeded those of the negative control HEK 293T cells of 222 **(Figures 28 and 29).** Notably, the higher MFI values in CD14-positive cells compared to the HEK 293T negative control cells suggested a more abundant presence of CD14 antigen on the surface of THP-1 cells. Comparable observations were reported in the studies by Shen DY *et al*, in 2014 when they developed a chimeric antibody 2F9, which displayed specific binding to CD14 antigen on PBMCs (monocytes population) and no detectable binding was observed when tested against the negative control line, NALM-6 (326). However, CD14 expression is higher in differentiated THP-1 cells compared to undifferentiated cells (327) (320). In a 2020 study conducted by Jimenez-Duran *et al*., when they were investigating for the regulators of macrophage differentiation, it was observed that after subjecting THP-1 cells to PMA treatment, there was a notable increase in both the percentage of CD14 positive cells and the MFI of CD14 expression per cell, in comparison to the isotype controls (320). Thus, it is worthwhile to consider treating THP-1 cells with PMA to enhance CD14 expression.

In the case of MPO, our analysis revealed that approximately 80% of the HL60 cells exhibited the presence of MPO. Importantly, these MPO-positive cells displayed MFI values of approximately 9194 that exceeded those of the negative control HEK 293T cells of approximately 2859 **(Figures 30 and 31).** The higher MFI values observed in MPO-positive HL60 cells in comparison to the HEK 293T negative control cells indicated a more abundant presence of the antigen in HL60 cells which exhibited a relatively strong binding. Similar findings were reported by Kazunori Nakase and colleagues in their study to demonstrate the reliable detection of MPO in the cytoplasm of leukemic cells, which also involved the HL60 cell line using antibody MPO-7 (Dako) (328).

Similarly, the newly developed anti-HLA-DR antibody (L243(scFv)-SNAP) conjugated to BG Alexa Fluor 488 was used to stain PBMCs. The results observed showed binding to HLA-DR-positive B cells and no binding was observed on CD4-positive lymphocytes, as well as CD4 and HLA-DR negative lymphocytes (which could encompass CD8+ cytotoxic T cells) as shown in **Figure 32**. To establish a positive control, a commercial anti-HLA-DR antibody clone L243 conjugated to PE (Biolegend, USA) and an anti-CD4 commercial antibody clone SK3 conjugated to BV786 (Biolegend, USA) were used. This allowed for the discrimination of lymphocytes positive for both CD4 and HLA-DR **(Figures 32 and 33)**. While the staining results demonstrated specific binding to HLA-DR expressing lymphocytes (i.e., B-cells) and a comparable distribution pattern between the L243 commercial antibody and the L243(scFv)-SNAP. However, it should be noted that the brightness of the staining was lower for L243(scFv)-SNAP than the commercial L243 antibody, which could be due to higher numbers of fluorochromes on the commercial antibody which resulted in a more distinct separation between the negative and positive populations. Adding to that, the commercial L243 antibody was conjugated to PE, which generally emits a brighter signal than Alexa Fluor 488, leading to a more enhanced fluorescence intensity (329). Furthermore, the commercial antibody is a full monoclonal antibody consisting of two antigen binding sites, compared to the monovalent scFv with a single antigen binding site. As a result, the commercial antibody had a higher affinity for the antigen, thereby facilitating

better separation between the HLA-DR negative and positive populations (330). Considering these findings, it is highly recommended to explore the development of a new bivalent version of the newly generated antibody L243(scFv)-SNAP. This involves the genetic attachment of a second antigen binding arm to the L243(scFv)-SNAP antibody, creating a bivalent antibody (L243(scFv)-SNAP-L243(scFv)). Notably, this technology was already established by Maryam Karran, a former master's student at the Medical Biotechnology and Immunotherapy Research Unit, when she generated an CSPG4 bivalent scFv fusion protein to increase the binding affinity of the monovalent version of the antibody (data not published). Secondly, by leveraging the antibody's precision in targeting cells expressing HLA-DR it can be speculated that increasing the number of fluorochromes conjugated SNAP tag-based antibody fusion proteins by protein engineering may be another advantageous avenue to enhance the MFI.

Chapter 5: Conclusion and future work

In conclusion, we successfully developed and demonstrated selective binding of 2F9(scFv)-SNAP, 8E2(ScFv)-SNAP and L243(scFv)-SNAP to antigen positive cells. Moreover, the absence of binding observed on antigen negative cells, further confirms the antibody specificity. This specificity is a key factor which opens possibilities for the developed antibodies diagnostic applications. Further investigations involving primary cancer cells and clinical samples are required for the developed antibodies to establish clinical relevance.

Future work offers an array of interesting possibilities to expand our research, but before exploring future research possibilities, we need to improve the productivity of our SNAP fusion proteins in HEK 293T cells. To achieve this, we aim to establish industrialized production processes through tight collaboration with biopharmaceutical companies. Secondly, our focus lies on refining purification methodologies to attain the desired protein purities exceeding 95%, by incorporating multiple protein purification steps. Furthermore, we need to evaluate the newly developed antibodies on a wide range of alternative cell lines that express CD14, MPO, and HLA-DR before moving to patient samples. This

expansion of our tests will provide a full understanding of the antibodies' specificity, sensitivity and overall performance in multiple circumstances, verifying their adaptability and possible clinical usefulness. Expanding on the antibody design strategy, we plan to develop bivalent versions of the antibodies derived from the single-chain variable fragments (scFv). This entails combining two scFv units to increase their affinity for target antigens. We hope to improve the accuracy and efficiency of our detection method by strengthening the interaction between the antibody and its intended target, which is particularly critical in scenarios with low antigen concentrations or complex sample matrices.

Similarly, we will investigate the possibility of increasing fluorescence signal strength by conjugating multiple fluorochromes to a single antibody molecule. This approach has the potential to significantly boost the emitted fluorescence, potentially leading to more robust and sensitive detection capabilities. We anticipate reaching a level of signal enhancement comparable to that of commercial antibodies by improving the conjugation process and carefully selecting the most appropriate fluorochromes, thereby pushing the boundaries of our detection technology. Incorporating these proposed strategies into our research endeavours would not only strengthen the scientific foundation of our work but will also pave avenues for innovative applications in AML diagnosis and treatment.

6. References.

1. Brunning RD. Classification of acute leukemias. Semin Diagn Pathol. 2003 Aug;20(3):142–53.

2. Tur MK, Huhn M, Jost E, Thepen T, Brümmendorf TH, Barth S. In vivo efficacy of the recombinant anti-CD64 immunotoxin H22(scFv)-ETA' in a human acute myeloid leukemia xenograft tumor model. Int J Cancer. 2011 Sep 1;129(5):1277–82.

3. Abutalib SA, Tallman MS. Monoclonal antibodies for the treatment of acute myeloid leukemia. Curr Pharm Biotechnol. 2006 Oct;7(5):343–69.

4. Fouad YA, Aanei C. Revisiting the hallmarks of cancer. Am J Cancer Res. 2017;7(5):1016–36.

5. Yamashita M, Dellorusso PV, Olson OC, Passegué E. Dysregulated haematopoietic stem cell behaviour in myeloid leukaemogenesis. Nat Rev Cancer. 2020 Jul;20(7):365–82.

6. Worldwide cancer data | World Cancer Research Fund International [Internet]. WCRF International. [cited 2023 Apr 28]. Available from: https://www.wcrf.org/cancer-trends/worldwide-cancer-data.

7. SEER [Internet]. [cited 2023 Jun 28]. Acute Myeloid Leukemia - Cancer Stat Facts. Available from: https://seer.cancer.gov/statfacts.

8. Zjablovskaja P, Florian MC. Acute Myeloid Leukemia: Aging and Epigenetics. Cancers. 2019 Dec 31;12(1):103.

9. Kantarjian H, Kadia T, DiNardo C, Daver N, Borthakur G, Jabbour E, et al. Acute myeloid leukemia: current progress and future directions. Blood Cancer J. 2021 Feb 22;11(2):1–25.

10. Molyneux E, Scanlan T, Chagaluka G, Renner L. Haematological cancers in African children: progress and challenges. Br J Haematol. 2017;177(6):971–8.

11. Fleming AF. Leukaemias in Africa. Leukemia. 1993 Aug;7 Suppl 2:S138-141.

12. GLOBOCAN (2020) Estimated cancer Incidence, Mortality, Prevalence and Disability adjusted life years (DALYs) Worldwide in 2020. International Agency for Research on Cancer, Lyon, France.

13. Weir EG, Borowitz MJ. Flow cytometry in the diagnosis of acute leukemia. Semin Hematol. 2001 Apr;38(2):124–38.

14. Arunachalam S. Applications of Machine Learning and Image Processing Techniques in the Detection of Leukemia. Int J Sci Res Comput Sci Eng. 2020 Apr 30;8:77–82.

15. Long NA, Golla U, Sharma A, Claxton DF. Acute Myeloid Leukemia Stem Cells: Origin, Characteristics, and Clinical Implications. Stem Cell Rev Rep. 2022 Apr;18(4):1211–26.

16. Terwilliger T, Abdul-Hay M. Acute lymphoblastic leukemia: a comprehensive review and 2017 update. Blood Cancer J. 2017 Jun;7(6):577–577.

17. Scarfò L, Ferreri AJM, Ghia P. Chronic lymphocytic leukaemia. Crit Rev Oncol Hematol. 2016 Aug;104:169–82.

18. Chen Y, Li J, Xu L, Găman MA, Zou Z. The genesis and evolution of acute myeloid leukemia stem cells in the microenvironment: From biology to therapeutic targeting. Cell Death Discov. 2022 Sep 26;8(1):1–10.

19. DiNardo CD, Cortes JE. Mutations in AML: prognostic and therapeutic implications. Hematol Am Soc Hematol Educ Program. 2016 Dec 2;2016(1):348–55.

20. Green K, Tandon S, Ahmed M, Toscano W, O'Connor D, Ancliff P, et al. Congenital acute myeloid leukemia: challenges and lessons. A 15-year experience from the UK. Leuk Lymphoma. 2021 Mar;62(3):688–95.

21. Schüz J, Erdmann F. Environmental Exposure and Risk of Childhood Leukemia: An Overview. Arch Med Res. 2016 Nov;47(8):607–14.

22. Xavier AC, Taub JW. Acute leukemia in children with Down syndrome. Haematologica. 2010 Jul;95(7):1043–5.

23. Hitzler JK, Zipursky A. Origins of leukaemia in children with Down syndrome. Nat Rev Cancer. 2005 Jan;5(1):11–20.

24. Childhood Acute Lymphoblastic Leukemia Treatment (PDQ®) - NCI [Internet]. 2023 [cited 2023 Sep 6]. Available from: https://www.cancer.gov/types/leukemia.

25. Marlow EC, Ducore J, Kwan ML, Cheng SY, Bowles EJA, Greenlee RT, et al. Leukemia Risk in a Cohort of 3.9 million Children With and Without Down Syndrome. J Pediatr. 2021 Jul;234:172-180.

26. Lupo PJ, Schraw JM, Desrosiers TA, Nembhard WN, Langlois PH, Canfield MA, et al. Association Between Birth Defects and Cancer Risk Among Children and Adolescents in a Population-Based Assessment of 10 million Live Births. JAMA Oncol. 2019 Aug;5(8):1–10.

27. Mateos MK, Barbaric D, Byatt SA, Sutton R, Marshall GM. Down syndrome and leukemia: insights into leukemogenesis and translational targets. Transl Pediatr. 2015 Apr;4(2):76–92.

28. Roy A, Roberts I, Norton A, Vyas P. Acute megakaryoblastic leukaemia (AMKL) and transient myeloproliferative disorder (TMD) in Down syndrome: a multi-step model of myeloid leukaemogenesis. Br J Haematol. 2009;147(1):3–12.

29. Horsman DE, Pantzar JT, Dill FJ, Kalousek DK. Klinefelter's syndrome and acute leukemia. Cancer Genet Cytogenet. 1987 Jun;26(2):375–6.

30. Swaminathan M, Bannon SA, Routbort M, Naqvi K, Kadia TM, Takahashi K, et al. Hematologic malignancies and Li-Fraumeni syndrome. Cold Spring Harb Mol Case Stud. 2019 Feb;5(1):3210.

31. Alter BP. Fanconi anemia and the development of leukemia. Best Pract Res Clin Haematol. 2014;27(3–4):214–21.

32. Sartor C, Papayannidis C, Chiara Abbenante M, Curti A, Polverelli N, Ottaviani E, et al. A Case Report of Acute Myeloid Leukemia and Neurofibromatosis 1. Hematol Rep. 2013 Jul 3;5(2):28–9.

33. Tsushima H, Iwanaga M, Miyazaki Y. Late effect of atomic bomb radiation on myeloid disorders: leukemia and myelodysplastic syndromes. Int J Hematol. 2012 Mar 1;95(3):232–8.

34. Finch SC. Leukemia: lessons from the Japanese experience. Stem Cells Dayt Ohio. 1997;15 Suppl 2:135–9.

35. Poynter JN, Richardson M, Roesler M, Blair CK, Hirsch B, Nguyen P, et al. Chemical exposures, and risk of acute myeloid leukemia and myelodysplastic syndromes in a population-based study. Int J Cancer. 2017 Jan 1;140(1):23–33.

36. North CM, Schnatter AR, Rooseboom M, Aygun Kocabas N, Dalzell A, Williams SD. Key event-informed risk models for benzene-induced acute myeloid leukaemia. Toxicol Lett. 2021 Apr 1;340:141–52.

37. Fircanis S, Merriam P, Khan N, Castillo JJ. The relation between cigarette smoking and risk of acute myeloid leukemia: an updated meta-analysis of epidemiological studies. Am J Hematol. 2014 Aug;89(8):125-132.

38. Behrmann L, Wellbrock J, Fiedler W. Acute Myeloid Leukemia and the Bone Marrow Niche-Take a Closer Look. Front Oncol. 2018;8:444.

39. Miles LA, Bowman RL, Merlinsky TR, Csete IS, Ooi AT, Durruthy-Durruthy R, et al. Single-cell mutation analysis of clonal evolution in myeloid malignancies. Nature. 2020 Nov;587(7834):477–82.

40. Whiteley AE, Price TT, Cantelli G, Sipkins DA. Leukaemia: a model metastatic disease. Nat Rev Cancer. 2021 Jul;21(7):461–75.

41. Falini B. Acute myeloid leukemia with mutated nucleophosmin (NPM1): molecular, pathological, and clinical features. Cancer Treat Res. 2010;145:149–68.

42. NPM1-mutated acute myeloid leukemia: from bench to bedside - PubMed [Internet]. [cited 2023 Jun 30]. Available from: https://pubmed.ncbi.nlm.nih.gov.

43. Becker H, Marcucci G, Maharry K, Radmacher MD, Mrózek K, Margeson D, et al. Favorable Prognostic Impact of NPM1 mutations in older patients with cytogenetically normal De Novo acute myeloid leukemia and associated gene- and MicroRNA-expression Signatures: A Cancer and Leukemia Group B Study. J Clin Oncol. 2010 Feb 1;28(4):596–604.

44. Fu W, Huang A, Xu L, Peng Y, Gao L, Chen L, et al. Cytogenetic abnormalities in NPM1-mutated acute myeloid leukemia. Leuk Lymphoma. 2022 Aug;63(8):1956–63.

45. Daver N, Schlenk RF, Russell NH, Levis MJ. Targeting FLT3 mutations in AML: review of current knowledge and evidence. Leukemia. 2019 Feb;33(2):299–312.

46. Daver N, Venugopal S, Ravandi F. FLT3 mutated acute myeloid leukemia: 2021 treatment algorithm. Blood Cancer J. 2021 May 27;11(5):104.

47. Stone RM, Mandrekar SJ, Sanford BL, Laumann K, Geyer S, Bloomfield CD, et al. Midostaurin plus chemotherapy for acute myeloid leukemia with a FLT3 mutation. N Engl J Med. 2017 Aug 3;377(5):454–64.

48. K L, De Z. RUNX1 and RUNX1-ETO: roles in haematopoiesis and leukemogenesis. Front Biosci Landmark Ed [Internet]. 2012 Jan 1 [cited 2023 Jun 30];17(3). Available from: https://pubmed.ncbi.nlm.nih.gov.

49. DeKelver RC, Lewin B, Weng S, Yan M, Biggs J, Zhang DE. RUNX1-ETO induces a type I interferon response which negatively effects t(8;21)-induced increased self-renewal and leukemia development. Leuk Lymphoma. 2014 Apr;55(4):884–91.

50. Ichikawa M, Yoshimi A, Nakagawa M, Nishimoto N, Watanabe-Okochi N, Kurokawa M. A role for RUNX1 in hematopoiesis and myeloid leukemia. Int J Hematol. 2013 Jun;97(6):726–34.

51. Montalban-Bravo G, DiNardo CD. The role of IDH mutations in acute myeloid leukemia. Future Oncol Lond Engl. 2018 Apr;14(10):979–93.

52. Issa GC, DiNardo CD. Acute myeloid leukemia with IDH1 and IDH2 mutations: 2021 treatment algorithm. Blood Cancer J. 2021 Jun 3;11(6):1–7.

53. Mannelli F, Ponziani V, Bencini S, Bonetti MI, Benelli M, Cutini I, et al. CEBPA-double-mutated acute myeloid leukemia displays a unique phenotypic profile: a reliable screening method and insight into biological features. Haematologica. 2017 Mar;102(3):529–40.

54. Su L, Shi YY, Liu ZY, Gao SJ. Acute myeloid leukemia with *CEBPA* mutations: Current Progress and Future Directions. Front Oncol. 2022 Feb 1;12:806137.

55. Niparuck P, Police P, Noikongdee P, Siriputtanapong K, Limsuwanachot N, Rerkamnuaychoke B, et al. TP53 mutation in newly diagnosed acute myeloid leukemia and myelodysplastic syndrome. Diagn Pathol. 2021 Oct 31;16(1):100.

56. Khan M, Din M, Naeem Z, Sajid Z, Khan D, Amjad M, et al. Insights into Acute Myeloid Leukemia: Critical Analysis on its Wide Aspects. 2020 Dec 31;Volume 3:1–9.

57. Rawat J, Virmani J, Singh A, Bhadauria HS, Kumar I, Devgan JS. FAB classification of acute leukemia using an ensemble of neural networks. Evol Intell. 2022 Mar;15(1):99–117.

58. Walter RB, Othus M, Burnett AK, Löwenberg B, Kantarjian HM, Ossenkoppele GJ, et al. Significance of FAB subclassification of "acute myeloid leukemia, NOS" in the 2008 WHO classification: Analysis of 5848 newly diagnosed patients. Blood. 2013;121(13):2424–31.

59. Bennett JM, Catovsky D, Daniel MT, Flandrin G, Galton DA, Gralnick HR, et al. Criteria for the diagnosis of acute leukemia of megakaryocyte lineage (M7). A report of the French-American-British Cooperative Group. Ann Intern Med. 1985 Sep;103(3):460–2.

60. Acute Myeloid Leukemia (AML) Staging: FAB and WHO classifications for acute myeloid leukemia. 2021 Jan 15 [cited 2023 Sep 6]; Available from: https://emedicine.medscape.com/article/2006750-overview

61. Ladines-Castro W, Barragán-Ibañez G, Luna-Pérez MA, Santoyo-Sánchez A, Collazo-Jaloma J, Mendoza-García E, et al. Morphology of leukaemia. Rev Médica Hosp Gen México. 2016 Apr 1;79(2):107–13.

62. Acute Myeloid Leukemia (AML) Subtypes and Prognostic Factors [Internet]. [cited 2023 Apr 5]. Available from: https://www.cancer.org/cancer/acute-myeloid-leukemia/detection-diagnosis-staging/how-classified.

63. Vardiman JW, Harris NL, Brunning RD. The World Health Organization (WHO) classification of the myeloid neoplasms. Blood. 2002 Oct 1;100(7):2292–302.

64. De Kouchkovsky I, Abdul-Hay M. 'Acute myeloid leukemia: a comprehensive review and 2016 update'. Blood Cancer J. 2016 Jul;6(7):441.

65. Visani G, Loscocco F, Isidori A, Piccaluga PP. Genetic profiling in acute myeloid leukemia: a path to predicting treatment outcome. Expert Rev Hematol. 2018 May 24;11:1–7.

66. Canaani J, Beohou E, Labopin M, Socié G, Huynh A, Volin L, et al. Impact of FAB classification on predicting outcome in acute myeloid leukemia, not otherwise specified, patients undergoing allogeneic stem cell transplantation in CR1: An analysis of 1690 patients from the acute leukemia working party of EBMT. Am J Hematol. 2017 Apr;92(4):344–50.

67. Chemotherapy to Treat Cancer - NCI [Internet]. 2015 [cited 2023 Oct 24]. Available from: https://www.cancer.gov/about-cancer/treatment/types/chemotherapy.

68. Lancet JE, Uy GL, Cortes JE, Newell LF, Lin TL, Ritchie EK, et al. CPX-351 (cytarabine and daunorubicin) Liposome for injection versus onventional cytarabine plus daunorubicin in older patients with newly diagnosed secondary acute myeloid leukemia. J Clin Oncol Off J Am Soc Clin Oncol. 2018 Sep 10;36(26):2684–92.

69. Alfayez M, Kantarjian H, Kadia T, Ravandi-Kashani F, Daver N. CPX-35 in AML. Leuk Lymphoma. 2020 Feb;61(2):288–97.

70. Samra B, Konopleva M, Isidori A, Daver N, DiNardo C. Venetoclax-Based combinations in acute myeloid leukemia: Current Evidence and Future Directions. Front Oncol. 2020;10:562558.

71. Research C for DE and FDA grants regular approval to venetoclax in combination for untreated acute myeloid leukemia. FDA [Internet]. 2021 Nov 6 [cited 2023 Sep 7]; Available from: https://www.fda.gov/drugs/resources-information-approved-drugs/fda-grants-regular-approval-venetoclax-combination-untreated-acute-myeloid-leukemia.

72. A Randomized, Double-Blind, Placebo Controlled Phase 3 Study of Venetoclax in combination with azacitidine versus azacitidine in treatment naïve subjects with acute myeloid leukemia who are ineligible for standard induction therapy [Internet]. clinicaltrials.gov; 2023 Jun [cited 2023 Sep 5]. Report No.: NCT02993523. Available from: https://clinicaltrials.gov/study/NCT02993523.

73. Fitting J, Blume T, Ten Haaf A, Blau W, Gattenlöhner S, Tur MK, et al. Phage display-based generation of novel internalizing antibody fragments for immunotoxin-based treatment of acute myeloid leukemia. mAbs. 2015;7(2):390–402.

74. Mardiana S, Gill S. CAR T Cells for Acute Myeloid Leukemia: State of the art and future directions. Front Oncol. 2020 May 6;10:697.

75. Blau CA. E. Donnall Thomas, M.D. (1920–2012). Stem Cells. Transl Med. 2013 Feb;2(2):81–2.

76. Mandelli F, Vignetti M, Suciu S, Stasi R, Petti MC, Meloni G, et al. Daunorubicin versus mitoxantrone versus idarubicin as induction and consolidation chemotherapy for adults with acute myeloid leukemia: the EORTC and GIMEMA Groups Study AML-10. J Clin Oncol Off J Am Soc Clin Oncol. 2009 Nov 10;27(32):5397–403.

77. Baron F, Stevens-Kroef M, Kicinski M, Meloni G, Muus P, Marie JP, et al. Impact of induction regimen and allogeneic hematopoietic cell transplantation on outcome in younger adults with acute myeloid leukemia with a monosomal karyotype. Haematologica. 2019 Jun;104(6):1168–75.

78. Cancer.Net [Internet]. 2013 [cited 2023 Sep 7]. Side effects of a bone marrow transplant (stem cell transplant). Available from: https://www.cancer.net/navigating-cancer-care/how-cancer-treated/bone-marrowstem-cell-transplantation/side-effects-bone-marrow-transplant-stem-cell-transplant.

79. Grafone T, Palmisano M, Nicci C, Storti S. An overview on the role of FLT3-tyrosine kinase receptor in acute myeloid leukemia: biology and treatment. Oncol Rev. 2012 Apr 17;6(1):8.

80. Percival ME, Estey E. Emerging treatments in acute myeloid leukemia: current standards and unmet challenges. Clin Adv Hematol Oncol HO. 2017 Aug;15(8):632–42.

81. Numan Y, Abdel Rahman Z, Grenet J, Boisclair S, Bewersdorf JP, Collins C, et al. Gilteritinib clinical activity in relapsed/refractory FLT3 mutated acute myeloid leukemia previously treated with FLT3 inhibitors. Am J Hematol. 2022 Mar 1;97(3):322–8.

82. Research C for DE and FDA approves quizartinib for newly diagnosed acute myeloid leukemia. FDA [Internet]. 2023 Jul 21 [cited 2023 Sep 19]; Available from: https://www.fda.gov/drugs/drug-approvals-and-databases/fda-approves-quizartinib-newly-diagnosed-acute-myeloid-leukemia.

83. Reitman ZJ, Yan H. Isocitrate Dehydrogenase 1 and 2 Mutations in Cancer: Alterations at a crossroads of cellular metabolism. JNCI J Natl Cancer Inst. 2010 Jul 7;102(13):932–41.

84. Byun JM, Yoo SJ, Kim HJ, Ahn JS, Koh Y, Jang JH, et al. IDH1/2 mutations in acute myeloid leukemia. Blood Res. 2022 Mar 31;57(1):13–9.

85. Abou Dalle I, DiNardo CD. The role of enasidenib in the treatment of mutant IDH2 acute myeloid leukemia. Ther Adv Hematol. 2018 Jul;9(7):163–73.

86. Research C for DE and FDA granted regular approval to enasidenib for the treatment of relapsed or refractory AML. FDA [Internet]. 2019 Sep 2 [cited 2023 Sep 22]; Available from: https://www.fda.gov/drugs/resources-information-approved-drugs/fda-granted-regular-approval-enasidenib-treatment-relapsed-or-refractory-aml.

87. Megías-Vericat JE, Ballesta-López O, Barragán E, Montesinos P. IDH1-mutated relapsed or refractory AML: current challenges and future prospects. Blood Lymphat Cancer Targets Ther. 2019 Jun 27;9:19–32.

88. Research C for DE and. FDA approves ivosidenib for relapsed or refractory acute myeloid leukemia. FDA [Internet]. 2019 Sep 2 [cited 2023 Sep 22]; Available from: https://www.fda.gov/drugs/resources-information-approved-drugs/fda-approves-ivosidenib-relapsed-or-refractory-acute-myeloid-leukemia.

89. Research C for DE and FDA approves olutasidenib for relapsed or refractory acute myeloid leukemia with a susceptible IDH1 mutation. FDA [Internet]. 2022 Jan 12 [cited 2023 Sep 22]; Available from: https://www.fda.gov/drugs/resources-information-approved-drugs/fda-approves-olutasidenib-relapsed-or-refractory-acute-myeloid-leukemia-susceptible-idh1-mutation.

90. Hatok J, Racay P. Bcl-2 family proteins: master regulators of cell survival. Biomol Concepts. 2016 Aug 1;7(4):259–70.

91. Hardwick JM, Soane L. Multiple Functions of BCL-2 Family Proteins. Cold Spring Harb Perspect Biol. 2013 Feb;5(2):a008722.

92. Qian S, Wei Z, Yang W, Huang J, Yang Y, Wang J. The role of BCL-2 family proteins in regulating apoptosis and cancer therapy. Front Oncol. 2022 Oct 12;12:985363.

93. Perini GF, Ribeiro GN, Pinto Neto JV, Campos LT, Hamerschlak N. BCL-2 as therapeutic target for hematological malignancies. J Hematol OncolJ Hematol Oncol. 2018 May 11;11(1):65.

94. Borg MA, Clemmons A. Venetoclax: A Novel Treatment for Patients With del(17p) Chronic Lymphocytic Leukemia. J Adv Pract Oncol. 2017;8(6):647–52.

95. Terao T, Minami Y. Targeting Hedgehog (Hh) Pathway for the Acute Myeloid Leukemia Treatment. Cells. 2019 Apr 3;8(4):312.

96. Agren M, Kogerman P, Kleman MI, Wessling M, Toftgård R. Expression of the PTCH1 tumor suppressor gene is regulated by alternative promoters and a single functional Gli-binding site. Gene. 2004 Apr 14;330:101–14.

97. Jamieson C, Martinelli G, Papayannidis C, Cortes JE. Hedgehog Pathway Inhibitors: A New Therapeutic Class for the Treatment of Acute Myeloid Leukemia. Blood Cancer Discov. 2020 Aug 11;1(2):134–45.

98. Norsworthy KJ, By K, Subramaniam S, Zhuang L, Del Valle PL, Przepiorka D, et al. FDA Approval Summary: Glasdegib for Newly Diagnosed Acute Myeloid Leukemia. Clin Cancer Res Off J Am Assoc Cancer Res. 2019 Oct 15;25(20):6021–5.

99. Krzyszczyk P, Acevedo A, Davidoff EJ, Timmins LM, Marrero-Berrios I, Patel M, et al. The growing role of precision and personalized medicine for cancer treatment. Technology. 2018;6(3–4):79–100.

100. Liu L, Chen J. Therapeutic antibodies for precise cancer immunotherapy: current and future perspectives. Med Rev. 2022 Dec 1;2(6):555–69.

101. Naran K, Nundalall T, Chetty S, Barth S. Principles of Immunotherapy: Implications for Treatment Strategies in Cancer and Infectious Diseases. Front Microbiol. 2018 Dec 21;9:3158.

102. Tur MK, Barth S. Immunotherapy. In: Schwab M, editor. Encyclopedia of cancer. Berlin, Heidelberg: Springer; 2017 Jan 1; 27(1): 2237–9.

103. Ecker DM, Jones SD, Levine HL. The therapeutic monoclonal antibody market. mAbs. 2015;7(1):9–14.

104. Lu RM, Hwang YC, Liu IJ, Lee CC, Tsai HZ, Li HJ, et al. Development of therapeutic antibodies for the treatment of diseases. J Biomed Sci. 2020 Jan 2;27(1):1.

105. Huysamen AM, Fadeyi OE, Mayuni G, Dogbey DM, Mungra N, Biteghe FAN, et al. Click Chemistry-Generated Auristatin F–Linker–Benzylguanine for a SNAP-Tag-Based Recombinant Antibody–Drug Conjugate Demonstrating Selective Cytotoxicity toward EGFR-Overexpressing Tumor Cells. ACS Omega. 2023 Jan 31;8(4):4026–37.

106. Liu L, Chen J. Therapeutic antibodies for precise cancer immunotherapy: current and future perspectives. Med Rev (Berl). 2023 Jan 16;2(6):555-569.

107. Ludwig DL, Pereira DS, Zhu Z, Hicklin DJ, Bohlen P. Monoclonal antibody therapeutics and apoptosis. Oncogene. 2003 Dec 8;22(56):9097–106.

108. Haddish-Berhane N, Shah DK, Ma D, Leal M, Gerber HP, Sapra P, et al. On translation of antibody drug conjugates efficacy from mouse experimental tumors to the clinic: a PK/PD approach. J Pharmacokinet Pharmacodyn. 2013 Oct;40(5):557–71.

109. Bross PF, Beitz J, Chen G, Chen XH, Duffy E, Kieffer L, et al. Approval summary: gemtuzumab ozogamicin in relapsed acute myeloid leukemia. Clin Cancer Res Off J Am Assoc Cancer Res. 2001 Jun;7(6):1490–6.

110. Petersdorf SH, Kopecky KJ, Slovak M, Willman C, Nevill T, Brandwein J, et al. A phase 3 study of gemtuzumab ozogamicin during induction and postconsolidation therapy in younger patients with acute myeloid leukemia. Blood. 2013 Jun 13;121(24):4854–60.

111. Research C for DE and FDA Approves Gemtuzumab Ozogamicin for CD33-positive AML. FDA [Internet]. 2019 Sep 2 [cited 2023 Apr 5]; Available from: https://www.fda.gov/drugs/resources-information-approved-drugs/fda-approves-gemtuzumab-ozogamicin-CD33-positive-aml.

112. Swaminathan M, Cortes JE. Update on the role of gemtuzumab-ozogamicin in the treatment of acute myeloid leukemia. Ther Adv Hematol. 2023;14:20406207231154708.

113. Jen EY, Ko CW, Lee JE, Del Valle PL, Aydanian A, Jewell C, et al. FDA Approval: Gemtuzumab Ozogamicin for the Treatment of Adults with Newly Diagnosed CD33-Positive Acute Myeloid Leukemia. Clin Cancer Res Off J Am Assoc Cancer Res. 2018 Jul 15;24(14):3242–6.

114. Pagel JM, Gooley TA, Rajendran J, Fisher DR, Wilson WA, Sandmaier BM, et al. Allogeneic hematopoietic cell transplantation after conditioning with 131I-anti-CD45 antibody plus fludarabine and low-dose total body irradiation for elderly patients with advanced acute myeloid leukemia or high-risk myelodysplastic syndrome. Blood. 2009 Dec 24;114(27):5444–53.

115. Bunjes D, Buchmann I, Duncker C, Seitz U, Kotzerke J, Wiesneth M, et al. Rhenium 188-labelled anti-CD66 (a, b, c, e) monoclonal antibody to intensify the conditioning regimen prior to stem cell transplantation for patients with high-risk acute myeloid leukemia or myelodysplastic syndrome: results of a phase I-II study. Blood. 2001 Aug 1;98(3):565–72.

116. Hristodorov D, Mladenov R, Pardo A, Pham AT, Huhn M, Fischer R, et al. Microtubule-associated protein tau facilitates the targeted killing of proliferating cancer cells in vitro and in a xenograft mouse tumour model in vivo. Br J Cancer. 2013 Sep 17;109(6):1570–8.

117. Hussain AF, Kampmeier F, von Felbert V, Merk HF, Tur MK, Barth S. SNAP-tag technology mediates site specific conjugation of antibody fragments with a photosensitizer and improves target specific phototoxicity in tumor cells. Bioconjug Chem. 2011 Dec 21;22(12):2487–95.

118. Aru B, Pehlivanoğlu C, Dal Z, Dereli-Çalışkan NN, Gürlü E, Yanıkkaya-Demirel G. A potential area of use for immune checkpoint inhibitors: Targeting bone marrow microenvironment in acute myeloid leukemia. Front Immunol. 2023 Jan 20;14:1108200.

119. Elliot TAE, Lecky DAJ, Bending D. T-cell response to checkpoint blockade immunotherapies: from fundamental mechanisms to treatment signatures. Essays Biochem. 2023 Jun 30;EBC20220247.

120. Tsirigotis P, Savani BN, Nagler A. Programmed death-1 immune checkpoint blockade in the treatment of hematological malignancies. Ann Med. 2016 Aug 17;48(6):428–39.

121. Liao D, Wang M, Liao Y, Li J, Niu T. A Review of Efficacy and Safety of Checkpoint Inhibitor for the Treatment of Acute Myeloid Leukemia. Front Pharmacol. 2019;10:609.

122. Bewersdorf JP, Stahl M, Zeidan AM. Immune checkpoint-based therapy in myeloid malignancies: a promise yet to be fulfilled. Expert Rev Anticancer Ther. 2019 May;19(5):393–404.

123. Andrechak JC, Dooling LJ, Discher DE. The macrophage checkpoint CD47 : SIRPα for recognition of 'self' cells: from clinical trials of blocking antibodies to mechanobiological fundamentals. Philos Trans R Soc Lond B Biol Sci. 2019 Aug 19;374(1779):20180217.

124. Ritchie DS, Neeson PJ, Khot A, Peinert S, Tai T, Tainton K, Chen K, Shin M, Wall DM, Hönemann D, Gambell P, Westerman DA, Haurat J et al, Persistence and efficacy of second generation CAR T cell against the LeY antigen in acute myeloid leukemia. Mol Ther. 2013 Nov;21(11):2122-9.

125. Kabel AM, Zamzami F, Al-Talhi M, Al-Dwila K, Hamza R. Acute Myeloid Leukemia: A focus on Risk Factors, Clinical Presentation, Diagnosis and Possible Lines of Management. J Cancer Res Treat. 2017 Jun 13;5(2):62–7.

126. Signs and Symptoms of Acute Myeloid Leukemia (AML) [Internet]. [cited 2023 Jun 30]. Available from: https://www.cancer.org/cancer/types/acute-myeloid-leukemia/detection-diagnosis-staging/signs-symptoms.

127. Soon GS, Laxer RM. Approach to recurrent fever in childhood. Can Fam Physician. 2017 Oct;63(10):756.

128. Namazzi R, Gaikwad A, Wasswa P, Cubbage M, Kambugu JB, Kasirye P, et al. Improving diagnosis and treatment of acute childhood leukemia in Uganda: impact of flow cytometry. Blood Adv. 2018 Nov 30;2(Suppl 1):21–3.

129. Howard SC, Pedrosa M, Lins M, Pedrosa A, Pui CH, Ribeiro RC, et al. Establishment of a pediatric oncology program and outcomes of childhood acute lymphoblastic leukemia in a resource-poor area. JAMA. 2004 May 26;291(20):2471–5.

130. Nandakumar A, Anantha N, Venugopal T, Reddy S, Padmanabhan B, Swamy K, et al. Descriptive epidemiology of lymphoid and haemopoietic malignancies in Bangalore, India. Int J Cancer. 1995 Sep 27;63(1):37–42.

131. Heuser M, Ofran Y, Boissel N, Mauri SB, Craddock C, Janssen J, et al. Acute myeloid leukaemia in adult patients: ESMO Clinical Practice Guidelines for diagnosis, treatment and follow-up†. Ann Oncol. 2020 Jun 1;31(6):697–712.

132. Alessandrini M, Beltchev E, Pool R, Pepper M. Evaluation of The AMLprofiler in The South African Context: Report On Preliminary Findings. Blood. 2013 Nov 15;122(21):5590.

133. Tucker J, Dorey E, Gregory WM, Simpson AP, Amess JA, Lister TA, Horton MA. Immunophenotype of blast cells in acute myeloid leukemia may be a useful predictive factor for outcome. Hematol Oncol. 1990 Jan-Feb;8(1):47-58.

134. Paietta E. Assessing minimal residual disease (MRD) in leukemia: a changing definition and concept? Bone Marrow Transplant. 2002 Mar;29(6):459–65.

135. Al-Mawali A, Gillis D, Lewis I. The role of multiparameter flow cytometry for detection of minimal residual disease in acute myeloid leukemia. Am J Clin Pathol. 2009 Jan;131(1):16–26.

136. Bendari M, Sraidi S, Khoubila N. Overview of the recent progresses in genetics intechopen; 2021:96913.

137. Ozkan E, Lacerda MP. Genetics, Cytogenetic Testing And conventional karyotype. In: StatPearls [Internet]. Treasure Island (FL): StatPearls Publishing; 2023 [cited 2023 Apr 10]. Available from: http://www.ncbi.nlm.nih.gov/books/NBK563293.

138. Gonzales PR, Mikhail FM. Diagnostic and Prognostic Utility of Fluorescence In situ Hybridization (FISH) Analysis in Acute Myeloid Leukemia. Curr Hematol Malig Rep. 2017 Dec;12(6):568–73.

139. Custom AML Panel - CD Genomics [Internet]. [cited 2023 Apr 10]. Available from: https://www.cd-genomics.com/diseasepanel/custom-aml-panel.

140. Schuurhuis GJ, Heuser M, Freeman S, Béné MC, Buccisano F, Cloos J, et al. Minimal/measurable residual disease in AML: a consensus document from the European LeukemiaNet MRD Working Party. Blood. 2018 Mar 22;131(12):1275–91.

141. Hubmann M, Köhnke T, Hoster E, Schneider S, Dufour A, Zellmeier E, et al. Molecular response assessment by quantitative real-time polymerase chain reaction after induction therapy in NPM1-mutated patients identifies those at high risk of relapse. Haematologica. 2014 Aug 1;99(8):1317–25.

142. Nardi V, Hasserjian RP. Genetic Testing in Acute Myeloid Leukemia and Myelodysplastic Syndromes. Surg Pathol Clin. 2016 Mar;9(1):143–63.

143. Craig FE, Foon KA. Flow cytometric immunophenotyping for hematologic neoplasms. Blood. 2008 Apr 15;111(8):3941–67.

144. Bösmüller H, Fischer A, Pham DL, Fehm T, Capper D, von Deimling A, et al. Detection of the BRAF V600E mutation in serous ovarian tumors: a comparative analysis of immunohistochemistry with a mutation-specific monoclonal antibody and allele-specific PCR. Hum Pathol. 2013 Mar;44(3):329–35.

145. Axup JY, Bajjuri KM, Ritland M, Hutchins BM, Kim CH, Kazane SA, et al. Synthesis of site-specific antibody-drug conjugates using unnatural amino acids. Proc Natl Acad Sci U S A. 2012 Oct 2;109(40):16101–6.

146. Gong H, Kovar JL, Cheung L, Rosenthal EL, Olive DM. A comparative study of affibody, panitumumab, and EGF for near-infrared fluorescence imaging of EGFR- and EGFRvIII-expressing tumors. Cancer Biol Ther. 2014 Feb;15(2):185–93.

147. Alley SC, Okeley NM, Senter PD. Antibody-drug conjugates: targeted drug delivery for cancer. Curr Opin Chem Biol. 2010 Aug;14(4):529–37.

148. Reichert JM. Antibodies to watch in 2016. mAbs. 2016;8(2):197–204.

149. Furia L, Pelicci P, Faretta M. Confocal microscopy for high-resolution and high-content analysis of the cell cycle. Curr Protoc Cytom. 2014 Oct 1;70:7.42.1-14.

150. Laser Systems for Confocal Microscopy | Olympus LS [Internet]. [cited 2023 Apr 10]. Available from: https://www.olympus-lifescience.com/en/microscope resource/primer/techniques.

151. Saxena R, Anand H. Flow cytometry in acute leukemia. Indian J Hematol Blood Transfus Off J Indian Soc Hematol Blood Transfus. 2008 Dec;24(4):146–50.

152. Cools J, Vandenberghe P. New flow cytometry in hematologic malignancies. Haematologica. 2009 Dec;94(12):1639–41.

153. Barlogie B, Latreille J, Freireich EJ, Fu CT, Mellard D, Meistrich M, et al. Characterization of hematologic malignancies by flow cytometry. Blood Cells. 1980;6(4):719–44.

154. Neale G a. M, Coustan-Smith E, Stow P, Pan Q, Chen X, Pui CH, et al. Comparative analysis of flow cytometry and polymerase chain reaction for the detection of minimal residual disease in childhood acute lymphoblastic leukemia. Leukemia. 2004 May;18(5):934–8.

155. Percival ME, Lai C, Estey E, Hourigan CS. Bone marrow evaluation for diagnosis and monitoring of acute myeloid leukemia. Blood Rev. 2017 Jul;31(4):185–92.

156. Tests for Acute Myeloid Leukemia (AML) [Internet]. [cited 2023 Jul 1]. Available from: https://www.cancer.org/cancer/types/acute-myeloid-leukemia/detection-diagnosis-staging/how diagnosed.

157. Schoch C, Haferlach T. Cytogenetics in acute myeloid leukemia. Curr Oncol Rep. 2002 Sep;4(5):390–7.

158. Qin D. Molecular testing for acute myeloid leukemia. Cancer Biol Med. 2022 Jan 15;19(1):4–13.

159. Chen X, Cherian S. Acute Myeloid Leukemia Immunophenotyping by Flow Cytometric Analysis. Clin Lab Med. 2017 Dec 1;37(4):753–69.

160. Tabata R, Chi S, Yuda J, Minami Y. Emerging Immunotherapy for Acute Myeloid Leukemia. Int J Mol Sci. 2021 Feb 16;22(4):1944.

161. Vergez F, Largeaud L, Bertoli S, Nicolau ML, Rieu JB, Vergnolle I, et al. Phenotypically-defined stages of leukemia arrest predict main driver mutations subgroups, and outcome in acute myeloid leukemia. Blood Cancer J. 2022 Aug 16;12(8):1–11.

162. Ghosh S, Shinde SC, Kumaran GS, Sapre RS, Dhond SR, Badrinath Y, et al. Haematologic and immunophenotypic profile of acute myeloid leukemia: an experience of Tata Memorial Hospital. Indian J Cancer. 2003;40(2):71–6.

163. Gorczyca W, Sun ZY, Cronin W, Li X, Mau S, Tugulea S. Immunophenotypic pattern of myeloid populations by flow cytometry analysis. Methods Cell Biol. 2011;103:221–66.

164. Lin KM, Austin GE. Functional activity of three distinct myeloperoxidase (MPO) promoters in human myeloid cells. Leukemia. 2002 Jun;16(6):1143–53.

165. Leong CF, Kalaichelvi AVM, Cheong SK, Hamidah NH, Rahman J, Sivagengei K. Comparison of myeloperoxidase detection by flow cytometry using two different clones of monoclonal antibodies. Malays J Pathol. 2004 Dec;26(2):111–6.

166. Choi Y, Lee JH, Kim SD, Kim DY, Lee JH, Seol M, et al. Prognostic implications of CD14 positivity in acute myeloid leukemia arising from myelodysplastic syndrome. Int J Hematol. 2013 Feb;97(2):246–55.

167. Kim Y, Yoon S, Kim SJ, Kim JS, Cheong JW, Min YH. Myeloperoxidase Expression in Acute Myeloid Leukemia Helps Identifying Patients to Benefit from Transplant. Yonsei Med J. 2012 May 1;53(3):530–6.

168. Roerden M, Märklin M, Salih HR, Bethge WA, Klein R, Rammensee HG, et al. Expression levels of HLA-DR in acute myeloid leukemia: implications for antigenicity and clinical outcome. Leuk Lymphoma. 2021 Aug;62(8):1907–19.

169. Shiina T, Hosomichi K, Inoko H, Kulski JK. The HLA genomic loci map: expression, interaction, diversity and disease. J Hum Genet. 2009 Jan;54(1):15-39.

170. Schafer PH, Pierce SK, Jardetzky TS. The structure of MHC class II: a role for dimer of dimers. Semin Immunol. 1995 Dec;7(6):389–98.

171. Wetzler M, McElwain BK, Stewart CC, Blumenson L, Mortazavi A, Ford LA, et al. HLA-DR antigen-negative acute myeloid leukemia. Leukemia. 2003 Apr;17(4):707–15.

172. Döhner H, Estey E, Grimwade D, Amadori S, Appelbaum FR, Büchner T, et al. Diagnosis and management of AML in adults: 2017 ELN recommendations from an international expert panel. Blood. 2017 Jan 26;129(4):424–47.

173. Döhner H, Wei AH, Appelbaum FR, Craddock C, DiNardo CD, Dombret H, et al. Diagnosis and management of AML in adults: 2022 recommendations from an international expert panel on behalf of the ELN. Blood. 2022 Sep 22;140(12):1345–77.

174. Stein R, Gupta P, Chen X, Cardillo TM, Furman RR, Chen S, Chang CH, Goldenberg DM. Therapy of B-cell malignancies by anti-HLA-DR humanized monoclonal antibody, IMMU-114, is mediated through hyperactivation of ERK and JNK MAP kinase signaling pathways. Blood. 2010 Jun 24;115(25):5180-90.

175. Dechant M, Bruenke J, Valerius T. HLA class II antibodies in the treatment of hematologic malignancies. Semin Oncol. 2003 Aug 1;30(4):465–75.

176. Yamamoto W, Nakamura N, Tomita N, Takeuchi K, Ishii Y, Takahashi H, et al. Human leukocyte antigen-DR expression on flow cytometry and tumor-associated macrophages in diffuse large B-cell lymphoma treated by rituximab, cyclophosphamide, doxorubicin, vincristine and prednisone therapy: retrospective cohort study. Leuk Lymphoma. 2014 Dec;55(12):2721–7.

177. Ren F, Zhang N, Xu Z, Xu J, Zhang Y, Chen X, et al. The CD9+ CD11b- HLA-DR- immunophenotype can be used to diagnose acute promyelocytic leukemia. Int J Lab Hematol. 2019 Apr;41(2):168–75.

178. Colloby PS, West KP, Fletcher A. Is poor prognosis really related to HLA-DR expression by malignant melanoma cells? Histopathology. 1992 May;20(5):411–6.

179. Maleki LA, Shanehbandi D, Majidi J, Yusefi M, Abdolalizadeh J, Orangi M, et al. Production of anti-CD14 monoclonal antibody using synthetic peptide of human CD14 as immunizing antigen. Hum Antibodies. 2013;22(3–4):67–71.

180. Płóciennikowska A, Hromada-Judycka A, Borzęcka K, Kwiatkowska K. Co-operation of TLR4 and raft proteins in LPS-induced pro-inflammatory signaling. Cell Mol Life Sci. 2015 Feb 1;72(3):557–81.

181. Harris CL, Vigar MA, Rey Nores JE, Horejsi V, Labeta MO, Morgan BP. The lipopolysaccharide co-receptor CD14 is present and functional in seminal plasma and expressed on spermatozoa. Immunology. 2001 Nov;104(3):317–23.

182. Kitchens RL, Thompson PA. Modulatory effects of sCD14 and LBP on LPS-host cell interactions. J Endotoxin Res. 2005;11(4):225–9.

183. Krasinskas AM, Wasik MA, Kamoun M, Schretzenmair R, Moore J, Salhany KE. The usefulness of CD64, other monocyte-associated antigens, and CD45 gating in the subclassification of acute myeloid leukemias with monocytic differentiation. Am J Clin Pathol. 1998 Dec;110(6):797–805.

184. Gupta D, Shah HP, Malu K, Berliner N, Gaines P. Differentiation and characterization of myeloid cells. Curr Protoc Immunol. 2014 Feb 4;104:22.

185. Klebanoff SJ. Myeloperoxidase. Proc Assoc Am Physicians. 1999 Sep-Oct;111(5):383-9.

186. Itonaga H, Imanishi D, Wong YF, Sato S, Ando K, Sawayama Y, et al. Expression of myeloperoxidase in acute myeloid leukemia blasts mirrors the distinct DNA methylation pattern involving the downregulation of DNA methyltransferase DNMT3B. Leukemia. 2014 Jul;28(7):1459–66.

187. Matsuo T, Kuriyama K, Miyazaki Y, Yoshida S, Tomonaga M, Emi N, et al. The percentage of myeloperoxidase-positive blast cells is a strong independent prognostic factor in acute myeloid leukemia, even in the patients with normal karyotype. Leukemia. 2003 Aug;17(8):1538–43.

188. Matsuo T, Cox C, Bennett JM. Prognostic significance of myeloperoxidase positivity of blast cells in acute myeloblastic leukemia without maturation (FAB: M1): an ECOG study. Hematol Pathol. 1989;3(4):153–8.

189. Lanza F, Latorraca A, Moretti S, Castagnari B, Ferrari L, Castoldi G. Comparative analysis of different permeabilization methods for the flow cytometry measurement of cytoplasmic myeloperoxidase and lysozyme in normal and leukemic cells. Cytometry. 1997;30(3):134–44.

190. Chiu ML, Goulet DR, Teplyakov A, Gilliland GL. Antibody Structure and Function: The Basis for Engineering Therapeutics. Antibodies. 2019 Dec 3;8(4):55.

191. Myung Y, Pires DEV, Ascher DB. Understanding the complementarity and plasticity of antibody–antigen interfaces. Bioinformatics. 2023 Jul 1;39(7):btad392.

192. Schroeder HW Jr, Cavacini L. Structure and function of immunoglobulins. J Allergy Clin Immunol. 2010 Feb;125(2 Suppl 2):S41-52.

193. Ryman JT, Meibohm B. Pharmacokinetics of Monoclonal Antibodies. CPT Pharmacomet Syst Pharmacol. 2017 Sep;6(9):576–88.

194. VanDyk L, Meek K. Assembly of IgH CDR3: mechanism, regulation, and influence on antibody diversity. Int Rev Immunol. 1992;8(2–3):123–33.

195. D'Angelo S, Ferrara F, Naranjo L, Erasmus MF, Hraber P, Bradbury ARM. Many Routes to an Antibody Heavy-Chain CDR3: Necessary, Yet Insufficient, for Specific Binding. Front Immunol. 2018 Mar 8;9:395.

196. Imkeller K, Wardemann H. Assessing human B cell repertoire diversity and convergence. Immunol Rev. 2018;284(1):51–66.

197. Roth DB. V(D)J Recombination: Mechanism, Errors, and Fidelity. Microbiol Spectr. 2014 Dec;2(6):10.

198. Chi X, Li Y, Qiu X. V(D)J recombination, somatic hypermutation and class switch recombination of immunoglobulins: mechanism and regulation. Immunology. 2020;160(3):233–47.

199. von Mehren M, Adams GP, Weiner LM. Monoclonal antibody therapy for cancer. Annu Rev Med. 2003;54:343–69.

200. Biteghe FAN, Chalomie NET, Mungra N, Vignaux G, Gao N, Vergeade A, et al. Antibody-Based immunotherapy: Alternative Approaches for the Treatment of Metastatic Melanoma. Biomedicines. 2020 Sep;8(9):327.

201. Leavy O. The birth of monoclonal antibodies. Nat Immunol. 2016 Dec;17(1):S13–S13.

202. Muhsin A, Rangel R, Vien L, Bover L. Monoclonal Antibodies Generation: Updates and Protocols on Hybridoma Technology. Methods Mol Biol Clifton NJ. 2022;2435:73–93.

203. Batra SK, Jain M, Wittel UA, Chauhan SC, Colcher D. Pharmacokinetics and biodistribution of genetically engineered antibodies. Curr Opin Biotechnol. 2002 Dec;13(6):603-8.

204. Sauter M, Strieker M, Kleist C, Wischnjow A, Daniel V, Altmann A, et al. Improving antibody-based therapies by chemical engineering of antibodies with multimeric cell-penetrating peptides for elevated intracellular delivery. J Control Release Off J Control Release Soc. 2020 Jun 10;322:200–8.

205. Chapman K, Pullen N, Coney L, Dempster M, Andrews L, Bajramovic J, Baldrick P, Buckley L, Jacobs A, Hale G, Green C, Ragan I, Robinson V. Preclinical development of monoclonal antibodies: considerations for the use of non-human primates. MAbs. 2009 Sep-Oct;1(5):505-16.

206. Jin S, Sun Y, Liang X, Gu X, Ning J, Xu Y, et al. Emerging new therapeutic antibody derivatives for cancer treatment. Signal Transduct Target Ther. 2022 Feb 7;7(1):1–28.

207. Miller RA, Maloney DG, Warnke R, Levy R. Treatment of B-cell lymphoma with monoclonal anti-idiotype antibody. N Engl J Med. 1982 Mar 4;306(9):517–22.

208. Khazaeli MB, Conry RM, LoBuglio AF. Human immune response to monoclonal antibodies. J Immunother Emphas Tumor Immunol Off J Soc Biol Ther. 1994 Jan;15(1):42–52.

209. Waldmann H. Human Monoclonal Antibodies: The Benefits of Humanization. Methods Mol Biol Clifton NJ. 2019;1904:1–10.

210. Shepard HM, Phillips GL, Thanos CD, Feldmann M. Developments in therapy with monoclonal antibodies and related proteins. Clin Med. 2017 Jun 1;17(3):220–32.

211. Dreyer R, Pfukwa R, Barth S, Hunter R, Klumperman B. The Evolution of SNAP-Tag Labels. Biomacromolecules. 2023 Feb 13;24(2):517–30.

212. Cole NB. Site-specific protein labeling with SNAP-tags. Curr Protoc Protein Sci. 2013 Sep 24;73:30.

213. Hussain AF, Heppenstall PA, Kampmeier F et al. One-step site-specific antibody fragment auto-conjugation using SNAP-tag technology. Nat Protoc. 2019 Oct 11;3101–3125.

214. Sun X, Zhang A, Baker B, Sun L, Howard A, Buswell J, et al. Development of SNAP-Tag Fluorogenic Probes for Wash-Free Fluorescence Imaging. Chembiochem. 2011 Sep 19;12(14):2217–26.

215. Sun X, Zhang A, Baker B, Sun L, Howard A, Buswell J, Maurel D, Masharina A, Johnsson K, Noren CJ, Xu MQ, Corrêa IR Jr. Development of SNAP-tag fluorogenic probes for wash-free fluorescence imaging. Chembiochem. 2011 Sep 19;12(14):2217-26.

216. Dempsey GT, Vaughan JC, Chen KH, Bates M, Zhuang X. Evaluation of fluorophores for optimal performance in localization-based super-resolution imaging. Nat Methods. 2011 Nov 6;8(12):1027–36.

217. Mungra N, Biteghe FAN, Malindi Z, Huysamen AM, Karaan M, Hardcastle NS, Bunjun R, Chetty S, Naran K, Lang D, Richter W, Hunter R, Barth S. CSPG4 as a target for the specific killing of triple-negative breast cancer cells by a recombinant SNAP-tag-based antibody-auristatin F drug conjugate. J Cancer Res Clin Oncol. 2023 Oct;149(13):12203-12225.

218. Hussain AF, Amoury M, Barth S. SNAP-tag technology: a powerful tool for site specific conjugation of therapeutic and imaging agents. Curr Pharm Des. 2013;19(30):5437–42.

219. Niesen J, Sack M, Seidel M, Fendel R, Barth S, Fischer R, et al. SNAP-Tag Technology: A Useful Tool To Determine Affinity Constants and Other Functional Parameters of Novel Antibody Fragments. Bioconjug Chem. 2016 Aug 17;27(8):1931–41.

220. MACHEREY-NAGEL [Internet]. [cited 2023 Oct 21]. NucleoBond PC 100, Midi kit for transfection-grade plasmid DNA. Available from: https://www.mn-net.com/nucleobond-pc-100-midi-kit-for-transfection-grade-plasmid-dna.

221. Ligation Protocol with T4 DNA Ligase (M0202) | NEB [Internet]. [cited 2023 Oct 1]. Available from: https://www.neb.com/en/protocols/0001/01/01/dna-ligation-with-t4-dna-ligase.

222. Zymo Research International [Internet]. [cited 2023 Oct 27]. Zyppy Plasmid Miniprep Kit. Available from: https://zymoresearch.eu/products/zyppy-plasmid-miniprep-kit.

223. Chong ZX, Yeap SK, Ho WY. Transfection types, methods and strategies: a technical review. PeerJ. 2021 Apr 21;9:11165.

224. X-tremeGENE™ HP DNA Transfection Reagent Protocol [Internet]. [cited 2023 Oct 27]. Available from: https://www.sigmaaldrich.com/ZA/en/technical-documents/protocol/cell-culture-and-cell-culture-analysis/transfection-and-gene-editing/xtghp-general-protocol.

225. Smith BJ. SDS Polyacrylamide Gel Electrophoresis of Proteins. Methods Mol Biol Clifton NJ. 1984;1:41–55.

226. Hulspas R, O'Gorman MRG, Wood BL, Gratama JW, Sutherland DR. Considerations for the control of background fluorescence in clinical flow cytometry. Cytometry B Clin Cytom. 2009;76B(6):355–64.

227. Szalóki G, Goda K. Compensation in multicolor flow cytometry. Cytometry A. 2015;87(11):982–5.

228. Chang CH, Goldenberg DM, Hansen HJ, Qu Z. Humanized L243 antibodies [Internet]. AU2006218454B2, 2011 [cited 2023 Jul 2]. Available from: https://patents.google.com/patent/AU2006218454B2.

229. Goldenberg DM, Hansen HJ, Chang CH. Humanized anti-HLA-DR antibodies [Internet]. US10174114B2, 2019 [cited 2023 Jul 2]. Available from: https://patents.google.com/patent/US10174114B2.

230. Shen DY, Ning BT, Tang YM, Li SS. Human-mouse chimeric anti-human CD14 antibody Hm2F9 and purpose thereof [Internet]. CN102260350A, 2011 [cited 2023 Jul 2]. Available from: https://patents.google.com/patent/CN102260350A.

231. Jethwa HS, Clarke SH, Itoh-Lindstrom Y, Falk RJ, Jennette JC, Nachman PH. Restriction in V kappa gene use and antigen selection in anti-myeloperoxidase response in mice. J Immunol Baltim Md 1950. 2000 Oct 1;165(7):3890–7.

232. Owji H, Nezafat N, Negahdaripour M, Hajiebrahimi A, Ghasemi Y. A comprehensive review of signal peptides: Structure, roles, and applications. Eur J Cell Biol. 2018 Aug;97(6):422–41.

233. Knecht S, Ricklin D, Eberle AN, Ernst B. Oligohis-tags: mechanisms of binding to Ni2+-NTA surfaces. J Mol Recognit JMR. 2009;22(4):270–9.

234. Volkmann G, Volkmann V, Liu XQ. Site-specific protein cleavage in vivo by an intein-derived protease. FEBS Lett. 2012 Jan 2;586(1):79–84.

235. Tudek A, Schmid M, Jensen TH. Escaping nuclear decay: the significance of mRNA export for gene expression. Curr Genet. 2019 Apr;65(2):473–6.

236. Marques R, Lacerda R, Romão L. Internal Ribosome Entry Site (IRES)-Mediated Translation and Its Potential for Novel mRNA-Based Therapy Development. Biomedicines. 2022 Aug 2;10(8):1865.

237. Dai C, Cao Z, Wu Y, Yi H, Jiang D, Li W. Improved fusion protein expression of EGFP via the mutation of both Kozak and the initial ATG codon. Cell Mol Biol Lett. 2007 Sep;12(3):362–9.

238. Batt DB, Luo Y, Carmichael GG. Polyadenylation and transcription termination in gene constructs containing multiple tandem polyadenylation signals. Nucleic Acids Res. 1994 Jul 25;22(14):2811–6.

239. Gros MF, te Riele H, Ehrlich SD. Replication origin of a single-stranded DNA plasmid pC194. EMBO J. 1989 Sep;8(9):2711–6.

240. Prasad TK, Rao NM. The role of plasmid constructs containing the SV40 DNA nuclear-targeting sequence in cationic lipid-mediated DNA delivery. Cell Mol Biol Lett. 2005;10(2):203–15.

241. Choi KH, Mima T, Casart Y, Rholl D, Kumar A, Beacham IR, et al. Genetic tools for select-agent-compliant manipulation of Burkholderia pseudomallei. Appl Environ Microbiol. 2008 Feb;74(4):1064–75.

242. Ata-abadi NS, Forouzanfar M, Dormiani K, Varnosfaderani SR, Pirjamali L, Nasr-Esfahani MH, et al. Site-specific integration as an efficient method for production of recombinant human hyaluronidase PH20 in semi-adherent cells. Appl Microbiol Biotechnol. 2022 Feb 1;106(4):1459–73.

243. Li SP, Feng JJ, Wang HG, Wang XF, Lv ZJ. [The effects of SV40 PolyA sequence and its AATAAA signal on upstream GFP gene expression and transcription termination]. Yi Chuan Hered. 2012 Jan;34(1):113–9.

244. Roberts TC, Langer R, Wood MJA. Advances in oligonucleotide drug delivery. Nat Rev Drug Discov. 2020 Oct;19(10):673–94.

245. Lewis M. The lac repressor. C R Biol. 2005 Jun;328(6):521–48.

246. Poirel L, Madec JY, Lupo A, Schink AK, Kieffer N, Nordmann P, et al. Antimicrobial Resistance in Escherichia coli. Microbiol Spectr. 2018 Jul;6(4).

247. Johari YB, Scarrott JM, Pohle TH, Liu P, Mayer A, Brown AJ, et al. Engineering of the CMV promoter for controlled expression of recombinant genes in HEK293 cells. Biotechnol J. 2022 Aug;17(8): 2200062.

248. Conrad T, Plumbom I, Alcobendas M, Vidal R, Sauer S. Maximizing transcription of nucleic acids with efficient T7 promoters. Commun Biol. 2020 Aug 14;3(1):1–8.

249. Aldo PB, Craveiro V, Guller S, Mor G. Effect of culture conditions on the phenotype of THP-1 monocyte cell line. Am J Reprod Immunol N Y N 1989. 2013 Jul;70(1):80–6.

250. Naito K, Takeshita A, Shigeno K, Nakamura S, Fujisawa S, Shinjo K, et al. Calicheamicin-conjugated humanized anti-CD33 monoclonal antibody (gemtuzumab zogamicin, CMA-676) shows cytocidal effect on CD33-positive leukemia cell lines but is inactive on P-glycoprotein-expressing sublines. Leukemia. 2000 Aug;14(8):1436–43.

251. Purified anti-human HLA-DR Antibody anti-HLA-DR - L243 [Internet]. [cited 2023 Jun 25]. Available from:https://www.biolegend.com/en-us/products/purified-anti-human-hla-dr-antibody-792.

252. Saif A, Kazmi SFA, Naseem R, Shah H, Butt MO. Acute Myeloid Leukemia: Is that all there is? Cureus. 10(8):3198.

253. Li W. Flow Cytometry in the diagnosis of leukemias. In: Li W, editor. Leukemia. Brisbane (AU): Exon Publications; 2022 Oct 16. Chapter 4. [cited 2023 Oct 7]. Available from: http://www.ncbi.nlm.nih.gov/books/NBK586209.

254. Holmes KL, Lantz LM, Russ W. Conjugation of fluorochromes to monoclonal antibodies. Curr Protoc Cytom. 2001 May;Chapter 4:Unit 4.2.

255. Ivell R, Teerds K, Hoffman GE. Proper Application of Antibodies for Immunohistochemical Detection: Antibody Crimes and How to Prevent Them. Endocrinology. 2014 Mar;155(3):676–87.

256. McKinnon KM. Flow Cytometry: An Overview. Curr Protoc Immunol. 2018 Feb 21;120:5.1.1-5.1.11.

257. Magaki S, Hojat SA, Wei B, So A, Yong WH. An Introduction to the Performance of Immunohistochemistry. Methods Mol Biol Clifton NJ. 2019;1897:289–98.

258. Teixeira A, Carreira L, Abalde-Cela S, Sampaio-Marques B, Areias AC, Ludovico P, et al. Current and Emerging Techniques for Diagnosis and MRD Detection in AML: A Comprehensive Narrative Review. Cancers. 2023 Feb 21;15(5):1362.

259. Papaioannou NE, Beniata OV, Vitsos P, Tsitsilonis O, Samara P. Harnessing the immune system to improve cancer therapy. Ann Transl Med. 2016 Jul;4(14):261–261.

260. Marconi G, Guolo F, Nanni J, Papayannidis C. Editorial: Precision medicine for acute myeloid leukemia. Front Oncol. 2023 Jul 25;13:1233757.

261. Webber BA, Cushing MM, Li S. Prognostic Significance of Flow Cytometric Immunophenotyping in Acute Myeloid Leukemia. Int J Clin Exp Pathol. 2008 Jan 1;1(2):124–33.

262. Espinoza-Gutarra MR, Green SD, Zeidner JF, Konig H. CD123-targeted therapy in acute myeloid leukemia. Expert Rev Hematol. 2021 Jun;14(6):561–76.

263. El-Meligui YM, Abd Elrhman HE, Salahuddin A, Hamouda MA, Kassem AB. Correlation Study on HLA-DR and CD117 (c-Kit) Expressions: Its Prognosis and Treatment Response in Acute Myeloid Leukemia Patients. Pharmacogenomics Pers Med. 2021 Mar 30;14:381–93.

264. Campos L, Guyotat D, Archimbaud E, Devaux Y, Treille D, Larese A, et al. Surface marker expression in adult acute myeloid leukaemia: correlations with initial characteristics, morphology and response to therapy. Br J Haematol. 1989 Jun 1;72(2):161–6.

265. Landmann R, Knopf HP, Link S, Sansano S, Schumann R, Zimmerli W. Human monocyte CD14 is upregulated by lipopolysaccharide. Infect Immun. 1996 May;64(5):1762–9.

266. van den Ancker W, Wijnands PGJTB, Westers TM, Bontkes HJ, van Wetering S, Kruisbeek AM, et al. Expansion of AML Blasts Induces CD14 Expression and Facilitates Leukemic DC Development for Therapeutic Application In AML. Blood. 2010 Nov 19;116(21):2193.

267. Salem DA, Abd El-Aziz SM. Flowcytometric Immunophenotypic Profile of Acute Leukemia: Mansoura Experience. Indian J Hematol Blood Transfus. 2012 Jun;28(2):89–96.

268. Bradstock K, Matthews J, Benson E, Page F, Bishop J. Prognostic value of immunophenotyping in acute myeloid leukemia. Australian Leukaemia Study Group. Blood. 1994 Aug 15;84(4):1220–5.

269. Wang D, An G, Xie S, Yao Y, Feng G. The clinical and prognostic significance of CD14+HLA-DR−/low myeloid-derived suppressor cells in hepatocellular carcinoma patients receiving radiotherapy. Tumor Biol. 2016 Aug 1;37(8):10427–33.

270. Skopek R, Palusińska M, Kaczor-Keller K, Pingwara R, Papierniak-Wyglądała A, Schenk T, et al. Choosing the Right Cell Line for Acute Myeloid Leukemia (AML) Research. Int J Mol Sci. 2023 Mar 11;24(6):5377.

271. Alabdulmonem W, Rasheed Z, Aljohani ASM, Almakrami M, Ssadh HA, Fernandez N. LPS Subtypes Activate Inflammatory Signaling Through CD-14 and TLR-4 in Human Monocytic Cells. Res J Immunol. 2020 Jan 16;13(1):1–9.

272. Bosshart H, Heinzelmann M. THP-1 cells as a model for human monocytes. Ann Transl Med. 2016 Nov;4(21):438.

273. Tsuchiya S, Yamabe M, Yamaguchi Y, Kobayashi Y, Konno T, Tada K. Establishment and characterization of a human acute monocytic leukemia cell line (THP-1). Int J Cancer. 1980;26(2):171–6.

274. Khan AA, Alsahli MA, Rahmani AH. Myeloperoxidase as an Active Disease Biomarker: Recent Biochemical and Pathological Perspectives. Med Sci. 2018 Apr 18;6(2):33.

275. Omman RA, Kini AR. 31 - Acute leukemias. In: Keohane EM, Otto CN, Walenga JM, editors. Rodak's Hematology (Sixth Edition) [Internet]. St. Louis (MO): Elsevier; 2020 [cited 2023 Oct 8]. p. 540–54. Available from: https://www.sciencedirect.com.

276. Pant S, Misra R. Role of Immunohistochemistry in diagnosis and subtyping of acute leukemia using selected ihc markers in a resource limited setting. Int J Contemp Med Res IJCMR. 2020 Jun 1;7.

277. Guy J, Antony-Debré I, Arnoux I, Fossat C, Benayoun E, Le Garff-Tavernier M, et al. flow cytometry thresholds of myeloperoxidase detection to discriminate between acute lymphoblastic or myeloblastic leukemia. Blood. 2012 Nov 16;120(21):1450.

278. Arber DA, Orazi A, Hasserjian R, Thiele J, Borowitz MJ, Le Beau MM, et al. The 2016 revision to the World Health Organization classification of myeloid neoplasms and acute leukemia. Blood. 2016 May 19;127(20):2391–405.

279. HL-60 - CCL-240 | ATCC [Internet]. [cited 2023 Sep 1]. Available from: https://www.atcc.org.

280. Meier RW, Chen T, Friis RR, Tobler A. Myeloperoxidase is a primary response gene in HL60 cells, directly regulated during hematopoietic differentiation. Biochem Biophys Res Commun. 1991 May 15;176(3):1345–50.

281. Cruz-Tapias P, Castiblanco J, Anaya JM. Major histocompatibility complex: Antigen processing and presentation. In: Autoimmunity: From Bench to Bedside [Internet] [Internet]. El Rosario University Press; 2013 [cited 2023 Aug 3]. Available from: https://www.ncbi.nlm.nih.gov/books/NBK459467/

282. Alexovič M, Lindner JR, Bober P, Longuespée R, Sabo J, Davalieva K. Human peripheral blood mononuclear cells: A review of recent proteomic applications. Proteomics. 2022 Aug;22(15–16):2200026.

283. Acosta Davila JA, Hernandez De Los Rios A. An Overview of Peripheral Blood Mononuclear Cells as a Model for Immunological Research of *Toxoplasma gondii* and Other Apicomplexan Parasites. Front Cell Infect Microbiol. 2019 Feb 8;9:24.

284. Coupling of Monoclonal Antibodies with Fluorophores | Springer Nature Experiments [Internet]. [cited 2023 Aug 8]. Available from: https://experiments.springernature.com/articles/10.1385/0-89603-308-2:205.

285. J. Walsh S, D. Bargh J, M. Dannheim F, R. Hanby A, Seki H, J. Counsell A, et al. Site-selective modification strategies in antibody–drug conjugates. Chem Soc Rev. 2021;50(2):1305–53.

286. Ward CC, Kleinman JI, Nomura DK. NHS-Esters as Versatile Reactivity-Based Probes for Mapping Proteome-Wide Ligandable Hotspots. ACS Chem Biol. 2017 Jun 16;12(6):1478–83.

287. Kuang J, Tao Y, Song Y, Chemmalil L, Mussa N, Ding J, et al. Understanding the pathway and kinetics of aspartic acid isomerization in peptide mapping methods for monoclonal antibodies. Anal Bioanal Chem. 2021 Mar 1;413(8):2113–23.

288. Engineering THIOMABs for Site-Specific Conjugation of Thiol-Reactive Linkers | SpringerLink [Internet]. [cited 2023 Aug 8]. Available from: https://link.springer.com/protocol/10.1007/978-1-62703-541-5_11.

289. Sadiki A, Kercher EM, Lu H, Lang RT, Spring BQ, Zhou ZS. Site-specific Bioconjugation and Convergent Click Chemistry Enhances Antibody–Chromophore Conjugate Binding Efficiency. Photochem Photobiol. 2020 May;96(3):596–603.

290. Wilhelm J, Kühn S, Tarnawski M, Gotthard G, Tünnermann J, Tänzer T, et al. Kinetic and Structural Characterization of the Self-Labeling Protein Tags HaloTag7, SNAP-tag, and CLIP-tag. Biochemistry. 2021 Aug 24;60(33):2560–75.

291. Gautier A, Juillerat A, Heinis C, Corrêa IR, Kindermann M, Beaufils F, et al. An engineered protein tag for multiprotein labeling in living cells. Chem Biol. 2008 Feb;15(2):128–36.

292. Kolberg K, Puettmann C, Pardo A, Fitting J, Barth S. SNAP-tag technology: a general introduction. Curr Pharm Des. 2013;19(30):5406–13.

293. Keppler A, Kindermann M, Gendreizig S, Pick H, Vogel H, Johnsson K. Labeling of fusion proteins of O6-alkylguanine-DNA alkyltransferase with small molecules in vivo and in vitro. Methods. 2004 Apr;32(4):437-44.

294. Woitok M, Grieger E, Akinrinmade OA, Bethke S, Pham AT, Stein C, et al. Using the SNAP-Tag technology to easily measure and demonstrate apoptotic changes in cancer and blood cells with different dyes. PLOS ONE. 2020 Dec 3;15(12):0243286.

295. Woitok M, Klose D, Niesen J, Richter W, Abbas M, Stein C, et al. The efficient elimination of solid tumor cells by EGFR-specific and HER2-specific scFv-SNAP fusion proteins conjugated to benzylguanine-modified auristatin F. Cancer Lett. 2016 Oct 28;381(2):323–30.

296. Hussain AF, Kampmeier F, von Felbert V, Merk HF, Tur MK, Barth S. SNAP-tag technology mediates site specific conjugation of antibody fragments with a photosensitizer and improves target specific phototoxicity in tumor cells. Bioconjug Chem. 2011 Dec 21;22(12):2487–95.

297. Mauro VP, Chappell SA. A critical analysis of codon optimization in human therapeutics. Trends Mol Med. 2014 Nov;20(11):604–13.

298. Restriction Digest - an overview | ScienceDirect Topics [Internet]. [cited 2023 Aug 11]. Available from: https://www.sciencedirect.com/topics/biochemistry-genetics-and-molecular-biology/restriction-digest.

299. Addgene: Protocol - How to Run an Agarose Gel [Internet]. [cited 2023 Aug 12]. Available from: https://www.addgene.org/protocols/gel-electrophoresis.

300. Sample Preparation & Gel Electrophoresis Troubleshooting [Internet]. [cited 2023 Aug 12]. Available from: https://www.sigmaaldrich.com/ZA/en/technical-documents/technical-article/protein-biology/gel-electrophoresis/sample-preparation-gel-electrophoresis.

301. Inoue H, Nojima H, Okayama H. High efficiency transformation of Escherichia coli with plasmids. Gene. 1990 Nov 30;96(1):23–8.

302. Hanahan D. Studies on transformation of Escherichia coli with plasmids. J Mol Biol. 1983 Jun 5;166(4):557–80.

303. Barnes LM, Dickson AJ. Mammalian cell factories for efficient and stable protein expression. Curr Opin Biotechnol. 2006 Aug;17(4):381–6.

304. Jäger V, Büssow K, Wagner A, Weber S, Hust M, Frenzel A, et al. High level transient production of recombinant antibodies and antibodies fusion proteins in HEK293 cells. BMC Biotechnol. 2013 Jun 26;13:52.

305. Mungra N, Biteghe FAN, Malindi Z, Huysamen AM, Karaan M, Hardcastle NS, et al. CSPG4 as a target for the specific killing of triple-negative breast cancer cells by a recombinant SNAP-tag-based antibody-auristatin F drug conjugate. J Cancer Res Clin Oncol. 2023 Oct 1;149(13):12203–25.

306. Potter H. Transfection by electroporation. Curr Protoc Immunol. 2001 May;Chapter 10:10.15.1-10.15.3.

307. Nimesh S, Chandra R. Guanidinium-grafted polyethylenimine: an efficient transfecting agent for mammalian cells. Eur J Pharm Biopharm Off J Arbeitsgemeinschaft Pharm Verfahrenstechnik EV. 2008 Mar;68(3):647–55.

308. Carson M, Johnson DH, McDonald H, Brouillette C, Delucas LJ. His-tag impact on structure. Acta Crystallogr D Biol Crystallogr. 2007 Mar;63(Pt 3):295–301.

309. Marvelgent Biosciences [Internet]. 2018 [cited 2023 Oct 11]. PolyHis tag: how length matters in protein purification. Available from: https://marvelgent.com/blogs/marvoblog/how-his-tag-length-matters-in-protein-purification.

310. Wang W, Ignatius AA, Thakkar SV. Impact of residual impurities and contaminants on protein stability. J Pharm Sci. 2014 May;103(5):1315–30.

311. Cytiva [Internet]. [cited 2023 Aug 15]. His-tagged protein purification protocol. Available from: https://www.cytivalifesciences.com/en/us/solutions/protein-research/knowledge-center/protein-purification-methods/how-to-combine-chromatography-techniques/his-tagged-protein-purification-protocols.

312. Saraswat M, Musante L, Ravidá A, Shortt B, Byrne B, Holthofer H. Preparative purification of recombinant proteins: current status and future trends. BioMed Res Int. 2013;2013:312709.

313. Gibert S, Bakalara N, Santarelli X. Three-step chromatographic purification procedure for the production of a his-tag recombinant kinesin overexpressed in E. coli. J Chromatogr B Biomed Sci App. 2000 Jan 14;737(1–2):143–50.

314. Ryan BJ, Henehan GT. Overview of approaches to preventing and avoiding proteolysis during expression and purification of proteins. Curr Protoc Protein Sci. 2013 Feb;Chapter 5:Unit5.25.

315. Cell line development. In: Therapeutic Antibody Engineering [Internet]. Elsevier; 2012 [cited 2023 Sep 2]. p. 421–595. Available from: https://linkinghub.elsevier.com.

316. Lemire L, Pham PL, Durocher Y, Henry O. Practical Considerations for the Scale-Up of Chinese Hamster Ovary (CHO) Cell Cultures. In: Pörtner R, editor. Cell Culture Engineering and Technology: In appreciation to Professor Mohamed Al-Rubeai [Internet]. Cham: Springer International Publishing; 2021 [cited 2023 Aug 19]. p. 367–400.

317. Yang W, Zhang J, Xiao Y, Li W, Wang T. Screening Strategies for High-Yield Chinese Hamster Ovary Cell Clones. Front Bioeng Biotechnol. 2022 Jun 17;10:858478.

318. Poussin C, Foti M, Carpentier JL, Pugin J. CD14-dependent Endotoxin Internalization via a Macropinocytic Pathway*. J Biol Chem. 1998 Aug 7;273(32):20285–91.

319. Genin M, Clement F, Fattaccioli A, Raes M, Michiels C. M1 and M2 macrophages derived from THP-1 cells differentially modulate the response of cancer cells to etoposide. BMC Cancer. 2015 Aug 8;15(1):577.

320. Jimenez-Duran G, Luque-Martin R, Patel M, Koppe E, Bernard S, Sharp C, et al. Pharmacological validation of targets regulating CD14 during macrophage differentiation. EBioMedicine. 2020 Oct 7;61:103039.

321. Tominaga-Sato S, Tsushima H, Ando K, Itonaga H, Imaizumi Y, Imanishi D, et al. Expression of myeloperoxidase and gene mutations in AML patients with normal karyotype: double CEBPA mutations

are associated with high percentage of MPO positivity in leukemic blasts. Int J Hematol. 2011 Jul;94(1):81–9.

322. www.rndsystems.com [Internet]. [cited 2023 Sep 2]. Human/Mouse Myeloperoxidase/MPO Antibody. Available from: https://www.rndsystems.com/products/human-mouse-myeloperoxidase-mpo-antibody.

323. Anti-Myeloperoxidase antibody (ab45977) [Internet]. [cited 2023 Sep 3]. Available from: https://www.abcam.com/products/primary-antibodies/myeloperoxidase-antibody.

324. Pink D, Basu A, Wong M, Pham D, Valencia J, Triana V, et al. Antibody titrations are critical for microflow cytometric analysis of extracellular vesicles. Cytometry A. 2023;103(8):670–83.

325. Mizrahi O, Ish Shalom E, Baniyash M, Klieger Y. Quantitative Flow Cytometry: Concerns and Recommendations in Clinic and Research. Cytometry B Clin Cytom. 2018;94(2):211–8.

326. Shen DY, Ning BT, Tang YM, Li SS. Construction and Expression of a Novel Anti-CD14 Human-Mouse Chimeric Antibody Hm2F9. DNA Cell Biol. 2014 Sep 1;33(9):599–604.

327. Starr T, Bauler T, Malik-Kale P, Steele-Mortimer O. The phorbol 12-myristate-13-acetate differentiation protocol is critical to the interaction of THP-1 macrophages with Salmonella Typhimurium. PLOS ONE. 2018 Mar 14;13:0193601.

328. Nakase K, Sartor M, Bradstock K. Detection of myeloperoxidase by flow cytometry in acute leukemia. Cytometry. 1998;34(4):198–202.

329. Brightness Index [Internet]. [cited 2023 Aug 31]. Available from: https://www.biolegend.com/en-us/brightness-index.

330. Bates A, Power CA. David vs. Goliath: The Structure, Function, and Clinical Prospects of Antibody Fragments. Antibodies Basel Switz. 2019 Apr 9;8(2):28.

7. Appendices.

1. Determining the ideal concentrations for 8E2(scFv)-SNAP-Alexa Flour 488

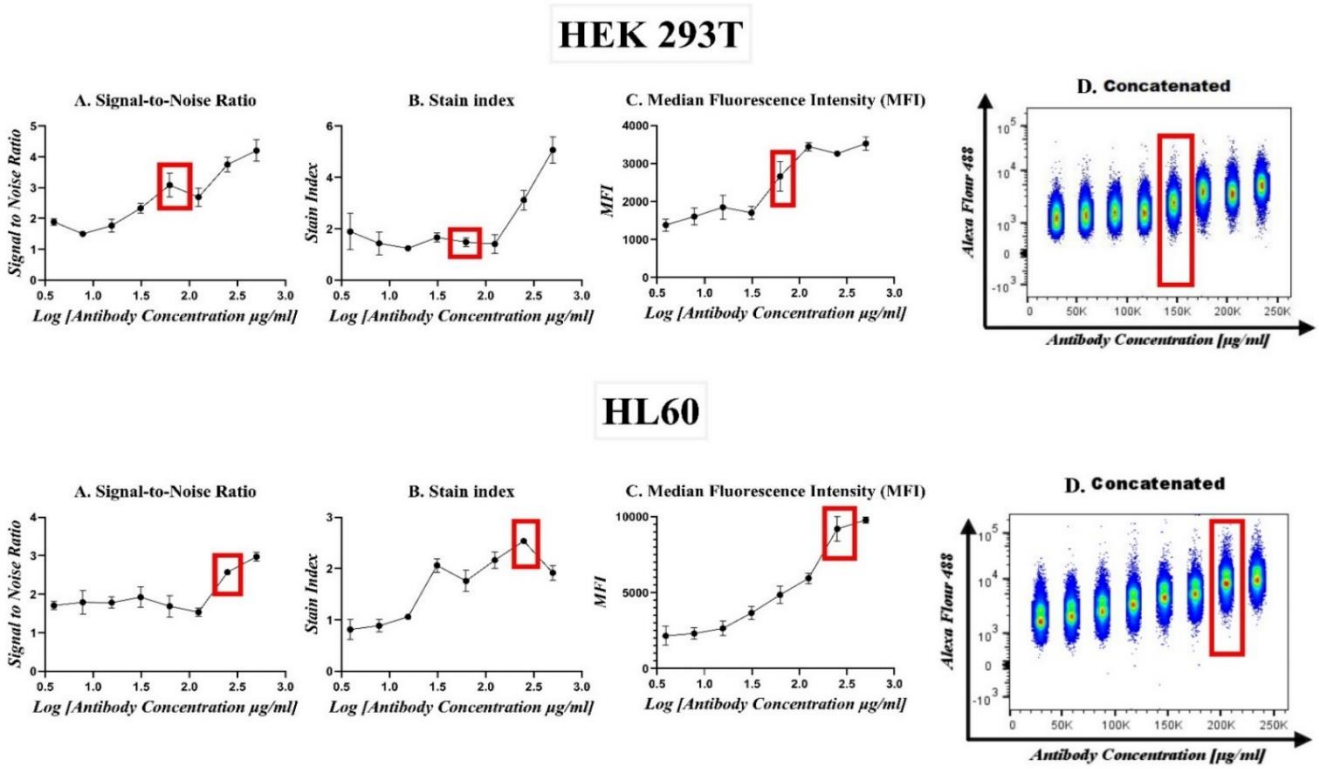

Figure A1. Titration of Anti-MPO antibody 8E2(scFv)-SNAP-Alexa Flour 488. HL60 and HEK 293T cells were incubated with increasing concentrations of antibody ranging from 3.9 µg/ml to 500 µg/ml. The experiments were done in replicates (A) Signal to noise ratio indicating the separation between the signal and the background noise. (B) Stain index showing the separation between positive and negative populations. (C) Median Fluorescence Intensity showing the fluorescence strength the stained population. (D) Concatenated pseudocolor plot showing combined multiple flow cytometry samples in a single plot. The red boxes indicate the chosen antibody concentrations for HEK 293T cells (62.5 µg/ml) and HL60 cells (250 µg/ml).

2. Determining the ideal concentrations for L243(scFv)-SNAP-Alexa Flour 488

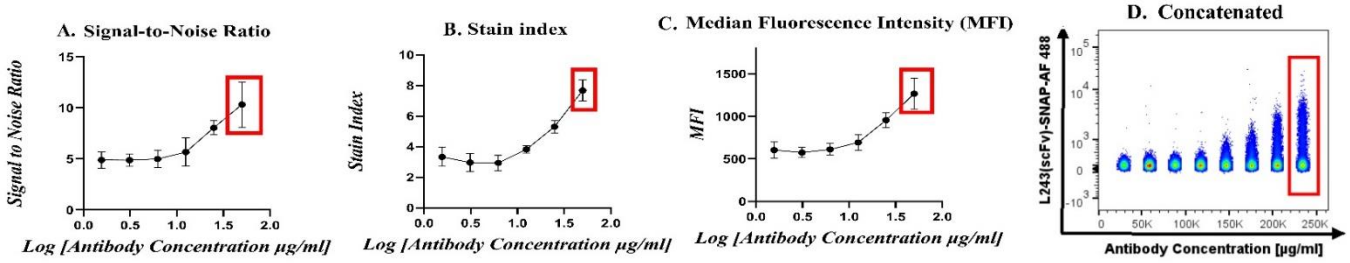

Figure A2. Titration of Anti-HLA-DR antibody L243(scFv)-SNAP-Alexa Flour 488. PBMCs cells were incubated with increasing concentrations of antibody ranging from 0.3 µg/ml to 50 µg/ml. (A) Signal to noise ratio indicating the separation between the signal and the background noise. (B) Stain index showing the separation

between positive and negative populations. (C) Median Fluorescence Intensity indicating the fluorescence strength the stained population. (D) Concatenated pseudocolor plot showing combined multiple flow cytometry samples in a single plot. The red boxes indicate the chosen antibody concentration of 50 µg/ml.

3. Analysing the staining of HLA-DR on Monocytes

A. **B.**

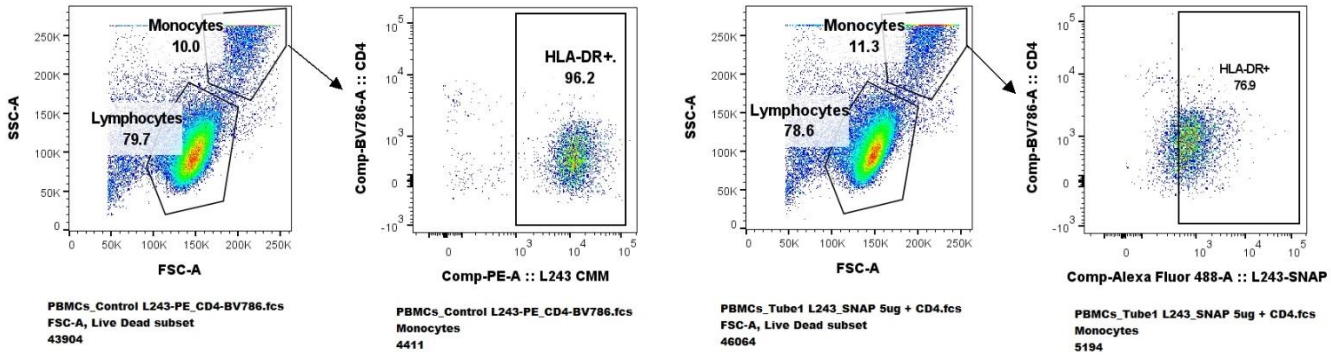

Figure A3. Representative flow cytometry plots showing HLA-DR staining on monocytes. The same gating strategy was use as mentioned above in figure 32. **(A)** Commercial L243 antibody was binding to monocytes with 96%. **(B)** L243(scFv)-SNAP was binding to monocytes with 66.4%.

4. Summary of buffers and media used for experiments in this study, including their compositions.

<u>Liquid transformation materials:</u>

Plasmid DNA

DH5α calcium competent cells *(E. coli)*

Luria-Bertani (LB) broth

(SOC) at room temperature

Heating block

Microfuge

Incubator with shaker

Nuclease free water

1.5 ml microfuge tubes

15 ml culture tubes

50 ml centrifuge tubes

LB agar plates

Glycerol (50%)

Ampicillin

Pipette, Pipette tips

Spectrophotometer (Denovix NanoDrop™)

Table A1. Buffer recipes and composition for DNA extraction

Buffer/Reagent	Description	Composition
LB Broth (1L, pH 7)	Bacterial culture media	35g LB agar powder dH_2O-top up to 1litre
LB Agar (20 ml)	Bacterial culture media	35g LB agar powder dH_2O-top up to 1litre
Ampicillin (100 mg/ml)	Antibiotic - selection for plasmids containing ampicillin resistance gene (AMPR)	1g ampicillin 10 ml dH_2O
50% Glycerol (100 ml)	Freezing down of bacterial culture	50 ml 100% Glycerol 50 ml dH_2O

Agarose Gel Electrophoresis materials:

Agarose powder

1x TAE buffer SYBR™ safe

Microwave

250 ml beaker

Scale, spatula

dH_20

Bio-Rad buffer tank

Gel casting tray, Gel comb

6X purple loading dye

Pipettes, Pipette tips

100 bp and/or 1000 bp DNA ladder

UV gel documentation system

Table A2. Buffer recipes and composition for Agarose Gel Electrophoresis

Reagent/Buffer	Composition
10x TAE buffer(1 litre):	48.5g Tris Base 20 ml 0.5M EDTA (pH8.0) 1.4 ml glacial acetic acid dH_2O - top up to 1 litre
1x TAE buffer(1 litre):	100 ml 10x TAE buffer 900 ml dH_2O
Agarose gel 1.2g agarose:	100 ml 1x TAE buffer 10 µl SYBR™safe (after cooling)

DNA Ligation reaction materials:

Insert DNA and Backbone DNA

Zyppy miniprep purification kit

T4 DNA Ligase

T4 DNA Ligase Buffer

Nuclease free water

SOC at room temperature

LB broth

Ampicillin (100 mg/ml)

1L flask, 15 ml culture tubes,

LB agar plates

1.5 ml microfuge tubes

Pipette, Pipette tips

Incubator with shaker

Heating block

Table A3. Reagents for T4 DNA Ligation

Component	Amount
Vector DNA	50ng
Insert DNA	Varies depending on fragment size. (use NEBio Calculator)
T4 DNA ligase buffer	2 µl
T4 DNA ligase	1 µl (added last)
Nuclease free water	Adjust to final volume of 20 µl

Protein purification

Materials needed:

ÄKTA Avant

Cell culture supernatant

Incubation buffer, Equilibration buffer, Elution buffer, Wash Buffer

96-deep well plate

PVDF membrane

5 ml His-Trap™ excel.

100kDA and 10kDa Amicon® Ultra 15 ml Centrifugal Filter

Table A4. Buffer recipes and for protein purification.

Buffer	Composition
Equilibration:	50 mM NaH_2PO_4 300 mM NaCl
Incubation:	200 mM (NaH_2PO_4) 1.2 M (NaCl), 10 mM ($C_3N_2H_4$)
Wash:	50 mM (NaH_2PO_4) 300 mM (NaCl) 40 mM ($C_3N_2H_4$)
Elution:	50 mM (NaH_2PO_4) 300 mM (NaCl), 250 mM ($C_3N_2H_4$)

SDS-PAGE & WB

Materials needed:

Mini-PROTEAN® system (Bio-Rad)

Micropipettes and tips Microfuge tubes

Acrylamide

10% SDS solution and 10% APS solution

TEMED

TRIS-HCl buffer (0.5M, pH 6.8) and TRIS-HCl buffer (1.5M, pH 8.8)

dH_2O

1x Running Buffer

4x Laemmli sample loading dye (1:9 ratio, 2-mercaptoethanol: Laemmli sample buffer)

Protein Ladder

Acqua Stain Protein Gel Stain (Vacutec, South Africa)

Tween® 20

1x Transfer Buffer

1x Tris-buffered saline, 0.1% (w/v) Tween®20(TBST)

Table A5. Buffer recipes and composition for SDS PAGE and Western Blot Analysis

Buffer	**Composition**
10% Ammonium per sulphate (APS)	Ammonium per sulphate powder (5g) dH_2O (50 ml)
10% SDS	SDS powder(10g) dH_2O (100 ml)
10x Running Buffer	Tris Base (30.3g) SDS (10g) Glycine (144g) dH_2O (fill up to 1litre)
1x Running Buffer	10x Running Buffer: dH_2O (1:9)

10x Transfer Buffer	Tris Base (30g) Glycine(144g)
1x Transfer Buffer	10X Transfer Buffer: 100% Methanol: dH_2O (1:2:7)
10x Tris-buffered saline (TBS)	Tris Base(200mM) NaCl (1.5M) dH_2O
1x TBS-Tween(TBST)	TBS: dH2O (1:9) 1 ml Tween®20

Conjugation

Materials needed:

Dimethyl sulfoxide (DMSO)

1x PBS

BG- Alexa Flour 488

BG- Alexa Flour 647

Heating block

Dithiothreitol (DTT)

SNAP fusion protein.

SDS-PAGE apparatus

Table A6. Conjugation reaction composition

Component	**Stock Concentration**	**Final Concentration**
PBS	1x	
Dithiothreitol DTT	10 mM	1 mM
BG-Alexa Flour 488/	25 µM	5 µM
BG-Alexa Flour 647		
SNAP fusion protein	50 µM	5 µM
Total volume		20 µl

Table A7. Conjugation reaction for live cell imaging and flow cytometry staining

Component	Initial Concentration	Final Concentration
PBS	1x	
Dithiothreitol (DTT)	50 mM	1 mM
BG-Alexa Flour 647/488	250 μM	5 μM
SNAP fusion protein	50 μM	5 μM
Final volume		200 μl

Table A8. The cell lines that were obtained and used in this study, the supplier and catalogue information, along with the medium they were cultured in is provided

Cell lines	Origin	Media	Species	Description
DH5α	New England Bio-Labs (C2987)	Luria-Bertani broth and agar	*E. coli*	*K12 strain and genotype fhuA2 (argF-lacZ) U169 phoA glnV44 Φ80 (lacZ)M15 gyrA96 recA1 relA1 endA1 thi-1 hsdR17*
HEK293T	ATCC(CRL-3216)	RPMI-1640	Human	Human embryonic kidney cell
THP-1	ATCC (TIB-202)	RPMI-1640	Human	Acute monocytic leukemia
HL60	ATCC (CCL-240)	RPMI-1640	Human	Acute promyelocytic leukemia
PBMCs	SATVI	N/A	Human	Peripheral blood mononucleated cells